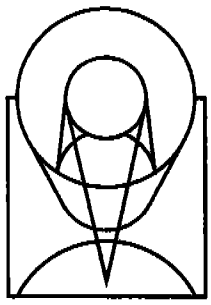

SPACE TELESCOPE SCIENCE INSTITUTE

1

Faint Object Spectrograph Instrument Handbook

V. 1.0

OCTOBER 1985

NASA

esa

Edwin P. Hubble Space Telescope

FAINT OBJECT SPECTROGRAPH
INSTRUMENT HANDBOOK

Holland C. Ford
Space Telescope Science Institute
and
Department of Physics and Astronomy
The Johns Hopkins University
Homewood Campus, Baltimore, MD 21218

Approved: F. Macchetto
F. Macchetto
Chief, Instrument Support Branch

SEPTEMBER, 1985

TABLE OF CONTENTS

1.0 HOW TO USE THIS MANUAL

User's manuals often begin with a detailed description of the instrument. If you like this traditional approach, you should begin by reading chapter 3. It should provide you with more than enough information to choose the FOS configurations needed to accomplish your proposed program. You can then read chapter 4, which tells you how to calculate exposure times and signal-to-noise ratios.

An alternative approach is to begin with chapter 2, which is meant to be light enough to not immediately swamp you with detail, yet deep enough to let you begin specifying the FOS configurations which you will use. You can then skip to chapter 4, which should allow you to estimate the feasibility of your program and calculate exposure times once you have finalized your list of objects. If you need still more detail (*e.g.*, for spectropolarimetry or time resolved spectrophotometry), you can then read all or selected parts of chapter 3. Chapter 5 discusses FOS calibrations and the types of programs which might require that you make special calibration observations, rather than use those which we provide at no charge. Chapter 6 outlines the kinds of data you get to take home (or analyze here). Finally, the Appendix is a catchall for information which only rarely will be needed to plan an FOS observing program.

2.0 A QUICK GUIDE TO USING THE FOS

2.1 BRIEF INSTRUMENT OVERVIEW

The Faint Object Spectrograph (FOS) is described in detail by Harms *et al.* (1979) and by Harms (1982). Briefly, the FOS has two independent optical paths which image a dispersed image of the entrance aperture onto two Digicon detectors with 2× demagnification. A schematic of the optical path is shown in Figure 2.1-1. The f/24 beam for either side passes through an entrance aperture, goes through a polarization analyzer (which includes a clear position), and then is reflected from the FOS corner nearest to the optical axis up into the spectrograph by a grazing incidence mirror. The diverging beam next passes through an order separating filter (if appropriate) in the filter-grating wheel and then is collimated by an off-axis paraboloidal mirror. The collimated light is reflected back to the filter-grating wheel where it is dispersed and imaged onto a Digicon detector by a concave grating, a camera mirror, or a camera mirror plus sapphire prism. The filter grating wheel allows selection of six slightly overlapping spectral regions between 1100 Å and 8000 Å with resolving power $R = \lambda/\Delta\lambda = 1300$, or three spectral regions with a resolving power of approximately 250 covered by two gratings and a prism. The polarizer can be used to measure linear and circular polarization over nearly the entire FOS wavelength range.

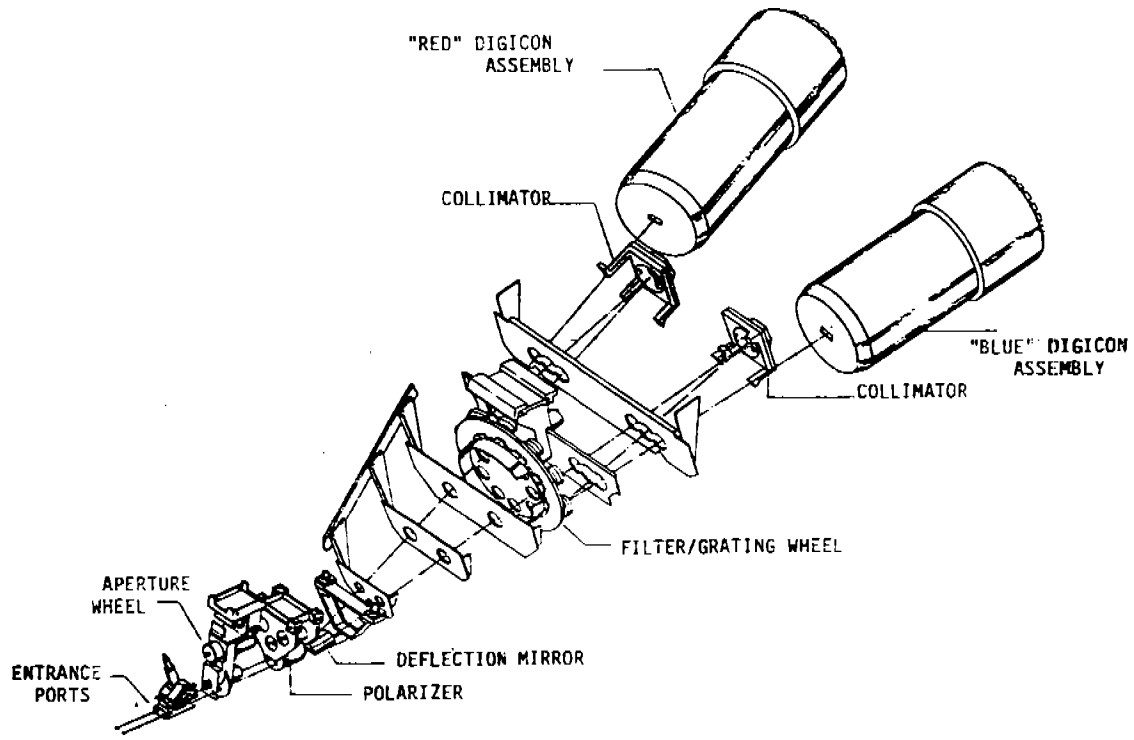

Figure 2.1-1. A Schematic Optical Diagram of the FOS

One Digicon has a bialkali photocathode on a magnesium fluoride faceplate and is sensitive to light between 1100 Å and 5500 Å. The second Digicon has a trialkali photocathode on a fused silica faceplate and is sensitve to light from 1800 Å to 8500 Å. The Digicons will be referred to respectively as the "blue" Digicon and the "red" Digicon. Each detector counts photoelectron pulses (if the pulse has an amplitude above a programmable threshold) in 512 independent silicon diode channels. There is a microprocessor for each side of the instrument which controls the electronics, mechanisms, and Digicons. The counts are summed into one of the microprocessor memories for a preset time (typically four minutes) and then read from the FOS to the HST SI C&HD computer which controls the instruments.

2.2 CONFIGURING THE FOS

The first step in using the FOS is to choose a set of configurations that will allow you to accomplish your scientific objectives. In a sentence, a configuration comprises a choice of an aperture, a waveplate (if you wish to do spectropolarimetry), a disperser with high resolution (R = 1300) or low resolution (R = 250) that covers the spectral region which interests you, and the appropriate red or blue detector to match the disperser. The second step is to decide if you want sky subtraction, unusual electronic substepping, or an observing mode such as time resolved spectrophotometry or rapid readout.

The choices which you can make and some of the considerations which should bear on the alternatives are given below.

2.2.1 Aperture Choice

The FOS entrance apertures and designations are given in Table 2.2.1-1. There are two sets of apertures, one for the blue side and one for the red side, etched sequentially along a circular ribbon which is mounted on the aperture wheel. The wheel positioning and locations of the apertures on the ribbon are such that the centers of the single apertures (including the target acquisition aperture) position to the same point on the sky for a fixed pointing of the Hubble Space Telescope (HST). This common point, which is different for the red and blue sides, coincides with the bisector of the line connecting the centers of the paired apertures,and with the geometrical centers of the slit and occulting apertures. The apertures are shown schematically in Figure 2.2.1-1.

The smallest apertures are suitable for isolating spatially resolved features on a scale of $0.1''$ to $0.25''$, and for spectroscopy of faint objects embedded in a bright background. However, unless you have a strong scientific reason for using the smallest apertures, there are two reasons why you should plan to use an $0.5''$ aperture (or larger). First, if you want a 95% probability of putting your object in an aperture, the RMS sum of all errors (*e.g.*, target relative positional errors in an offset and acquisition errors) must be less than $(D/4)$ arcseconds, where D is the aperture diameter. Second, the $0.1''$ and $0.25''$ apertures respectively block approximately 38% and 11% of the light (at 6300 Å) for a perfectly centered point source. Furthermore, the diffraction pattern from the $0.1''$ aperture overfills the FOS collimator, resulting in an additional light loss. The net light loss through the small apertures is shown in Figure 4.2-2 as a function of wavelength.

Table 2.2.1-1
FOS Apertures

Designation	Number	Shape	Size (″)	Separation (″)	Special Purpose
0.3	Single	Round	0.30 dia	NA	Spectroscopy and Spectropolarimetry
0.5	Single	Round	0.50 dia	NA	Spectroscopy and Spectropolarimetry
1.0	Single	Round	1.00 dia	NA	Spectroscopy and Spectropolarimetry
0.1- PAIR	Pair	Square	0.10	3.0	Object and Sky
0.25-PAIR	Pair	Square	0.25	3.0	Object and Sky
0.5- PAIR	Pair	Square	0.50	3.0	Object and Sky
1.0- PAIR	Pair	Square	1.00	3.0	Object and Sky
0.25 × 2.0	Single	Rectangular	0.25 × 2.0	NA	Extended Objects
0.7 × 2.0-BAR	Single	Rectangular	0.70 × 2.0	NA	Surrounding Nebulosity
2.0-BAR	Single	Square	2.0	NA	Surrounding Nebulosity
BLANK	NA	NA	NA	NA	Dark and Particle Events
4.3	Single	Square	4.3	NA	Target Acquisition
Failsafe	Pair	Square	0.5 and 4.3	NA	Target Acquisition and Spectroscopy

The first dimension of rectangular apertures is along the dispersion direction, the second dimension is perpendicular to the dispersion direction. The two apertures with the suffix designation "BAR" are bisected by an occulting bar which is 0.3″ wide in the direction perpendicular to the dispersion.

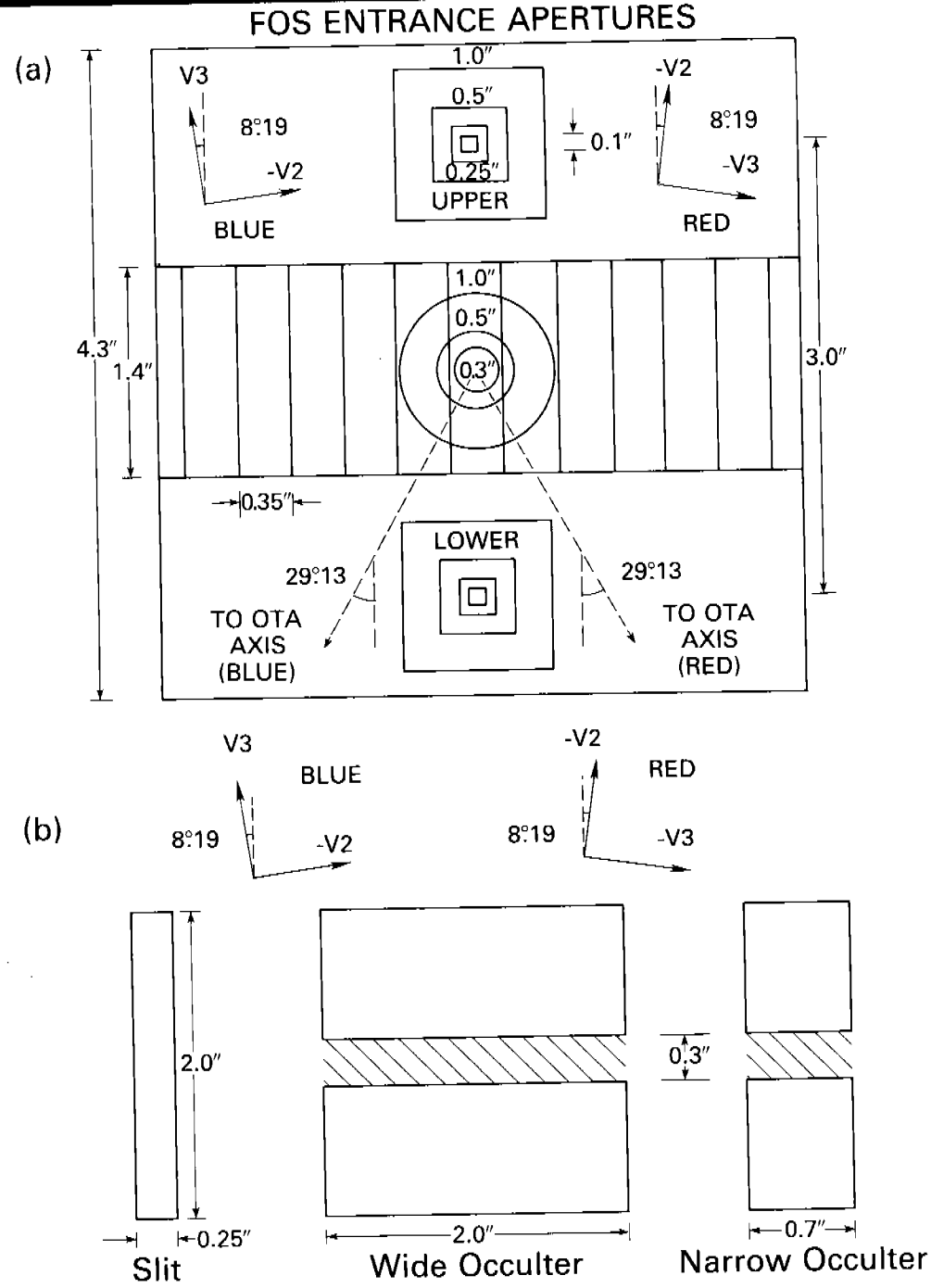

Figure 2.2.1-1 A Schematic of the FOS Apertures projected onto the sky. The upper panel shows the array of $0.35'' \times 1.4''$ diodes projected across the center of the $4.3'' \times 4.3''$ target acquisition aperture. The target acquisition aperture and the single circular apertures position to a common center. The pairs of square apertures position to common centers with respect to the target acquisition aperture as shown in the figure. Either the upper aperture (the "A" aperture, which is furtherest from the HST optical axis) or the lower aperture (the "B" aperture, which is closest to the HST optical axis) in a pair can be selected by an appropriate y-deflection in the Digicon detectors. The lower panel shows the three rectangular slits; two of the slits are bisected by an $0.3''$ opaque occulting bar. The centers of the three slits position to the center of the target acquisition aperture. The figure shows the orientation of the direction perpendicular to the dispersion in the HST V2, V3 focal plane on the blue and red sides. The FOS x-axis is parallel to the diode array and positive to the right; the y-axis is perpendicular to the diode array and positive toward the upper aperture.

If you are observing point sources the spectral resolution will be determined by the HST point spread function (including HST pointing jitter) and the grating's resolution. However, if you are observing an extended object the spectral resolution will be determined by the grating and the convolution of the FOS entrance aperture with the object's HST luminosity profile and the Digicon's diode response function. Consequently, there will be some loss of resolution with the larger apertures. The measured resolution as a function of aperture size (for a uniformly illuminated aperture) is given in Table 2.2.1-2. The full width at half maximum (FWHM) is tabulated in units of one diode width. The FWHM can be converted to spectral resolution by multiplying it times the dispersion, $\Delta\lambda(\text{Å Diode}^{-1})$, which is given in Table 2.2.3-1.

Table 2.2.1-2
FOS Line Widths (FWHM) as a Function of Aperture Size

Designation	Size (″)	G130H (Blue)	G570H (Red)
0.3	0.3 (circular)	1.00 ± .01	0.95 ± .02
0.5	0.5 (circular)	1.27 ± .04	1.20 ± .01
1.0	1.0 (circular)	2.29 ± .02	2.23 ± .01
0.1- PAIR	0.10 (square)	0.97 ± .03	0.92 ± .02
0.25-PAIR	0.25 (square)	0.98 ± .01	0.96 ± .01
0.5- PAIR	0.50 (square)	1.30 ± .04	1.34 ± .02
1.0- PAIR	1.00 (square)	2.65 ± .02	2.71 ± .02
0.25 × 2.0	0.25 × 2.0 (slit)	0.99 ± .01	0.96 ± .01
0.7 × 2.0-BAR	0.70 × 2.0	1.83 ± .02	1.90 ± .01
2.0-BAR	2.0	5.28 ± .07	5.43 ± .04

The FWHM are given in units of diodes.

A complete characterization of the FOS line profile must include the very low intensity wings which extend to large distances from the line center. The pseudo Voigt function given by equations (1) and (2) is a suitable representation of the FOS line profile.

$$V(x,\gamma,w) = y_o \left\{ \left[1 - \frac{\gamma}{w}\right] \exp\left[-\ln 2\left(\frac{x-x_o}{w}\right)^2\right] + \left[\frac{\gamma}{w}\right] \left[\frac{1}{1+\left(\frac{x-x_o}{w}\right)^2}\right] \right\} \qquad (1)$$

$$w = \frac{\gamma}{2} + \left(\frac{\gamma^2}{4} + 2\,(\ln 2)\,\sigma^2\right)^{\frac{1}{2}} \qquad (2)$$

The quantity y_o is the amplitude of the function (height of the line), γ is a parameter which characterizes the Lorentzian wings, σ is a parameter which characterizes the Gaussian core, and $x - x_o$ is the distance from the line center in diodes. In the limit that γ goes to zero, the function becomes a pure Gaussian.

The parameters of a good fit to an isolated emission line observed through the smallest aperture are $\sigma = 0.30$ and $\gamma = 0.07$. These parameters give values which are within 25% of the observed line profile out to 20 diodes from the line center.

The single circular apertures (0.3″, 0.5″, and 1.0″) should be used for polarization measurements. The paired apertures can be used for sky subtraction by alternately observing the "star plus sky" aperture and the "sky" aperture. If you are observing an isolated object with m_V brighter than 21, sky subtraction should not be necessary. Finally, there are two apertures with occulting bars which are intended for spectroscopy of nebulosity near a bright point source (*e.g.*, the parent galaxy of a quasar). When using these apertures you may require a particular position angle to place the nebulosity in the two windows perpendicular to the dispersion direction. The position angle is the angle of the positive y-axis (*cf.* Figure 2.2.1-1) projected onto the sky, measured from north through east. You must also specify a peak-up/peak-down target acquisition (*cf.* 2.4.2.3) in order to position the bright source on the occulting bar.

2.2.2 Choice of Waveplates for Spectropolarimetry

Observers who plan to use the FOS spectropolarimeter are strongly encouraged to read the paper by Allen and Angel (1982), which is reproduced as Appendix C. In order to achieve maximum sensitivity to linearly and circularly polarized light over the FOS spectral response (1150 Å to 8500 Å), there are two magnesium fluoride waveplates (A and B), one for each of the two Wollaston prisms in the polarimeter. Each waveplate-Wollaston combination can be used with either the red side or blue side.

Your choice of waveplate (or waveplates) will be dictated by whether you need high sensitivity to linearly polarized light or circularly polarized light in a particular spectral region. These efficiencies are given by

$$\eta_{linear} = \frac{(1 - \cos \Delta)}{2} \tag{1}$$

$$\eta_{circular} = \sin \Delta \tag{2}$$

where Δ is the waveplate retardation. The waveplate modulation efficiency for linear polarization will be a maximum near $\Delta = 180°$, and most efficient for circular polarization with retardations near $\Delta = 90°$ and 270°. Table 2.2.2-1 gives retardations and efficiencies for the FOS waveplates.

Figure 2.2.2-1 shows the polarimeter transmission, and waveplate retardations between 1200 Å and 1550 Å. In this spectral region the retardation is a strong function of wavelength.

TABLE 2.2.2-1
Retardations of the Flight Waveplates

λ(Å)	Δ	Waveplate A Efficiency		Δ	Waveplate B Efficiency	
		linear	circular		linear	circular
1175	-108°	.65	.95	-93 °	.53	.00
1200	100°	.59	.98	0 °	0.0	0.0
1216	215°	.91	.57	90 °	.50	1.00
1250	360°	0.0	0.0	161 °	.97	.33
1300	460°	.59	.98	228 °	.83	.74
1350	482°	.76	.85	247 °	.70	.92
1400	485°	.79	.82	250 °	.67	.94
1450	480°	.75	.87	241 °	.74	.87
1500	468°	.65	.95	238 °	.76	.85
1600	439°	.85	.98	226 °	.85	.72
2537	251°	.66	.94	123 °	.77	.86
3650	163°	.98	.29	84 °	.45	.99
6328	95°	.54	.99	43 °	.13	.68

Waveplate A has a high modulation efficiency at Lyα, whereas waveplate B does not. Both waveplates must be used if you wish to measure linear polarization over the entire spectral region between 1216 Å and 1350 Å.

2.2.3 Dispersers

Your choice of dispersers will depend on the combination of spectral regions and spectral resolution which you need. Table 2.2.3-1 lists the FOS dispersers; the first column lists the ST ScI grating designation (G for grating, the central wavelength in nanometers, and H or L for high or low dispersion), columns two and three and four and five respectively give the approximate diode number of the shortest and longest wavelengths covered by the grating, column six gives the dispersion (Å Diode^{-1}) at the central wavelength, column seven gives the maximum deviation of the dispersion from the central dispersion, and column eight gives the order separating blocking filter which is associated with the grating.

Each blocking filter has a fixed position in the filter-grating wheel and is used exclusively and mandatorily with its associated grating. The measured characteristics of the filters, gratings, and prism can be found in Appendix B. Appendix A is an atlas of Pt-Ne-Cr internal wavelength calibration spectra taken by the FOS before launch, and includes line identifications and polynomial fits of wavelength as a function of x-position.

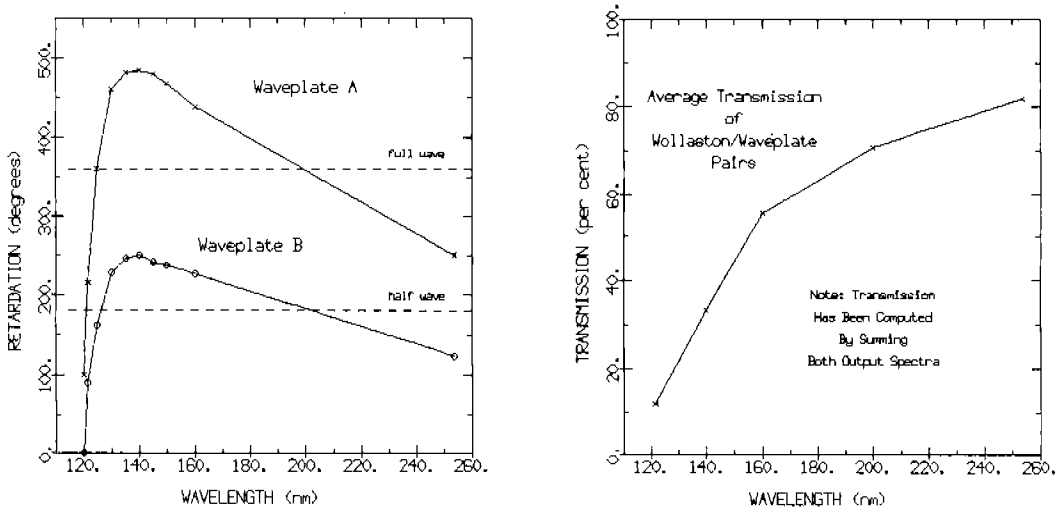

Figure 2.2.2-1 FOS waveplate retardation and polarimeter transmission (Allen and Angel 1982).

The nominal resolving power of the high resolution gratings is $R = \lambda/\Delta\lambda = 1300$ and the nominal resolving power of the two low resolution gratings is 250. Examples of simulated FOS spectra at high and low resolution are given in section 4.1. Because of its nonlinear dispersion the prism deserves special mention. Figure 2.2.3-1 shows the wavelength as a function of diode number. The figure shows that the resolving power approaches unity in the red. *Consequently, in order to avoid damaging the digicons by exceeding the maximum safe true counting rate of* 10^6 *counts* sec^{-1} *diode*$^{-1}$, *the internal comparison lamps cannot be observed with the prism unless two precautions are taken.* The first precaution is to use the smallest aperture and the second is to use the comparison lamp for the Digicon which is turned off. The lamp for each side has been optically cross strapped to the other side through a beam splitter which attenuates the lamp brightness by a factor of approximately 10 in the red. Also, because of the low dispersion of the prism, as a rule it will not be possible to observe stars brighter than $m_V = 6$.

2.2.4 Digicons

The final step in specifying an FOS configuration is to choose the Digicon (red or blue) with the best match in spectral sensitivity to the dispersers which you have selected. The measured preflight quantum efficiencies (QE) of the red and blue tubes are shown in Figure 2.2.4-1, and their dark count rates at $-20°$ C are given in Table 2.2.4-1.

Table 2.2.3-1

FOS Dispersers

Grating	Diode No.	λ(Å)	Diode No.	λ(Å)	Δλ(Å Diode^{-1})	Max Dev(%)	Blocking Filter
			Blue Digicon				
G130H	60	1150[1]	516[7]	1608	1.00	1.2	—
G190H	1	1575	516	2332	1.47	1.5	—
G270H	1	2227	516	3306	2.09	1.4	MgF
G400H	1	3244	516	4827	3.07	1.4	WG 305
G570H	1	4583	516	6885[6]	4.46	1.3	WG 375
G160L	318	1150[1]	516	2523[2]	6.50	2.4	—
G650L	295	3530	373	5500[6]	25.04	2.6	WG 375
PRISM	175	1850[4]	24	5500	—	—	—
			Red Digicon				
G190H	1	2323	516	1573[5]	- 1.45	0.4	—
G270H	1	3293	516	2225	- 2.07	0.4	MgF
G400H	1	4802	516	3237	- 3.04	0.4	WG 305
G570H	1	6849	516	4571	- 4.42	0.4	WG 375
G780H	1	9259	516	6274	- 5.79	0.5	OG 530
G160L	1	2473	126	1600[5]	- 6.96	—	—
G650L	1	8904[3]	205	3770	-25.05	0.6	WG 375
PRISM	497	8950	332	1850	—	—	—

1 The blue Digicon's MgF_2 faceplate absorbs light shortward of 1150Å.

2 The second order overlaps the first order longward of 2300Å.

3 The second order overlaps the first order longward of 7100Å.

4 The sapphire prism absorbs light shortward of 1650 Å; however, because of the large dispersion of the prism at the shortest wavelengths, the effective cutoff is longward of 1650 Å.

5 The red Digicon's fused silica faceplate strongly absorbs light shortward of 1700 Å.

6 The blue Digicon has little sensitivity longward of 5500 Å.

7 The photocathode electron image typically is deflected across 5 diodes, effectively adding 4 diodes to the diode length.

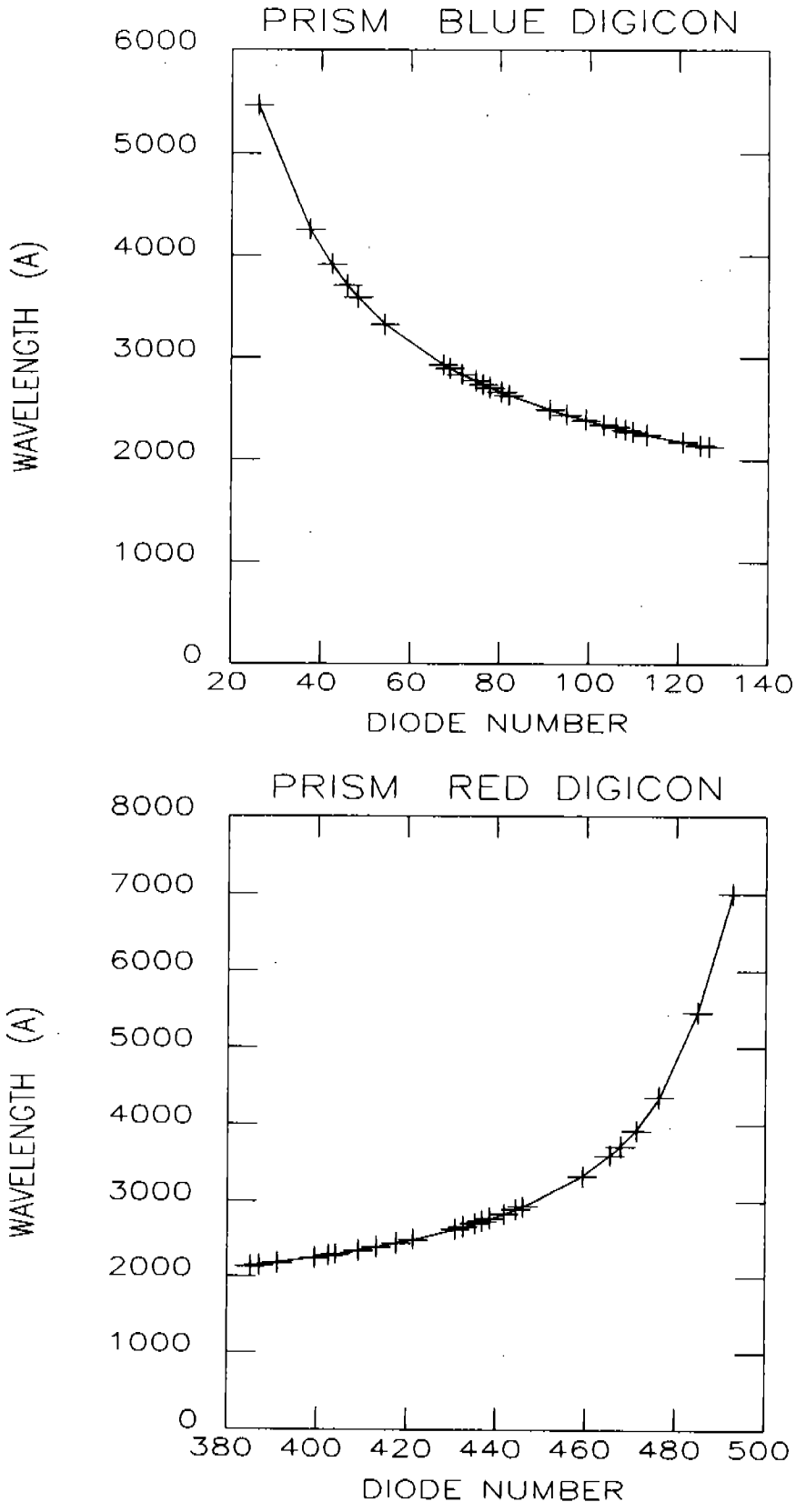

Figure 2.2.3-1. Wavelength as a function of pixel number for the prism with the blue and red Digicon (Sirk and Bohlin 1985).

Please be advised that at the time of the final editing of this manual, the previously selected Red Digicon (F3) has been removed from the FOS and will be replaced by one of two red spares, F8 or F9 (F8 is the most likely replacement). The quantum efficiencies of both tubes are shown in Figure 2.2.4-1. You will be advised in the STScI Newsletter which Digicon will be flown in the FOS.

High QE photocathodes have not been produced on magnesium fluoride substrates; consequently, the red Digicons were manufactured with fused silica faceplates. The rapid decline in the QE shortward of 1700 Å is caused by absorption in the faceplate. The rapid decline in the blue Digicon's QE longward of 5000 Å is characteristic of bialkali photocathodes.

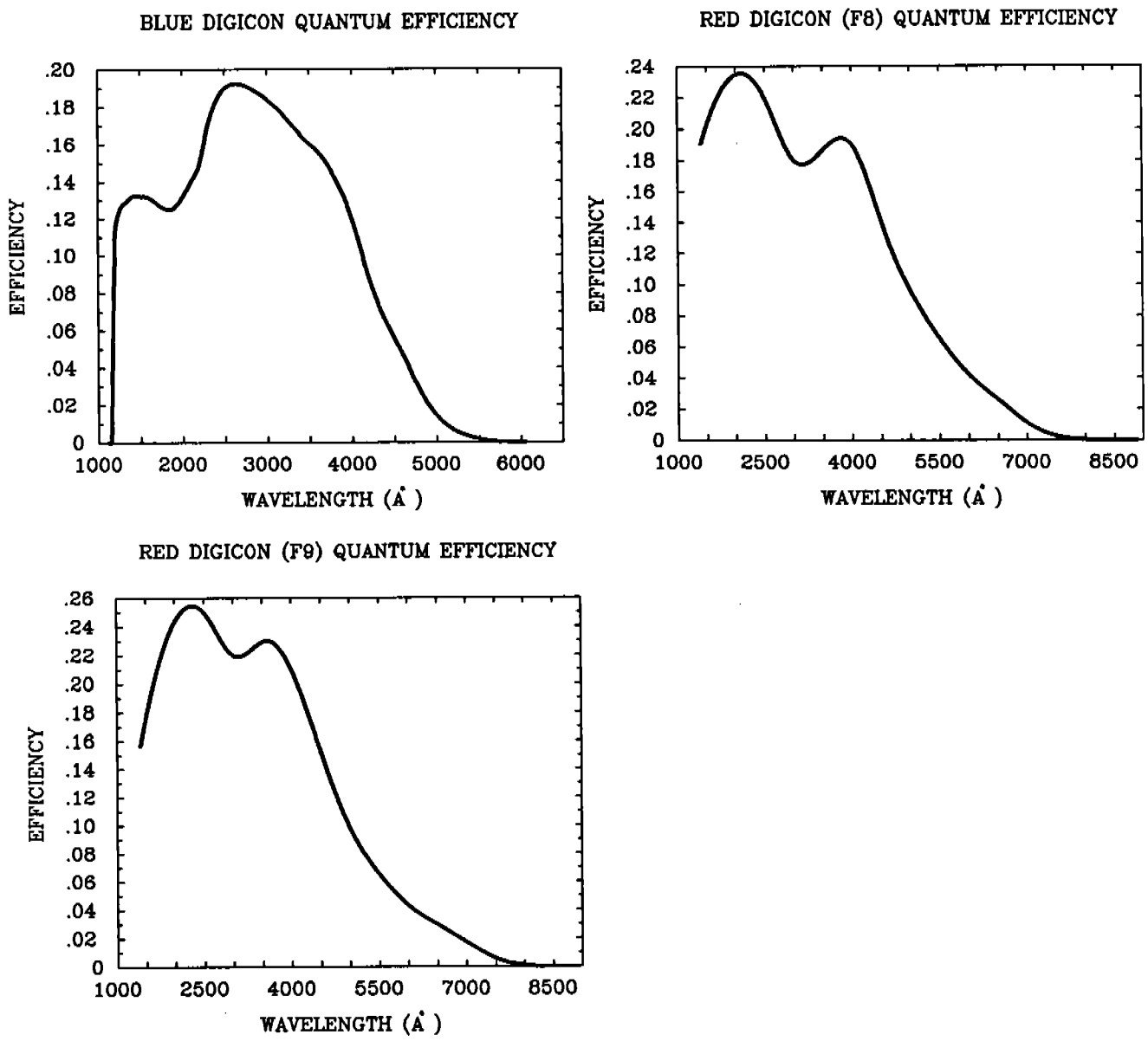

Figure 2.2.4-1 Digicon quantum efficiencies as a function of wavelength (courtesy of Ed Beaver and George Hartig).

If you plan to work shortward of 1700 Å you must use the blue Digicon, and longward of 5000 Å you must use the red Digicon. As a rule of thumb you will want to use the red Digicon longward of 3500 Å because of its better sensitivity. However, there are two additional considerations when selecting a Digicon or Digicons. First, if you are observing a faint UV source in an object with a strong red continuum, the blue tube may be preferable to the red tube in order to reduce scattered red light and the faint ghost images which can arise from high order multiple reflections of red light between the collimator and disperser. The second consideration is that it takes approximately 30 minutes for a Digicon to settle to less than a fraction of a diode spectral stability after having been turned on (but only 5 minutes for approximately one diode stability). Furthermore, one Digicon must be powered down before the other is powered up. Consequently, if your program requires frequent switching to the blue Digicon in order to observe shortward of 1700 Å, you may do better to continue with it for observations below 4000 Å, rather than pay the time penalty to warm up the red tube.

2.3 FOS OBSERVING MODES

2.3.1 Spectrophotometry - (ACCUM mode)

In normal spectrophotometric operation the FOS microprocessor will command data integration for an interval of time (referred to as the step-time) which usually will be 512 msec. At the end of this integration there is a burst-noise rejection option which, if set, causes the microprocessor to sum the counts from the 512 diodes. If the sum exceeds a preset level because of a cosmic ray induced noise burst,the microprocessor will reject the array. Depending on the option chosen (reject or retry), the microprocessor either increments a count of rejected arrays and continues, or keeps retrying until the specified number of integrations have been accepted. At the end of a successful integration the data is summed into 512 memory locations and the Digicon's magnetic deflection is adjusted to shift the electron image by a fraction of a diode (normally 1/4) along the direction of dispersion in order to satisfy the Nyquist theorem. After four such "x-steps" the process is repeated (for subtleties, see section 3.4), resulting in a 2048 data array (plus a few channels from overscanning at the end). After a nominal four minutes of summing into the microprocessor memory (16 bit integer), the data is nondestructively read from the FOS to the SI C&DH computer for telemetry to the ground or storage on the on-board tape recorder.

If your total exposure time is 28 minutes, the last of the 7 readouts contains the sum of all the data. The individual four minute sums can be reconstructed if necessary by differencing the sequential sums. Note that using 1/4-stepping has not caused any loss of signal- to-noise ratio (SNR) relative to not substepping, because you can always rebin the data to 512 channels (if you are willing to undersample the data).

If you choose paired apertures and specify sky subtraction by entering the optional parameter **STEP-PATT=STAR-SKY** on the ST ScI exposure logsheets, the Institute will set up a step pattern which will cause the microprocessor to command deflections (y-steps) back and forth between the two apertures (nominally every 10.24 seconds). When doing sky subtraction, one half the time will be spent on the "star plus sky" aperture and one half on the sky aperture. At the end of the exposure time there will be two 2064 data arrays, one for star plus sky and one for sky.

If you have exceptional requirements you can specify unusual x- steps, y-steps, and minimum integration times for spectrophotometry. However, be advised that unusual x-steps and y-steps may lead to data that cannot be automatically reduced by the Science Operations Ground System.

2.3.2 Spectropolarimetry

The birefringent Wollaston prism splits the incoming beam into a pair of spectra which correspond to orthogonal directions of polarization. In normal spectropolarimetry each of these spectra will be observed once at each of 16 position angles separated by 22.5°. The final data set will thus consist of 32 spectra, each 2064 channels long. If necessary you can rebin the data into low resolution bandpasses during the analysis in order to improve the SNR. When you specify spectropolarimetry by entering the optional parameter **POLSCAN** on the ST ScI exposure logsheets, the Institute will automatically schedule y- deflections (a step pattern) which will alternately deflect the two polarization spectra onto the diode array and step the polarizer through 16 position angles. This default setup is described at the end of section 3.5. If you want a different polarization sequence (*e.g.*, for position angles), you should use the optional parameter STEP-PATT=POL in the exposure logsheet, and then define the desired polarization sequence.

2.3.3 Time Resolved Spectrophotometry - (PERIOD mode)

You can use the time resolved-mode to study objects with known periodicity in the 50 msec to 100 second range. In this mode, the spectra are stored in separate memory locations corresponding to phase, with four to ten bins (the optional parameter **BINS** in the exposure logsheets) per full period being typical. Because the FOS has only 12K words of memory, regular x-stepping and overscanning cannot be used when doing time resolved spectrophotometry with more than 5 bins. The mode can be used synchronously by specifying an absolute start time which will lock the FOS phase to the source phase (assuming you have an up to date source ephemeris). If the source's period is shorter than 200 msec, you should read section 3.7 to understand the relations between integration time (Livetime) and the time required for housekeeping chores (Deadtime) at the end of a Livetime.

2.3.4 Rapid Readout - (RAPID mode)

Rapid readout is suitable for observing aperiodic phenomena or periodic phenomena with poorly established or unknown periods. When using rapid readout the FOS executes a long daisy chain consisting of a short integration, immediate readout, and automatic restart of the next itegration. If all 512 diodes are read out, the shortest practical integration time in the daisy chain is 18 msec, which is partitioned into 10 msec data integrations (Livetime) followed by 8 msec for housekeeping chores (Deadtime). Rapid readout will quickly generate a large volume of data, and requires either the 1-MHz TDRSS downlink, or storage on the on- board tape recorder.

2.3.5 *Time-Tagged Spectrophotometry* - (TAG mode)

The time-tagged mode uses the same daisy chain structure as the rapid readout mode. However, instead of counting photons, each of the 512 accumulators counts ticks from the 1.024 MHz SSM spacecraft clock. The counting in a particular accumulator is stopped when the first photoelectron pulse is detected by its associated diode. After completion of the integration time and housekeeping duties (*e.g.*, data readout), the accumulators are cleared and a new cycle of counting clock pulses begins.

2.4 TARGET ACQUISITION - (ACQ mode)

Centering objects in the small FOS apertures (target acquisition) with no recourse to a "slit-jaw" camera is a demanding task. Consequently, we have provided several independent ways to do target acquisition. The choice between particular modes will depend on the complexity of the field within a $2''$ to $5''$ radius around the object. Because you will know more about this than we, it is up to you to understand the methods of FOS target acquisition and specify which option should be used. *When filling out the exposure logsheets, enter 1 minute for each FOS on-board acquisition, and 10 minutes for real-time acquisitions (FOS imaging and WF/PC-assisted acquisitions.)* More realistic estimates will be made available at a later time.

2.4.1 *FOS Imaging (Interactive and Onboard)*

When using this method for an interactive target acquisition, which is selected by entering the option **INT-MAP=YES** on the exposure log sheet, a camera mirror images the $4.3'' \times 4.3''$ aperture onto the Digicon's photocathode. The Digicon is commanded through a sequence of x-steps and y- steps which "map" the aperture. The data is sent to the ground in real time and is passed through the ground system to the Observer Support System at the ST ScI where a picture of the aperture is constructed and displayed on a television monitor. The picture can be processed in various ways, and should have a spatial resolution of approximately $0.3''$ in x and y. You, the observer, sit at a console where you identify your object in the field (we hope) and mark it with a cursor. The object's position in the field is then used to calculate the offsets which will center the object in a specified aperture. These offsets are uplinked to the HST which then makes a small move to reposition the object to the desired aperture. When you select an interactive target acquisition, you must enter the special requirement "INTeractive ACQuisition FOR" on the exposure logsheet.

FOS imaging is most suitable for target acquisition in moderately crowded fields where there may be several stars in the $4.3'' \times 4.3''$ aperture with nearly the same magnitude. In many cases, such as observations in the core of a globular cluster, the target acquisition probably will be more reliable if you use a WF/PC assisted FOS target acquisition as discussed in section 2.4.4.

There are a couple of reasons why you should plan to use FOS imaging only if other acquisition methods will not work. First, it is the least efficient way to do FOS target acquisition, because 64 integrations are required to map the aperture (compared to 5 or 6 with binary search), and because you must spend time musing over the picture. More importantly, FOS imaging requires a TDRSS up-link, which may not be available more than 20% of the time.

Non interactive FOS imaging can be specified by entering the optional parameter **ONBOARD-TYPE=MAP** on the exposure logsheet. In this case, the target acquisition aperture will be mapped and the data will be sent to the ground at the same time as the science data. This option might be used to take a "picture" of your field before or after your observation in order to verify that the field was correct, or after an onboard target acquisition to verify that the target was properly centered.

2.4.2 FOS Autonomous Target Acquisition - (Onboard)

There are three independent ways of doing FOS autonomous target acquisition. By using an appropriate command sequence (which is not your responsibility), these can be used in combination. For example, a firmware target acquisition could be made on a bright reference star, followed by an offset and peak-up on a faint star.

2.4.2.1 NSSC-1 Binary Search - (**ACQ-TYPE=BINARY**)

The binary search target acquisition is controlled by an FOS program in the NSSC-1 computer. Under program control, the aperture is first mapped with three y-steps, and all stars (within an optional count window) which are $n\sigma$ above sky are identified and ranked. The program then uses an algorithm to control the y-deflection such that the n-th brightest star is driven to the edge of the diode array through a geometrically decreasing sequence of steps which are binary in direction (*i.e.*, either $+y$ or $-y$). The algorithm can handle fields with between 4 and 12 stars, depending on the circumstances, and requires only a few y-steps to drive a star to the edge of the diode array. Offsets are included in the command load which are added to the measured position of the star before being passed to the HST's engineering computer (the SSM) for an HST offset. Thus the object found by the binary search can be centered in a selected aperture or the offset can be to another object. The parameters which you must specify in order to use a binary search are listed in section 3.3.2 *a. Finally, because of the increasing nonlinearity in the true versus measured count rate at rates greater than* $\sim 30,000$ *counts* sec^{-1} *diode*$^{-1}$ *(cf. section 4.7), the binary search will give progressively poorer centering in the direction perpendicular to the dispersion for stars brighter than* $m_V = 15$. The binary search option is selected by entering the optional parameter **ACQ-TYPE=BINARY** on the exposure logsheets. The time required to do a binary search target acquisition will be a weak function of magnitude for stars brighter than $m_V = 18$, and a strong function of the rate at which the NSSC-1 intermediates between the FOS and the HST pointing and control system. As little more than an order of magnitude guess, you should allow approximately three minutes for binary search target acquisition.

2.4.2.2 Firmware Target Acquisition - (**ACQ-TYPE=FIRMWARE**)

The firmware target acquisition program resides in FOS read-only- memory and is controlled by parameters which are set by the NSSC-1 computer. The firmware uses a set of y-deflections to look for a star within a specified count-rate window. If the program finds more than one star in the window, it will terminate the search by setting a "field too crowded" bit. Because of this feature, the firmware target acquisition should be most useful for isolated objects.

The firmware has sophisticated filtering and centering algorithms; consequently, it should find very accurate centers of bright or faint isolated stars. The firmware target acquisition probably will be slower than binary search, but much faster than FOS imaging. In order for the ST ScI to plan a firmware target acquisition, you must specify the brightness of the object being acquired in order for the count rate window to be set properly (*cf.* 3.3.2 *b*). You probably should allow at least three minutes for a firmware target acquisition.

2.4.2.3 Peak-Up/Peak-Down - (**ACQ-TYPE=PEAK-UP OR PEAK-DOWN**)

When using peak-up (or peak-down) the HST is commanded to move through a preloaded step-and-integrate pattern. The time of maximum (or minimum) counts is saved and at the end of the pattern the HST is repositioned to point to the step which gave the maximum (or minimum) number of counts. Peak-up is primarily a back up method which will be used if FOS mechanism problems should eventually make binary search and firmware target acquisition difficult or impossible. It may also be necessary to use peak-up on stars which are too bright for a binary search target acquisition. A combination of peak-up and peak-down will be required to center point sources on the occulting bar of the occulting apertures. The time required for the HST to take a step of less than 1.0" is approximately 7 seconds. Consequently, approximately 11 minutes will be required for HST stepping if you

use the 0.1" aperture to a peak-up in an 0.5" area with 0.05" steps.

2.4.3 Blind Acquisition (Blind Man's Bluff)

Blind acquisition is a blind pointing based on the assumption that the position of your object is accurately known relative to the guide stars used by HST during the observation. Because of the stringent accuracy requirements needed to center objects in the small FOS apertures, we think that you should seldom, if ever, plan to use a blind acquisition.

2.4.4 WF/PC-Assisted FOS Target Acquisition - (Early and Interactive)

Some fields such as the centers of globular clusters will be too complicated for any of the preceding FOS acquistion methods to work. In such cases the WF/PC can be used in two ways to help the FOS acquisition. In the first method a WFC or PC picture is used to derive the $\Delta\alpha$, $\Delta\delta$ of the target relative to an isolated "bright" star. At any subsequent time (provided the old guide stars still work or new ones can be found) FOS acquires the bright star and offsets to the faint star. In the second method a WFC picture is used to measure the WFC x,y coordinates of your object. The known relative positions of the WFC and the FOS are then used to derive the HST offsets relative to the guide stars which will position your object in a selected FOS aperture. The second method can be used either in real time (INTeractive ACQ) or as an early acquisition (**EARLY ACQ**).

The accuracy of the second method will depend on the relative stability of the WFC, the FOS, and the Fine Guidance Sensors. If used in real time the second method most likely will be more accurate than the first; however,the restrictions which are discussed in 3.3.4 make it more difficult to find suitable guide stars for the second method than for the first. A real time acquisition with the WFC also poses the risk of a real time delay while you try to identify your target in a complex field. By sacrificing an as yet undetermined amount

of positional accuracy to thermal-induced changes in relative positions of the instruments, this risk can be avoided by using the second method as an early acquistion for the FOS exposure.

When requesting a WFC picture for an FOS assisted target acquisition you should use an appropriate set of SPECIAL REQUIREMENTS on the ST ScI exposure logsheet to indicate that the picture is an **EARLY ACQ**uisition or an **INT**eractive **ACQ**uisition for your FOS exposure. You should also use a special **BEFORE** requirement with the WFC picture to ensure that the exposure is close enough (two months being the present minimum) to your FOS observation to use the same guide stars. Because HST roll constraints decrease the likelihood of finding suitable guide stars for an early acquisition as the time interval increases, the two month minimum will be relaxed if possible. Consequently, you should use a comment in the exposure logsheet to show the shortest acceptable time between the WFC picture and your FOS observation.

3.0 DETAILED INSTRUMENT DESCRIPTION AND OBSERVING MODES

Instrument Description

The following instrument description is largely drawn from Harms' (1982) discussion of the FOS.

Light enters the FOS through a pair of entrance ports (shown at lower left of Figure 3.0-1) nominally located 60 mm = 215″ off the optical axis of the ST. The center position of the blue side, indirectly measured before launch, is $V2 = 1.438$ inches (130.77″), $V3 = -1.836$ inches (−166.96″), assuming a scale of 90.9384 arcsec inch^{-1}. The inferred position of the red side center is $V2 = 1.885$ inches (171.42″) and $V3 = -1.389$ inches (−126.31″). The light from the object of interest then passes through one of two independent optical channels, each of which focuses nearly stigmatic spectral images on the photocathodes of photon-counting Digicon detectors. These channels differ only in the wavelength sensitivity of their respective detectors. At the HST focal surface is placed the FOS aperture wheel, containing twelve sets of single or paired apertures (including one blank for background measurement) which range in size from 0.1″ to 4.3″ projected onto the sky. The optical beam then passes through the polarization analyzer (which includes a clear aperture position). The grazing incidence mirror, a "roof" prism, deflects the beam 22° upward. The reflection is required in order to allow the apertures to be placed near the HST optical axis to minimize astigmatism, while meeting packaging constraints within the FOS. The deflected beam passes through an order-sorting filter, when required, in the filter-grating wheel. It is collimated by an off-axis paraboloidal mirror and then both dispersed (except for one imaging position) and focused by the selected element on the filter-grating wheel.

FIGURE 3.0-1. Faint Object Spectrograph: dimensions of the axial ST instrument are about 1 x 1 x 2 meters.

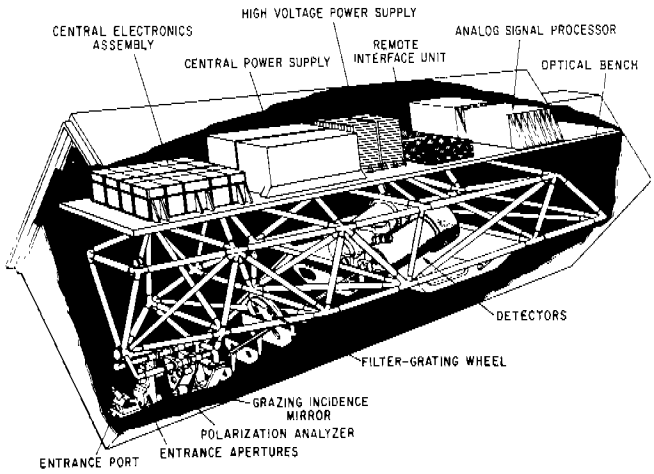

3.1 OPTICS

The design of the FOS optics is dominated by the desire to maximize throughput efficiency while utilizing the part of the HST focal plane as nearly on-axis as possible. The FOS design has eliminated any need to compensate for HST optical distortions, and has reduced to a minimum the number of optical surfaces. For example, a far-ultraviolet photon suffers only 3 reflections in the FOS before reaching a detector (grazing-incidence mirror, collimator, and focusing grating).

The entrance port has only two positions: one to close and one to open the FOS to external light. The port mechanism also contains mirrors which, in the closed position, allow light from the internal spectral calibration lamps to illuminate the entrance apertures for wavelength calibrations.

The entrance aperture mechanism selects one of the twelve aperture sets (in either optical path). Table 2.2.1-1 lists the various aperture choices provided. The largest aperture, $4.3''$ square, usually will be used for target acquisition. The smallest apertures, which are $0.1'' \times 0.1''$, will allow spectroscopy of fine spatial structure (*e.g.*, knots in the M87 jet), while the $1.0'' \times 1.0''$ aperture pair can be used for very accurate spectrophotometry or faint-nebula spectroscopy. Specialized occulting apertures are intended for the study of faint sources surrounding bright objects, particularly nebulosity surrounding quasars.

The FOS polarization analyzer allows positioning of any of three elements into either optical path: a clear aperture, a thin- waveplate (plate "B") plus Wollaston prism assembly, or a thick-waveplate (plate "A") plus Wollaston prism assembly. One waveplate is permanently located in front of each Wollaston. The polarimeter is designed so that only a single motor is required to rotate the waveplates and to move either of the Wollaston-waveplate pairs from one entrance port to the other or out of the way. A drum, which is only 1.9 inches in diameter, contains the two Wollaston-waveplate pairs. The Wollastons are permanently fixed to the drum, but the waveplates are mounted in rotatable cylinders inside the drum. The waveplate cylinders have a 16-tooth gear on the outside which meshes with a 17-tooth fixed center gear inside the drum. One revolution of the drum rotates the Wollastons by 360°. The waveplates, however, rotate 382.5°. Each rotation of the drum thus increments the position angle of the waveplate fast axis by a net 22.5°. Sixteen rotations of the drum bring the mechanism back to its original configuration. Figure 3.1-1 is a photograph of the flight polarizer mechanism.

The filter-grating wheel photographed in Figure 3.1-2 (still with dummy optical elements), allows selection from ten positions in each optical path. Table 2.2.3-1 presents the dispersion selections available, and lists the order separation filters used with five of the dispersers.

A considerable challenge in the FOS design was the requirement to maintain positional tolerances (initial alignment and stability) in the tens of micrometers for an optical structure over a meter long. Not surprisingly, the FOS optical bench is made of graphite-epoxy. However, as a photograph of the bench (Figure 3.1-3) and a photograph of its joints (Figure 3.1-4) make clear, the geometry is complex. The design selected uses pre-welded invar joints into which are inserted the graphite-epoxy tubes, all designed for near-zero thermal expansion coefficient at the optical compartment operating temperature of 20° C.

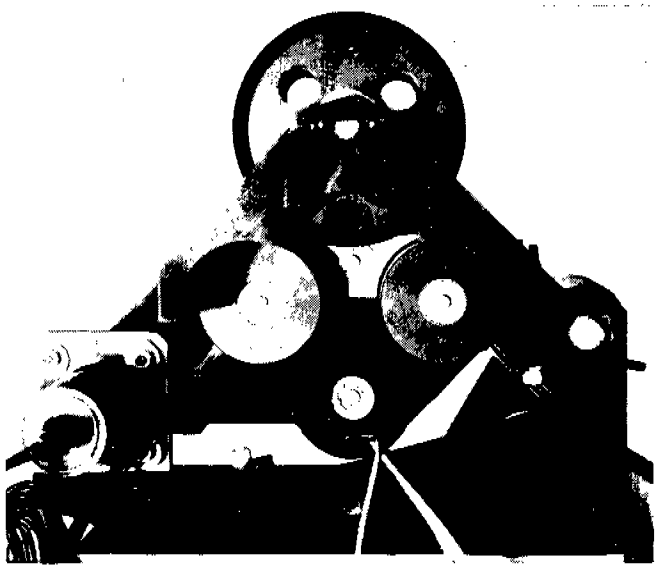

Figure 3.1-1. FOS Polarizer Analyzer. The upper rotating barrel is about 5 cm diameter.

3.2 DETECTORS

There are two independent assemblies, one for each optical channel. Each detector assembly consists of a Digicon tube (described in Harms *et al.* (1979) and references therein), deflection coils, a permanent magnet focus assembly, magnetic shielding, mounting and alignment structure, heat pipes, temperature sensors, hybrid preamplifiers, and connectors.

The two Digicon detector assemblies, designated "red" and "blue", differ only in their photocathode and faceplate materials. The blue detector has a bialkali photocathode (Na_2KSb) deposited on a magnesium fluoride window to cover the wavelength region 1150 Å $< \lambda <$ 5000 Å. The photocathode of the red detector, trialkali $Na_2KSb(Cs)$ deposited on fused silica, provides an extension of sensitivity to the red, covering the range 1700 Å$< \lambda <$ 8500 Å. To reduce dark background to the extremely low values required for FOS scientific programs ($<$ .002 counts sec^{-1} diode^{-1}), the detectors are cooled to the temperature range $-10°$ C to $-28°$ C by means of attached heat pipes.

The Digicons operate by accelerating (to 18-25 KeV) photoelectrons emitted by the transmissive photocathode onto a linear array of 512 silicon diodes. Figure 3.2-1 shows a photograph of a (reject) diode array mounted onto its 5 cm diameter ceramic header containing 520 vacuum-tight electrical feedthroughs. The charge pulse generated in each diode is amplified and counted by one of 512 independent electronic channels, beginning with the hybrid preamplifiers physically colocated with each Digicon. Figures 3.2-2 and 3.2-3 are photographs of one of the two flight detectors, showing the overall detector assembly and the preamplifiers at the aft end.

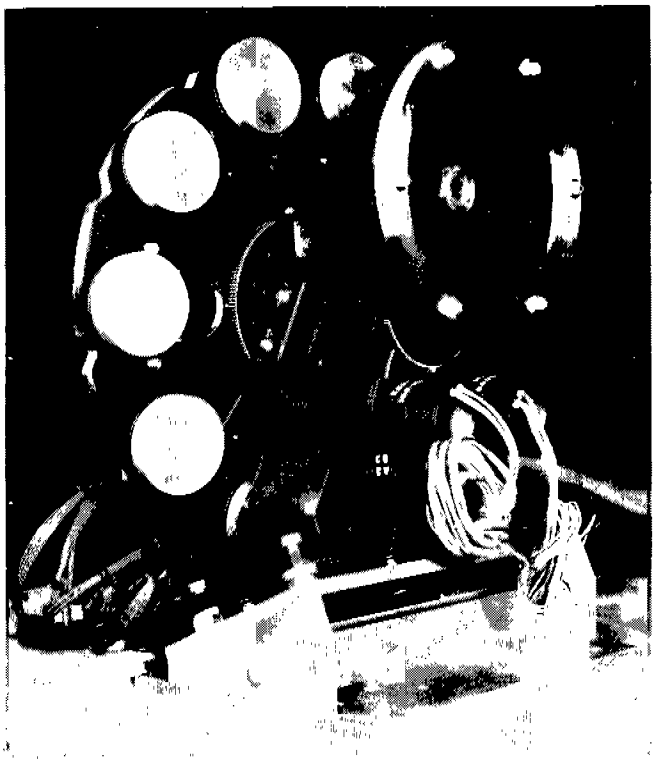

FIGURE 3.1-2 (upper left). FOS Filter/Grating Wheel. The outer ring of aluminum caps are disperser locations and the inner ring of holes are filter locations.

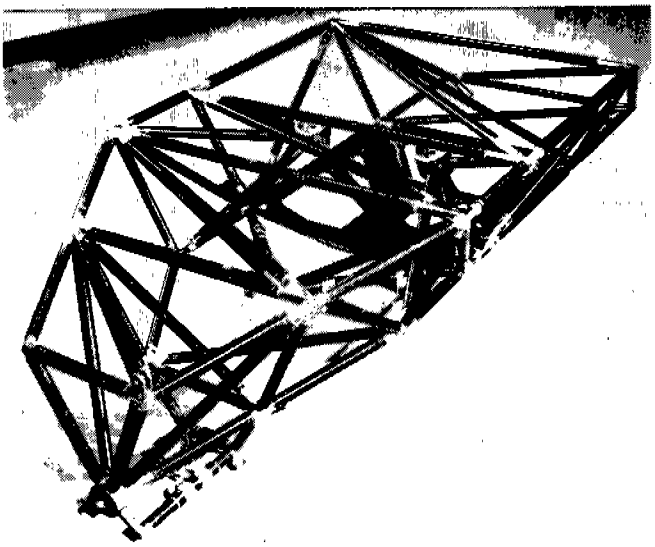

FIGURE 3.1-3. FOS Optical Bench. The bench is over one meter long and constructed of invar joints and graphite-epoxy tubes.

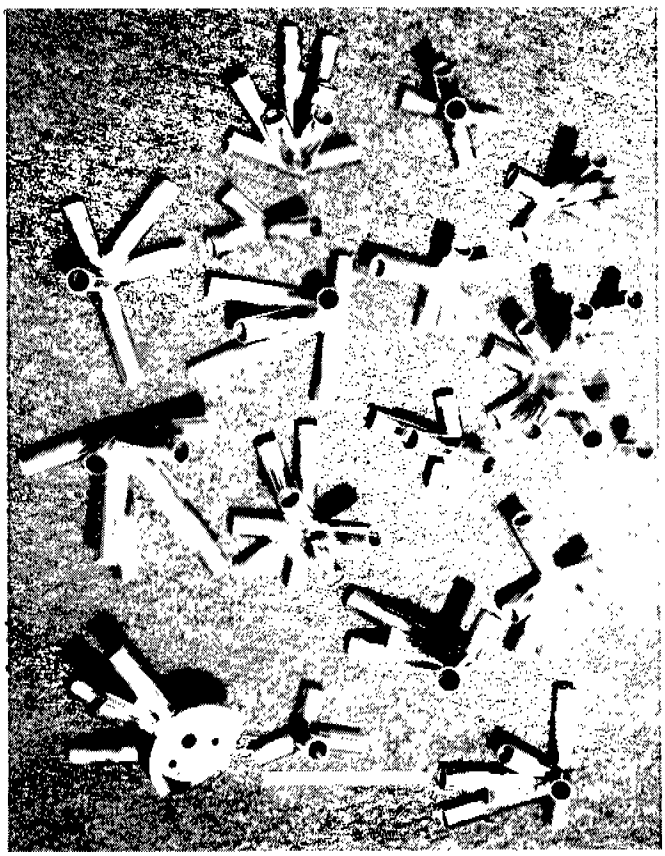

FIGURE 3.1-4. Optical Bench Invar Joints. Note geometrical complexity leading to choice of welded joint structure.

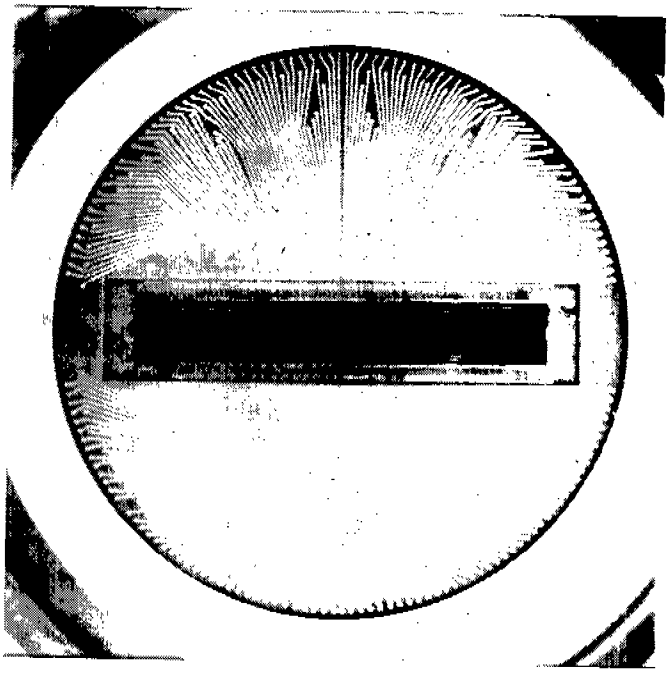

FIGURE 3.2-1. Digicon Array on Ceramic Header. The 512-element array is about 2.5 cm long. The 5 cm diameter header contains 520 vacuum feedthroughs.

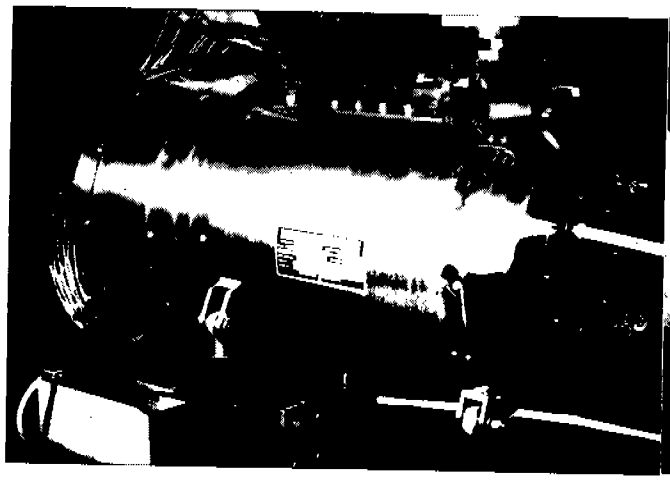

FIGURE 3.2-2. Red Flight Detector. Preamplifiers. The 512 preamps fit into back end of detector assembly. Each set consumes less than 10 watts.

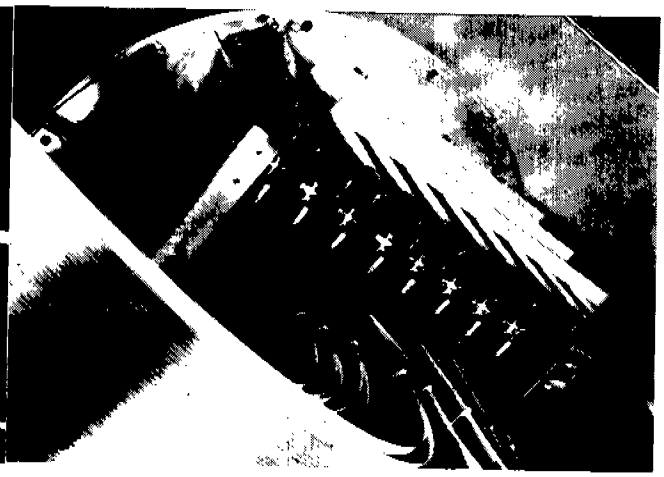

FIGURE 3.2-3. Detector Hybrid

Because so many FOS parameters can be set by using uplinked commands, the possible number of observing configurations is truly astronomical. However, in terms of intended use, the FOS performs one of six basic functions: 1) target acquisition, 2) spectroscopy, 3) spectropolarimetry, 4) time-resolved, 5) rapid- readout, and 6) time-tagged. Each offers the observer unique advantages (and limitations) for specific purposes.

3.3 TARGET ACQUISITIONS

As you might suspect, acquiring an extremely faint object with a one-dimensional detector in a viewing field of maximum size $4.3''$ square and then centering the object in an aperture as small as $0.1''$ is a nontrivial task. To quantify the difficulty, if we require a 95% probability ($\pm 2\sigma$) for placing a star in an aperture with a diameter d'', the sum of the pointing errors and relative positional errors must be less than $d''/4$. Because FOS observations will typically be made with a $0.5''$ aperture, and occasionally with $0.25''$ and $0.1''$ apertures, the positional tolerances are quite stringent. If we add an additional criterion that the star must be centered well enough to avoid vignetting, the positional tolerance becomes even tighter.

There are three generic ways to do FOS target acquisition.

3.3.1 FOS Imaging Target Acquisition - (Interactive and Onboard)

When using the FOS to make a target acquistion image the $4.3'' \times 4.3''$ aperture and the camera mirror are selected for the side (red or blue) you have chosen. The FOS is then commanded to "map" the aperture by taking a sequence of x-stepped integrations (nominal x-steps = 4) at different y-deflections. Normally the 614μ square image of the aperture will be mapped with 12.5μ steps in the y-direction. The sequential target acquisition integrations will be down linked through a TDRSS satellite and sent to the Observer Support System at the ST ScI. There the integrations are "stacked" and displayed as a "picture". Because the diodes in the Digicon detectors are 200μ high ($1.4''$), all stellar images will be $1.4''$ long in the y-direction. You have the option of sharpening the resolution in the x-direction by multiplying the picture by a psuedo-inverse x-restoration matrix (nominally 48×51). The y-elongation can be removed by multiplying the picture by a pseudo-inverse y- restoration matrix (nominally 48×63). You then mark your object with a cursor and its measured centroid is used to generate the offset commands which should center the target in a preselected FOS aperture. These commands are uplinked to the HST which then repoints. After (or during) the move the FOS is reconfigured to your desired setup and the observation begins after the SSM computer sends the appropriate flag to the NSSC-1 computer.

Note that to use the imaging mode for target acquisition you must be at the ST ScI, and it must be possible to schedule the TDRSS contact in order to get the data down and the offset commands back to the HST. You should also consider that this is the least efficient target acquisition mode, because the entire aperture must be mapped.

3.3.2 FOS Autonomous Target Acquisition - (Onboard)

FOS autonomous target acquisition is a scheme wherein the FOS, the NSSC-1 on board computer, and the HST act together to find and center a target. In reality, there are three independent ways of doing this.

a) NSSC-1 Binary Search

In principle, the binary search should give the fastest target acquisition. The binary search program begins by mapping the $4.3'' \times 4.3''$ aperture with three y-scans. The mean sky level is calculated at each y-step, and all peaks more than $n\sigma_{sky}$ (nominally $n = 3$) above the mean sky level and within the count window are noted. The program next uses a binary search pattern to deflect the image of the designated nth brightest peak onto the edge of the diode array. The derived Digicon x and y image coordinates are then converted to scaled microns and transformed into the ΔV_2, ΔV_3 offset which will center the object in the $4.3'' \times 4.3''$ aperture.

The processor includes an extraction of a ΔV_2, ΔV_3 from the command sequence. This ΔV_2, ΔV_3 will be the sum of the offset required to select a particular science aperture, and the offset required to move to a faint target if the peak-up was on a bright reference star. This ΔV_2, ΔV_3 will be added to the ΔV_2, ΔV_3 derived from the binary search. As an observer you need not be concerned with the telescope's V_2, V_3 coordinate system, which is fixed relative to the FOS focal plane. However, if you are peaking-up on a bright star and then offsetting to a faint object, you must bear in mind the relative positional accuracy of the bright and faint object which is required to drop the faint object into a small aperture.

In order to use binary search target acquisition, you must specify the following parameters:

1. Designation that the first star found is the target (*e.g.*, a bright offset star, or repeat visit), or that the first, second, or third brightest star is the target.
2. As an option, the approximate colors and magnitudes of the stars which you expect to be in the $4.3'' \times 4.3''$ acquisition field. These will be used to estimate a count rate window in which the target should be found. Although an acquisition can be made without setting a count rate window, succesful target acquisition in complex fields may require using a count rate window. As an example, the window could be used to exclude a large number of faint stars near a "bright" target.
3. Science aperture that will be used.
4. $\Delta\alpha$, $\Delta\delta$ for a blind offset if appropriate.

If the program fails to find a target, one of three events will occur:

1. If there is no scheduled OSS contact and no preplanned branch, the program will either stop the FOS data acquisition until the allocated time expires, or command a $4.3''$ move and try again. The latter option most likely will not be available until the telescope/target-acquisition performance is well understood.
2. If there is a scheduled OSS contact, the program will inform OSS that target acquisition failed and wait for the observer to make a decision.
3. If there is a preplanned branch, it will be executed.

b) Firmware Target Acquisition

The firmware target acquisition will work best for isolated objects. It will measure very accurate positions, and probably will take longer to do an acquisition than the more flexible NSSC-1 binary search. The firmware looks for an object within a specified count window. If the firmware finds more than one object within the window, it gives up in confusion, (this is after all, a firmware program, and is not meant to do pattern recognition). If the firmware does not find any objects in the window, an FOS processor in the NSSC-1 will respectively raise and lower the upper and lower windows, and command a retry.

The only parameters you must specify are the color ($B-V$; or, spectral index α), color excess $E(B-V)$, and magnitude of the target. These will be used by the ST ScI to estimate the count rate window settings, N_{min} and N_{max}. If your object is bright and the field is clean, the windows will be set far apart; otherwise, considerable care must be used.

If you wish to know even more about FOS firmware target acquisition, read on; otherwise, please skip to section *c*.

The firmware maps the FOS $4.3'' \times 4.3''$ target acquisition aperture with m y-steps, using x-stepping and overscan at each y-step. The nominal values for x-steps and overscan will be respectively 4 and 5. Although the target acquisition aperture images onto 12 diodes (the scale is 140 microns-arcsec^{-1} and each diode is $50\mu \times 200\mu$), the firmware will process the data from 20 diodes. Consequently, the nominal dimensions of the target acquisition data array will be $m \times (24 \times 4) = m \times 96$. There are 12K words of FOS microprocessor RAM which can be used for target acquisition, which allows us to command up to 120 y- steps, where each step of the 200μ-tall diodes is 5μ ($0.036''$). The firmware can be commanded to take any combination of y-steps, x-steps (*e.g.*, 1/8 steps), and overscan as long as the data will fit into the 12K bytes of memory.

The firmware processor includes an option to filter the data array before looking for peaks (stars) in the "picture". The default x-filtering filters the data array row-by-row with a 5 point isosceles triangle. The default y-filtering filters the data column-by-column with a 7 point piece-wise parabolic smoothing function. Graphically, the function looks like a saw tooth composed of an upright and an inverted isosceles triangle. The x-filter width should be odd with $2n-1$ points, and the y-filter width should be odd with $4n-1$ points. Zero values at the end points are not counted. The filter widths are specified by two serial magnitude commands YXFILWID and YYFILWID.

The objective of the y-filtering is to mark the edge of the diode with a feature which can be accurately centered. If the diodes have a sharp response function at the y-edges, the response to stepping the y-edge across a star will be a step function in the data. The convolution of the filter with a step function gives a piece-wise parabola. Consequently, the two edges of a diode will be marked with parabolas, positive at one end and negative at the other end.

The low pass filtering in x and y will reduce the amplitude of the peaks. The firmware processor has been written such that the data is renormalized after filtering in order to preserve intensity. Because of this care must be used when specifying the data window in which the peak (star) is to be found.

When the "fix bit" is set the firmware corrects for dead diodes and frames which were rejected because a burst-noise-rejection preset count was exceeded. Fixing the data significantly increases the processing time.

If we want to uplink filter functions which are different than those already described, YFILL and XFILL are set in order to suppress automatic filling of the filter function tables. If the double buffer bit is set, the 12K of memory will be partitioned and the filtered data will be written into the second half of the memory. If the double buffer bit is not set the filtered data will be written over the unfiltered data. Either filtered or unfiltered data can be read to the NSSC-1.

Note that the y-position is that of the upper edge, center, or lower edge, according to how the target acquisition is specified. If using an edge, the Y-BASE value returned to the NSSC-1 is in "Base units", and is the value which would drive the image to the upper edge of the diode (or center, or lower edge, as the case may be). Appropriate offsets must be applied to the y-position in the NSSC-1.

The processor looks line by line for peaks in the data array which fall within a commandable window. When a peak is found within the window two parameters, XSKIRT and YSKIRT, are used to see if the peak is a relative maximum. This is accomplished by looking at neighboring peaks out to the distance specified by XSKIRT and YSKIRT. If these parameters have their default values of 1, the 8 nearest points are examined. If a peak is in the window and is a relative maximum, the processor computes its x and y centroid by fitting an isosceles triangle to the peak's x-position and two nearest x-neighbors, and another triangle to the y-position and two nearest y-neighbors.

At the first occurrence of a peak in the window the processor increments the diagnostic "COUNT" to one. If a second peak is found the processor uses two parameters to decide if the new peak is part of the same stellar image or a new star. For unfiltered data the parameters are XPCLOSE and YPCLOSE with respective default values of 32 (one diode width) and 256 (one diode height).

If the new peak is within XPCLOSE and YPCLOSE of the last peak, count is incremented and the new x and y centroids are averaged with the previous values. If the data has been filtered, the parameters are XPCLOSE and YPCLOSE with respective default values of 32 and 64. If the new peak is not part of the previous image the processor sets the "crowded field" bit and quits. In this case the the x and y positions of the new peak are not averaged into the previous x and y positions.

c) FOS Peak-Up/Peak-Down

When executing a Peak-up/Peak-down target acquisition the NSSC-1 computer sets parameters or flags which cause the SSM computer to command the HST to step through a preloaded spatial pattern of dwell scans. After the SSM has commanded a small move and the HST has settled, the SSM sets global event flag #2. The NSSC-1 processor picks up this flag and initiates an FOS integration. The completed scan is summed over a specified number of diodes and the sum is saved. The processor records and updates the starting time of the integration which gives either the maximum number of counts (star centered in aperture) or the minimum number of counts (star centered on occulting bar). After the HST has stepped through the scan pattern the NSSC-1 computer returns the time of the

maximum or minimum sum to the SSM engineering computer. The SSM then repoints the HST to the position which gave the maximum or minimum sum.

The observer must specify:

1. The magnitude, color, and reddening $E(B-V)$ of your object, so the ST ScI can estimate the exposure time required for target acquisition.
2. The science aperture that will be used during the observation.
3. The estimated uncertainty in the position of your object, so we know how large an area must be searched.
4. Whether you want a peak-up or a peak-down.

3.3.3 FOS Blind Acquisition

Blind acquisition is a blind pointing based on the assumption that the position of your object is accurately known relative to the guide stars used by HST during the observation. Because of the previously stated stringent accuracy requirements, we expect blind acquisition to be used only for revisits to targets whose centered positions are already accurately known relative to the guide stars. Based on discussions with Barry Lasker, it is my opinion that you should seldom, if ever, plan to use blind acquisition on a first pointing at an HST target.

3.3.4 WF/PC-Assisted FOS Target Acquisition - (Early and Interactive)

Some fields such as the centers of globular clusters or active galaxies may be too complex for an FOS target acquisition. In such cases there are at least two ways you can use WF/PC pictures for your FOS target acquisition. The first way is to take a WFC or PC picture and then measure the x,y position of your target in the picture relative to an isolated star. The x,y coordinates can then be converted to $\Delta\alpha$, $\Delta\delta$. Subsequently, an offset to your target can be made after an FOS target acquisition on the bright star.

When the HST repoints from the offset star to the target, the FGSs must also move within the FGS fields of view (refered to as a "pickle;" *cf.* the HST focal plane layout in *The Call for Proposals*). If one of the guide stars happens to be too close to the edge of the pickle, the offset might move the star outside the pickle, in which case the offset could not be made. As a rule of thumb, the smaller the distance between the offset star and the target, the more likely it is that two suitable guide stars can be found.

Because the accuracy of the derived relative positions, $\Delta\alpha$, $\Delta\delta$, is not strongly dependent on the accuracy of the HST guide star positions, the first procedure does not require that the FOS observations be made with the same guide stars. Consequently, there are fewer restrictions on when the observations must be made (in order to find suitable guide stars) and the time interval between the WF/PC observations and the FOS observation than if the second method is chosen.

In order to understand the restrictions imposed by the second method, as you read the following please refer to the diagram of the HST focal plane layout, which can be found in *The Call for Proposals*. The second method requires finding two guide stars (one in each of two FGS "pickles") which can be accessed by the FGSs both when the HST is pointed to position the target on the WFC and when the HST is subsequently repositioned to place the target in one of the FOS apertures. If two such guide stars can be found, the acquistion is accomplished by measuring the x,y position of the target in the WFC picture and then relying on the ST ScI to use the known position of the FOS apertures relative to the WFC to calculate the pointing commands which will position the target in the selected FOS aperture. In principle this procedure will position your target to within a few milliarcseconds of the FOS aperture center. It is clear from the HST focal plane layout that the probability of finding suitable guide stars will be maximized if the target is near the $+V2$, $-V3$ edge of WFC CCD chip No.4 when using the red side of the FOS, and near the $+V2$, $-V3$ edge of WFC CCD chip No. 3 when using the blue side of the FOS. If your target is transitory (*e.g.*, a faint supernova), this procedure can be done in real time; otherwise, the FOS observations should be made within a few days (to prevent the guide stars from rolling out of the "pickles";the roll rate, which is set by the necessity to maximally illuminate the solar panels, obviously depends on the target's ecliptic latitude) after you have had time to confidently find and measure the position of your object in the WFC picture. You should be aware that the optical distortion in the WFC pictures can be as large as one pixel at the edges of the CCD chips. Consequently, the measured x,y coordinates must be corrected for this distortion before using the smallest FOS apertures.

If you plan to use a WF/PC assisted FOS target acquisition, when filling out the forms you should specify that the picture will be used for a target acquisition. If you are in doubt about where your object should be positioned in the WFC target acquistion picture, you can let the ST ScI decide where to place the target.

3.4 SPECTROPHOTOMETRY

The FOS probably will be used most commonly for spectrophotometry. Any one of the eleven possible apertures (Table 2.2.1-1 and Figure 2.2.1-1) can be used with any of nine dispersers (Table 2.2.3-1). Spectra of the FOS Pt-Ne-Cr lamps for the different FOS dispersers can be found in the Appendix A. The minimum data integration time (live time) can be as short as 3 msec; however, because approximately 20 msec are needed by the microprocessor at the end of each data integration for housekeeping chores (dead time), the integration time usually will be 512 msec. For a typical observation, lasting a few minutes to a few hours, the 512 msec integrations are internally summed in the FOS in software selectable intervals (now planned to be four minutes) between each readout to the ground or ST tape recorders. The frequent readouts result in negligible loss of observing efficiency and protect against catastrophic losses of data.

The following definitions (taken from FOS-UCSD-SE01C) will acquaint the most curious of readers with the details of data acquisition during spectrophotometry. The first four are the most important for understanding what happens during an integration. Most observers need not be concerned with this level of detail.

The order of operations in the FOS microprocessor are, from the innermost logic level to the outermost:

INTS —The number of repetitions of the livetime/deadtime cycle, whereby electrons are counted in the selected (normally, but not necessarily 512) diode accumulators with no changes in magnetic deflection. If "burst noise rejection" is enabled, the sum of the counts is examined at each closing of the accumulators before being transferred to an array of memory locations. A value greater than the commandable "reject limit", if enabled, will cause the data to be rejected as burst noise. The FOS microprocessor keeps track of the number of rejected integrations in a rejection array which is indexed by x-step, overscan, y-step, and slice (*cf.* the following definitions). The accumulator livetime is constrained by the hardware to be no larger than 512 msec; INTS provide a means for increasing the amount of time data is collected at a given deflection value while keeping livetime short so that as little good data as possible is rejected along with noisy data. The minimum livetime is normally constrained by the firmware to be greater than 10 msec, although this too can be circumvented (*cf.* section 3.6 for a detailed discussion of livetime). The number of integrations performed, with diode outputs added into the same memory locations each time, is determined by the parameter INTS. Subsequent data will go into other array locations.

X-STEPS (also widely called SUBSTEPS) —*X*-steps are magnetic field deflections of the electrons in the dispersion (x) direction. The default value for X-STEP is 4, the so-called "quarter stepping" that will place the electrons on the next diode after 4 steps. X-STEP = 8 would be "one eighth stepping," *etc.*: after X-STEP steps, the electrons reach the corresponding spot on the next diode. The data go into new memory locations with each X-STEP. The reason for x-stepping is to satisfy the Nyquist sampling criterion, which requires X-STEP ≥ 2.

OVERSCAN —The overscan parameter indicates the number of times to repeat the addition of counts into the memory array, with an offset of one memory location at each overscan. Each offset is accompanied by a corresponding magnetic deflection in the x-direction so that data from a photocathode location falls into the same memory location independent of the diode which sampled it. OVRSCN = 5 (which is the default) with X-STEP = 4 would result in each diode being read 4 times in each of 5 sets of reads. This increases the spectrum from X-STEP × 512 points to X-STEP × 512 + X-STEP × (OVRSCN -1). The purpose is to average out the response of different diodes, including dead ones.

Y-STEPS —A y-step is magnetic deflection of electrons at right angles to the dispersion direction. The value, YBASE, is set at the beginning of an observation and is the base for the entire y-deflection sequence, ending after a number (Y-STEPS-1) of deflection increments. The purposes of y-stepping include mapping the photocathode and switching between the two spectra from the polarizer or paired apertures.

SLICES —A single slice consists of an entire deflection sequence. A deflection sequence can be repeated up to SLICES number of times; the data from each repetition goes into a new set of memory locations. Slices can be used for time-resolved spectroscopy or as a means to accumulate more than 64,000 counts per step when observing a bright object.

PATTERN —A pattern is a completed series of slices; all memory locations allocated for the science data array (and the reject array, if applicable) are filled after completeion of the first pattern. Counts in subsequent patterns will be added to the coresponding previous values in the science data array. A typical pattern repetition rate might be on the order of a few seconds.

READOUT —A readout consists of sending the science data to the NSSC-1 computer for either storage on the tape recorder or telemetry to the ground. Readouts are non-destructive, and typically will be performed at regular intervals (nominally four minutes) without memory clears in order to protect against loss of data. The last readout contains all the data accumulated since the previous memory clear.

MEMORY CLEAR —A memory clear zeroes all locations in the science data array to allow input of new data. Memory clear is repeated YCLEARS times in a given observation.

ACQUISITION —An acquisition is the initiation of data taking with a specified set of parameters. If any parameters are changed, a new acquisition must be initiated. There may be several acquisitions on a given object; an acquisition probably will be terminated when the object is eclipsed by the Earth.

3.4.1 Nominal Observational Philosophy

Following are the steps involved in choosing parameters for a non-time resolved observation. These steps will differ somewhat for various types of observing modes, but the general ideas embodied herein may be applicable. Ordinarily the ST ScI set of default parameters will be suitable for your observations; only in unusual cases will it be necessary for you to specify parameters by the following prescription.

1. Choose an instrument set-up consistent with your desired science: select X-STEPS, OVERSCAN, etc. through SLICES.
2. Consider the expected count rate for a given target, and the desirability of not overflowing memory (2^{16} counts): choose how often readouts, memory clears and acquisition should occur in terms of time, taking into account the total desired observing time.
3. Juggle the remaining free parameters; live and dead times, INTS, and PATTERNS/READOUT, to be consistent with instrument capabilities and the following considerations:

   The time between readouts, TRO, is given by

   TRO = (LT + DT) × INTS × [X-STEPS × OVERSCAN × Y-STEPS × SLICES] × PATTERNS

a) When choosing livetimes and deadtimes (LT, DT) a compromise must be made between a high duty cycle (LT/(LT + DT)) and loss of efficiency due to rejection of the integration by the burst-noise rejection firmware program (*cf.* 4.3). If the cosmic ray induced background is low, choose a relatively long (default 512 msec) livetime in order to keep the duty cycle high. If the background is high choose LT as short as possible, remembering that the dead time can be as long as 18 ms (*cf.* Table 3.6-1).

b) Leaving INTS = 1, make PATTERNS/READOUT as large as necessary; if TRO is still too short, boost INTS. If this does not make TRO sufficiently long, adjust LT.

3.5 SPECTROPOLARIMETRY

The technique used for spectropolarimetry in the FOS is very similar to that developed for ground-based instruments. A polarizing prism of birefringent material (MgF_2) is introduced into the spectrophotometer, so as to form twin dispersed images of the slit in opposite senses of polarization at the detector. The analyzer is held in a fixed position behind a waveplate which is turned in 22.5° intervals to analyze for linear and circular polarization. In this way the polarization effects in the dispersing optics following the analyzing prism are of no consequence, and have no effect on the accuracy of the measurement. Two separate waveplates of differing retardation are included in order to allow measurement of linear and circular polarization throughout the ultraviolet region; the properties of the waveplates are such that the polarizer also can be used in the optical spectral region. Any spectral element can be used with either polarizer waveplate.

The sensitivity of the polarizer depends both upon its throughput efficiency and its modulation efficiency (refer to Allen and Angel's paper reproduced in the Appendix for a detailed discussion of the FOS polarizer). The transmission efficiency of the complete polarizer rises from about 20% at Lyα to around 60% at 1600 Å and thence rises more slowly to just over 80% at 2400 Å. Because, at any given time, the detector can observe only one of the two spectra produced by the polarizer, another factor of two loss in practical throughput occurs. Modulation efficiencies for each of the two waveplates are given in Table 2.2.2-1. Note that the polarizer is sensitive to both linear and circular polarization over nearly the entire wavelength range of the FOS. Table 3.5-1 tabulates the achievable accuracies in 100 Å bandpasses for a 14.4 magnitude A0 star for ultraviolet polarimetry in a 20 minute exposure.

When you enter the optional parameter **STEP-PATT=POLSCAN** on the ST ScI exposure logsheets, the Institute will automatically schedule a polarization sequence as follows. After the selected digicon is powered-up, the selected disperser is in place, and one of the circular apertures (typically the 0.3 or 0.5 aperture) has moved into position, the polarimeter will be commanded to the clear position. The polarimeter will then be commanded to rotate clockwise to the first position angle of the selected waveplate. A step pattern will be used such that first there will be a TBS minute integration on the lower spectrum and then after a y-step a TBS minute integration on the upper spectrum. At the end of the second integration 15 seconds will be required to move the polarizer through 22.5° to the next polarization position. This procedure will be repeated 16 times, requiring 4 + 32 TBS minutes of time and giving 32 TBS minutes of integration, where TBS is the exposure time which you enter in the exposure logsheet. At the end of this time you will have 16 pairs of spectra. If you need to use either another grating and/or the second waveplate, the process will be repeated, requiring another 4 + 32 TBS minutes of time. The rms accuracy of the measured linear polarization and the accuracy of the direction of the electric vector is given in Table 3.5-2 as a function of the maximum counts per spectral bin (the spectral interval over which you choose to bin the data) achieved during an integration on one of the two spectra at one of the polarizer positions.

TABLE 3.5-1
Polarization Accuracy for A0 Star, $V = 14.4$, Exposure Time = 20 Minutes

Å	% Accuracy For	
	Linear*	Circular**
1216	6.4	5.8
1500	1.9	1.5
2000	0.89	0.74
2500	0.66	0.54
3000	0.63	0.58

* Standard deviation in Stokes parameter ratios Q/I and U/I
** Standard deviation in Stokes parameter V

Spectropolarimetric observations can be made while using the time resolved mode or the rapid readout mode. Because such observations will require unusual command loads, you should discuss the observations with STScI personnel before submitting your proposal. You should also be aware that such data will not be reduced automatically by the Institute's "pipeline" software.

Table 3.5-2
Polarimetric Errors as a Function of Maximum Observed Counts

Maximum Counts per Spectral Bin	Intrinsic Source Polarization (%)	RMS Error in Linear Polarization (%)	RMS Error in $\theta(^\circ)$
$\approx 5,000$	10	0.5	1.4
$\approx 5,000$	1	0.5	14.3
≈ 500	10	1.6	4.5
≈ 500	1	1.6	45
≈ 50	10	5	14.3
≈ 50	1	5	143

3.6 TIME RESOLVED SPECTROPHOTOMETRY

The time-resolved mode will be used to study objects with known periodicity in about the 50 msec to 100 second range. In this mode, the data is stored in separate memory locations (bins) corresponding to phase, with four to ten bins per full period being typical. Interruptions of data acquisition to read out a completed pattern to the NSSC-1 computer (typically at four minute intervals) are set by commands either to last an integral number of periods or to precede a series of synchronous starts, so that the correspondence between phase and bin is the same in each pattern (so long as the period is correctly known!). Thus, all information should be contained in the readout of the last pattern (assuming no memory clears after the intermediate readouts). Finally, there exist synchronous and asynchronous submodes; these differ only as to whether or not the initial phase angle is explicitly locked to the source at the start of the observation (by commanding the start to occur at a specified Universal Time).

Table 3.6-1
Minimum FOS Livetimes and Deadtimes

Retry Mode

Precision	N(diodes)	DT(msec)	DT+LT(msec)
DPA	512	18	28
SPA	512	12	23
NA	512	8	18
DPA	8	8	12
SPA	8	8	12
NA	8	8	12

Reject Mode

DPA	512	10	30
SPA	512	10	25
NA	512	10	20
DPA	8	10	15
SPA	8	10	15
NA	8	10	15

The limitations on time resolution are set by two internal FOS time intervals, the livetime (LT) and the deadtime (DT). The livetime is the most fundamental unit of integration time, and is the time interval between opening and closing the 512 accumulators. The shortest possible LT is approximately 3 msec, and is set by the time required for the microprocessor to service the accumulator open and accumulator close interrupts. Each LT is followed by a dead time, which is the time required for housekeeping chores such

as summing the accumulators for a burst- noise rejection test and "overlight" safety test, adding the data into FOS memory, and clearing the accumulators for the next integration. As a rule of thumb LT + DT must be greater than 30 msec, and DT = 20 msec.

Table 3.6-1 gives the shortest possible times as a function of processing parameters and functions, which are N(diodes), the number of diodes which will be processed, double precision addition (DPA) for burst-noise rejection and maximum bright light protection, single precision addition (SPA), adder disabled (NA), and either retry or reject for burst-noise rejection. Single precision addition is sufficient for burst-noise rejection, but, because of the possibility of overflow and digital wrap around from accidental observation of a damagingly bright light, SPA gives considerably less bright light protection than DPA.

The table can be used for interpolation as a function of the number of diodes processed. In order to achieve maximum time resolution, you must disable the adder. Note that in order to achieve maximum time resolution your duty cycle for collecting data is only 50%, and you have no protection against noise-bursts (and FOS has no protection against damagingly bright light).

3.7 RAPID READOUT

There are certain astronomical targets where rapid time variability is suspected, but the precise period of variability is unknown, or aperiodic rapid variability is expected. Time-resolved mode is unsuitable for these observations, as the bin folding period must be preset in that mode. Instead, normal FOS data taking is used, but the spectra are read out at very frequent intervals, rather than the approximately 4 minute integration times we anticipate for normal FOS data-taking. The frequency of readout is again set by the observer's requirements, but the shortest possible integration times are limited by various processor overheads. We expect 20 msec (10 msec livetime and 10 msec deadtime) is a reasonable estimate of the shortest integrations. Burst-noise rejection must be turned off (adder off) in order to go this fast. Because you would not be able to recover phase if FOS should either reject or retry some of the integrations, you probably always will want the adder turned off. The rapid-readout capability obviously requires the 1 MHz downlink from HST through TDRSS to the ground (or storage onto magnetic tape within HST).

3.8 TIME-TAGGED SPECTROPHOTOMETRY

The time-tagged mode, probably to be the least used FOS mode, will allow study of the most rapid variability possible using the FOS. Periodic or aperiodic variability on timescales in the range of about 10μsec to 50 msec are well suited to time- tagged study. In time-tagged mode, each of the FOS accumulators counts the 1.024 MHz SSM spacecraft clock rather than sensor counts. When the first photon arrives in a given channel, this counting freezes and further counts are inhibited in that channel. To be of value, time-tagged mode data must normally be read out at high rates, *i.e.*, the 1 MHz telemetry rates, and will produce a very high data rate and large volume of data during its rare usage. The data outputs are each unsigned integers between 0 and 65,535. The selected integration time, for reasonable data, must be long enough to allow proper flight software operation, but be less than the clock overflow period, resulting in a range of allowed periods from about 10 msec to 64 msec. The author will give a bottle of 1981 Beaucastel to the first astronomer who submits a successful proposal to use the time- tagged mode.

3.9 TIMES REQUIRED TO MOVE FOS MECHANISMS

The times required for FOS mechanisms to move from one position to another are listed in Table 3.9-1. The table can be used for an order of magnitude estimate of the time which must be allowed to execute a particular program. Accurate estimates of the mechanisms' times require knowing the exact sequence of moves and how far it is on the wheels from one required position to the next. The largest overhead for mechanical movements will be incurred when using the polarimeter.

Table 3.9-1
FOS Mechanism Times

Mechanism:	Door
Cycle Time:	6.4 seconds, open or close
Power Up Position:	Closed
Mechanism:	Aperture wheel
Rotation:	Bi-directional
Sequence:	Group A: 4.3, 0.5 pair, 0.25 pair, 0.1 pair Group B: 0.5, 0.3, 1.0, blank Group C: 1.0 pair, 0.25 × 2.0, 2.0 bar, 0.7 × 2.0 bar
Cycle Time:	5.73 seconds between adjacent apertures in same group 28.65 seconds between adjacent apertures in different groups (*e.g.*, blank position to 4.3, or 0.1 pair to 1.0 pair)
Maximum Time:	109 seconds (0.5 to 0.7 × 2.0 bar)
Power Up Position:	0.3
Mechanism:	Filter/grating wheel
Rotation:	Unidirectional (for maximum repeatability)
Sequence:	Camera, G270H, G190H, G570H, G400H, G160L, G650L, Prism, G780H, Camera
Cycle Time:	7.2 seconds between adjacent positions
Maximum Time:	64.8 seconds (*e.g.*, Camera to G780H)
Power Up Position:	Camera
Mechanism:	Polarizer
Rotation:	Bi-directional
Sequence:	Clear, Pol 00° Plate A, Pol 00° Plate B, Clear, Pol 22.5° Plate A, Pol 22.5° Plate B, Clear, ..., Pol 337.5° Plate B
Cycle Time:	Clear to Pol(α) Plate A: 3.9 seconds Pol(α) Plate A to Pol(α) Plate B: 2.4 seconds Pol(α) Plate B to Clear: 2.1 seconds
Maximum Time:	67.2 seconds (*e.g.*, Pol 00° Plate A to Pol 180° Plate A)
Power Up Position:	Clear

4.0 ESTIMATING EXPOSURE TIMES AND SNRS

4.1 HOW MUCH SNR DO YOU NEED?

Before estimating your exposure times you must decide how much signal-to-noise ratio (SNR) you need. This decision will, of course, be based on your scientific objectives. If you have not had sufficient experience with pulse counting spectrophotometry to be certain of how much SNR you need for your particular program, the following discussion may be helpful; otherwise, please skip to the next section.

Figures 4.1-1 through 4.1-4 present simulated FOS observations of four classes of objects: quasars, early type stars, gaseous nebulae, and early type galaxies (or late type giants). Each figure shows what a 1/4- stepped spectrum would look like observed at high resolution ($R = 1300$) and low resolution ($R = 250$) with an SNR of 3, 10, 30, and 100 in the central 1/4- stepped pixel. The SNR at any other wavelength will be close to the square root of the number of counts at that wavelength unless sky subtraction was necessary. Spectra taken with other gratings will have similar amounts of information if the SNR is the same. You can use the figures to see how strong and weak absorption features emerge from the noise as the SNR increases, or how line profiles or close doublets (*e.g.*, H I λ6563 and [NII] $\lambda\lambda$6584,6548) can be resolved as a function of SNR. On all but the faintest objects a given SNR can be obtained approximately 7 times faster with the low dispersion grating G160L than with the high dispersion grating G130H, and approximately 5 times faster with the low dispersion grating G650L than with the high dispersion grating G570H. If you are willing to trade spectral resolution for speed or SNR, you can use the figures to see the effects of the tradeoff on spectral details in the different objects. However, you should remember that you can always rebin the high resolution data to a lower resolution in order to improve the SNR. Consequently, the low dispersion gratings and prism will be most useful for extremely faint targets whose count rates are comparable to the sky plus dark count rates, or for those targets which require only a low resolution,but complete, spectral energy distribution.

The simulated FOS observations were kindly provided by Ross Cohen. The starting point for the low redshift quasar simulations was a spectrum of a high redshift quasar observed with the Image Dissector Scanner (IDS) on the Shane 3-m telescope. The spectrum, which had 10 Å resolution, was smoothed until the SNR per pixel was better than 200. The spectrum was then blueshifted to near zero redshift to simulate a low redshfit quasar observed in the UV with a resolution of approximately 3 Å. Because the FOS resolution is approximately 1 Å in the far UV, this process degrades the appearance of narrow features, but preserves the profiles of the broad lines. A power law continuum which matched the slope longwards of Lyα was added below Lyα. All absorption lines were removed from the data and several Lyα absorption lines were simulated by adding absorption lines much narrower than the resolution of the FOS. The spectrum was then rebinned to the FOS wavelength spacing for a particular grating, smoothed with a Gaussian function (width equal to 4 quarter steps), and run through a program which accurately simulates observations with the FOS. The program convolves the intrinsic spectral energy distribution with the net FOS+ST spectral sensitivity and resolution for the specified FOS configuration, and then uses a Poisson distribution to simulate the shot noise in the signal.

Similar procedures were used for the simulated spectra of the star and galaxy. Lick IDS spectra of Feige 56 were the starting point for the spectrum of the B0V star, and Lick IDS spectra of M31 and M32 were used to simulate the FOS observations of a galaxy. The artificial spectrum of the panetary nebula was constructed by taking all emission lines in NGC 7027 (Kaler, 1976) with strengths greater than 1% of Hβ and using an intrinsic line profile which was much narrower than the FOS resolution.

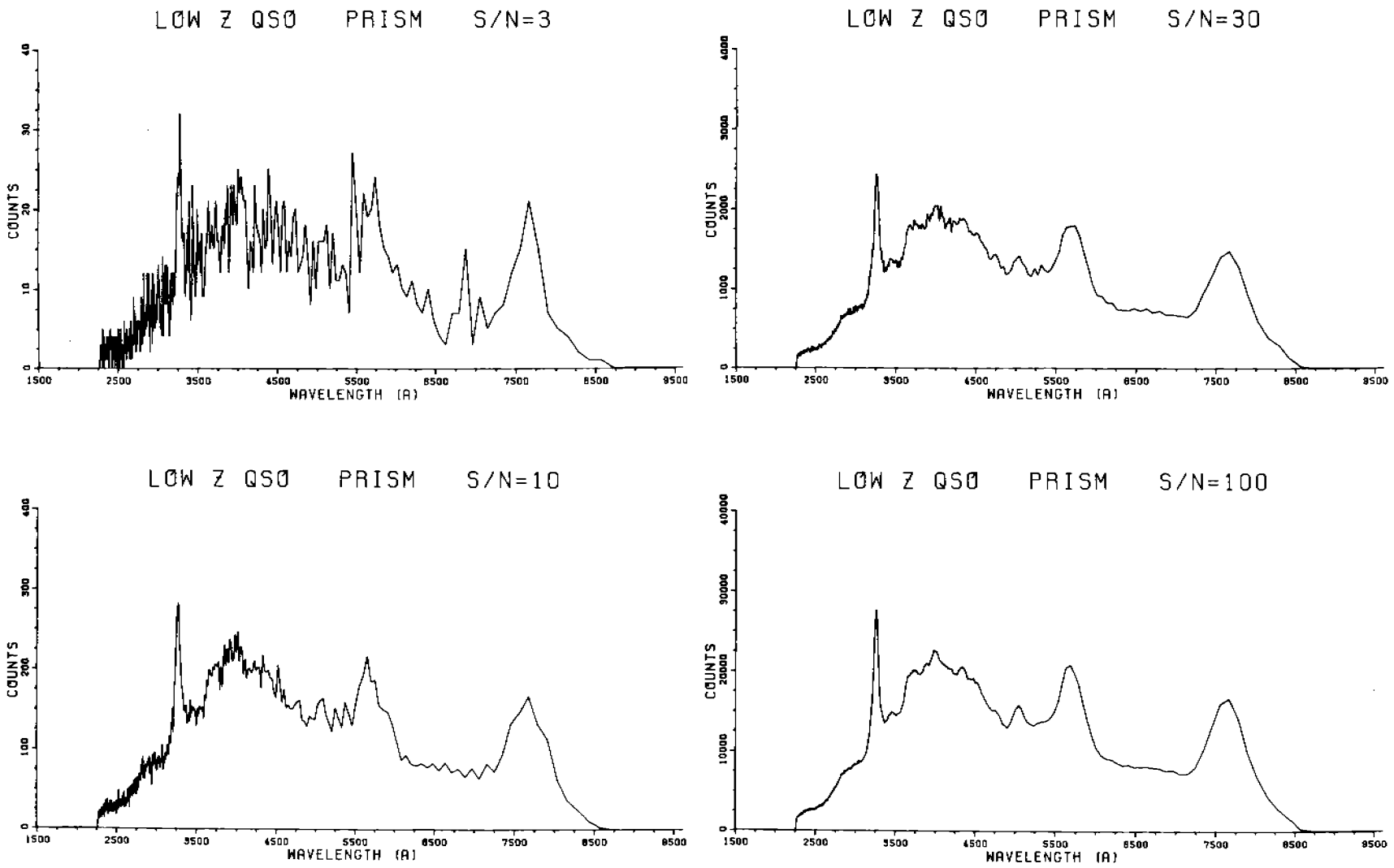

Fig. 4.1-1 Simulated FOS spectra of a low redshift quasar taken with the prism and the red digicon. The signal-to-noise ratio (SNR) is given at the central pixel, which corresponds to a wavelength of approximately 3250 Å. The nonlinear spectrum has been rebinned to a linear scale. The three sharp peaks correspond to MgII 2800, Hβ, and Hα at a redshift of 0.17.

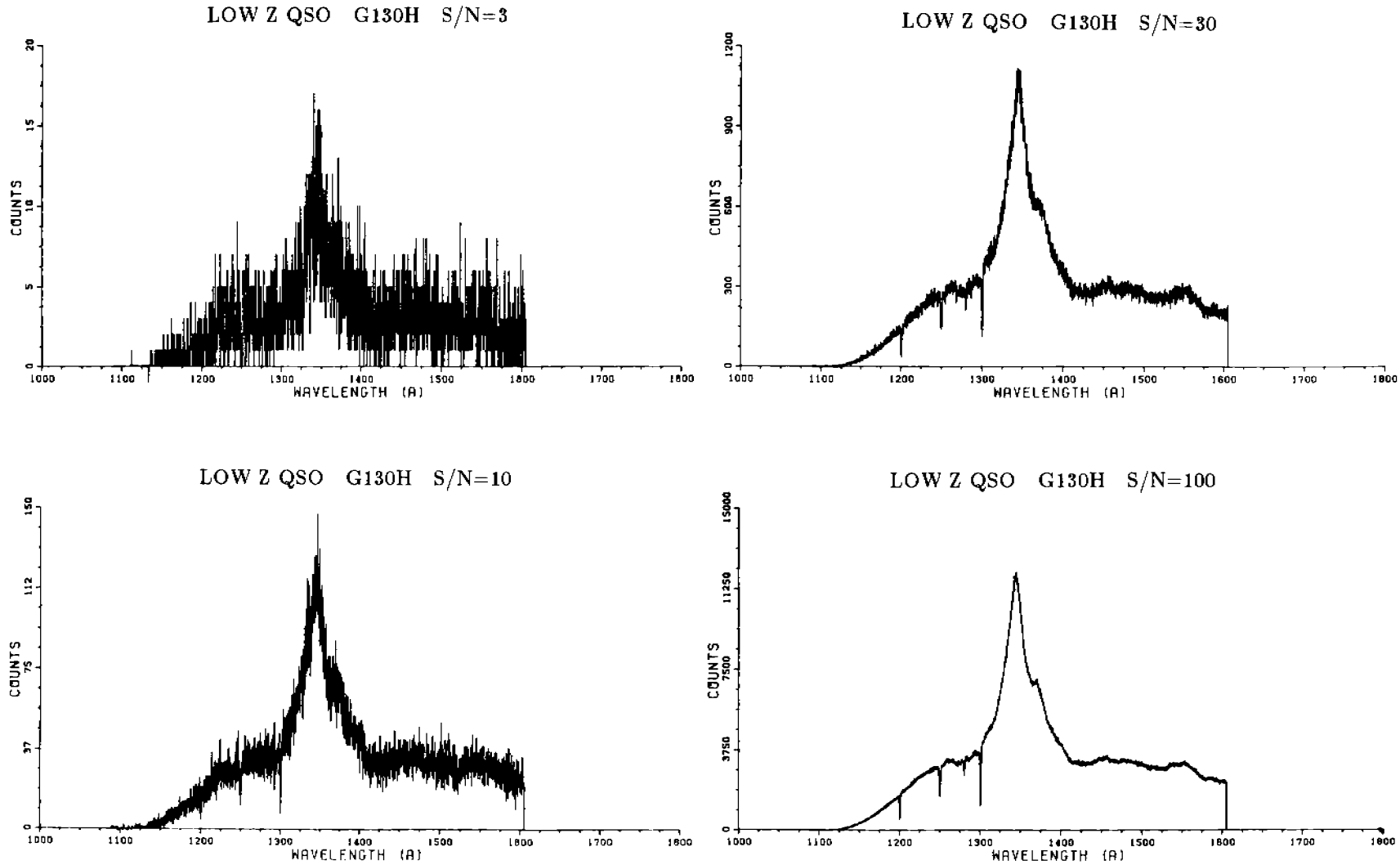

Fig. 4.1-2 Simulated FOS spectra of a low redshift quasar taken with grating G130H and the blue digicon. The signal-to-noise ratio (SNR) at a given wavelength is closely approximated by the square root of the number of counts per pixel at that wavelength. The strong emission feature is Lyα, and the four absorption lines from blue to red have equivalent widths of 1 Å, 1 Å (a doublet consisting of two 0.5 Å lines separated by 1 Å), 0.25 Å, and 1 Å.

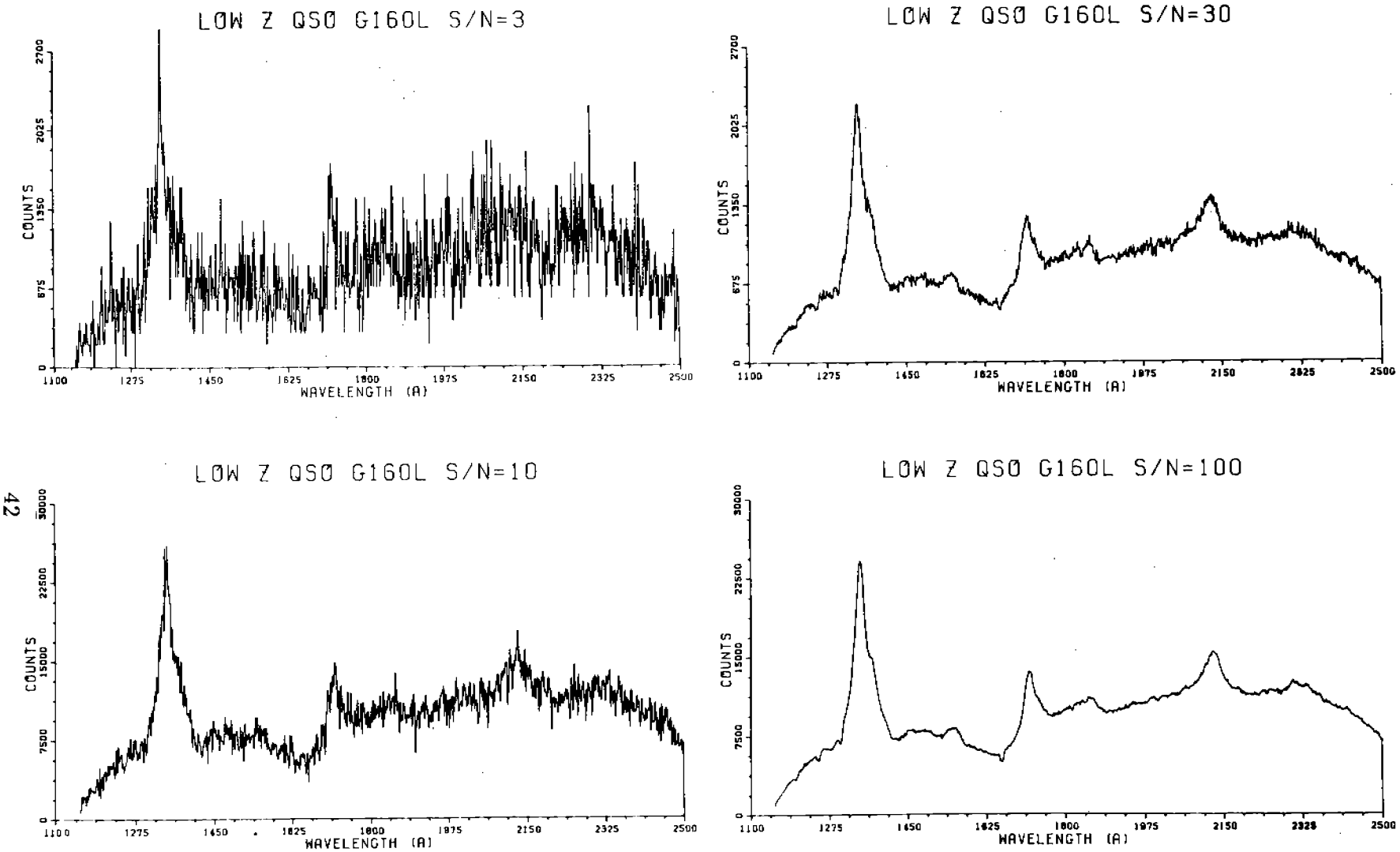

Fig. 4.1-3 Simulated FOS spectra of a low redshift quasar taken with grating L15 and the red digicon (courtesy Ross Cohen). The two strong emission lines are CIV and CIII]. The absorption feature at 1660 Å is a 1656.5/1659.3 doublet with respective equivalent widths of 1 Å and 0.5 Å.

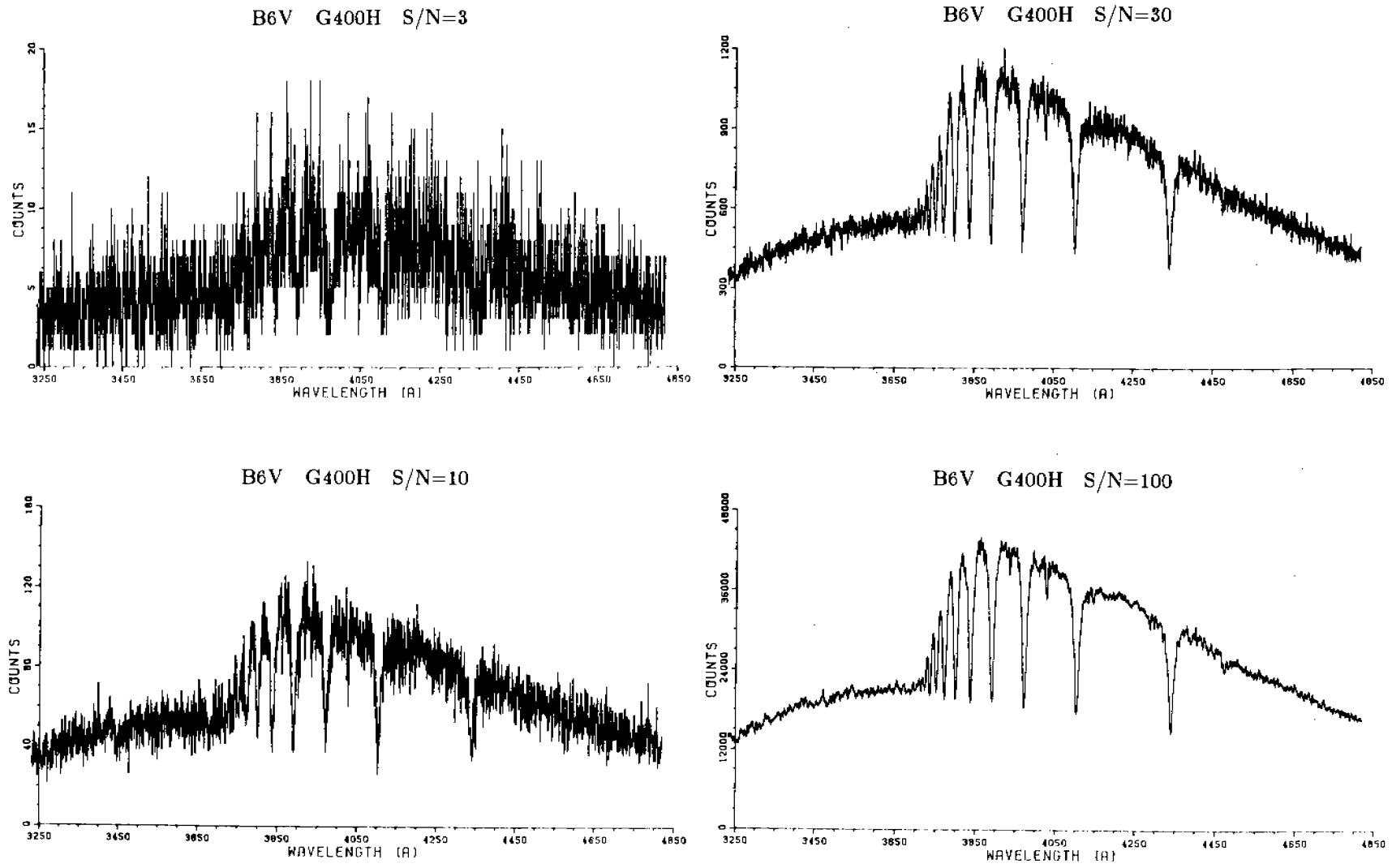

Fig. 4.1-4 Simulated FOS spectra of a B6 V star taken with grating G400H and the red digicon. The noise in the SNR= 100 spectrum is noise in the original data rather than shot noise in the FOS signal.

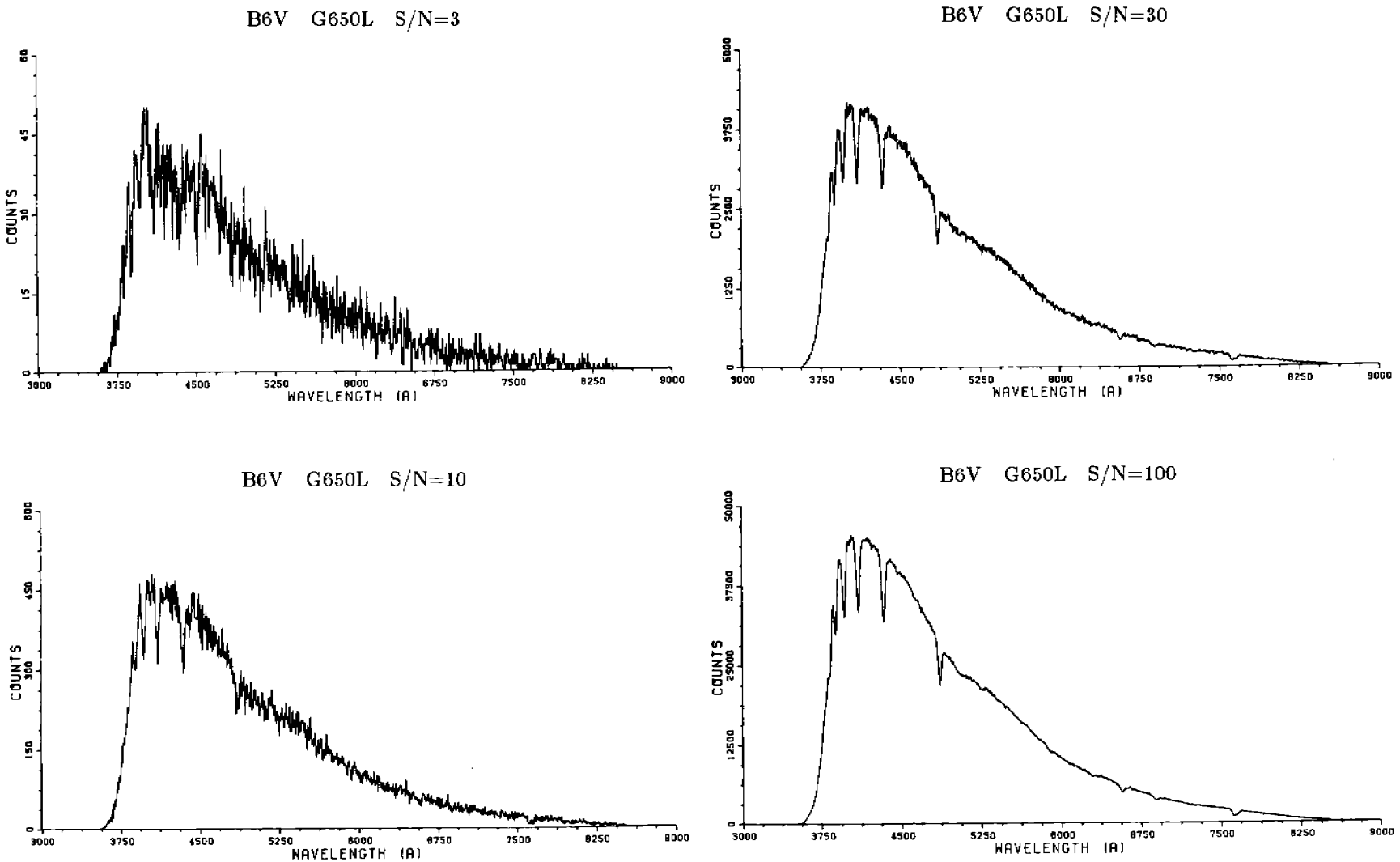

Fig. 4.1-5 Simulated FOS spectra of a B6 V star taken with grating G650L and the red digicon. The two absorption features redward of Hα are the atmospheric a-band and b-band.

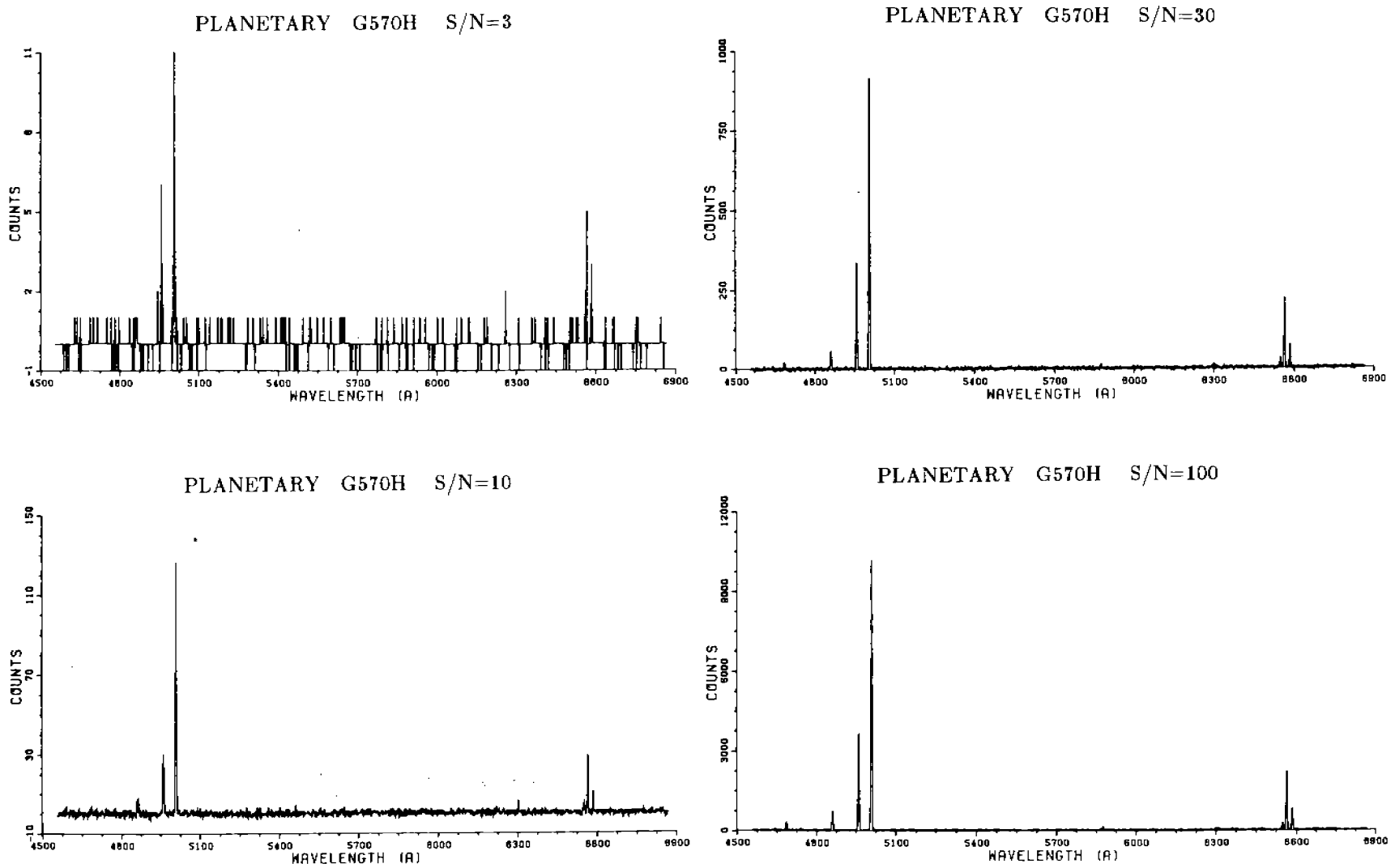

Fig. 4.1-6 Simulated FOS spectra of a high excitation planetary nebula taken with grating G570H and the red digicon. The negative counts result from simulating sky subtraction.

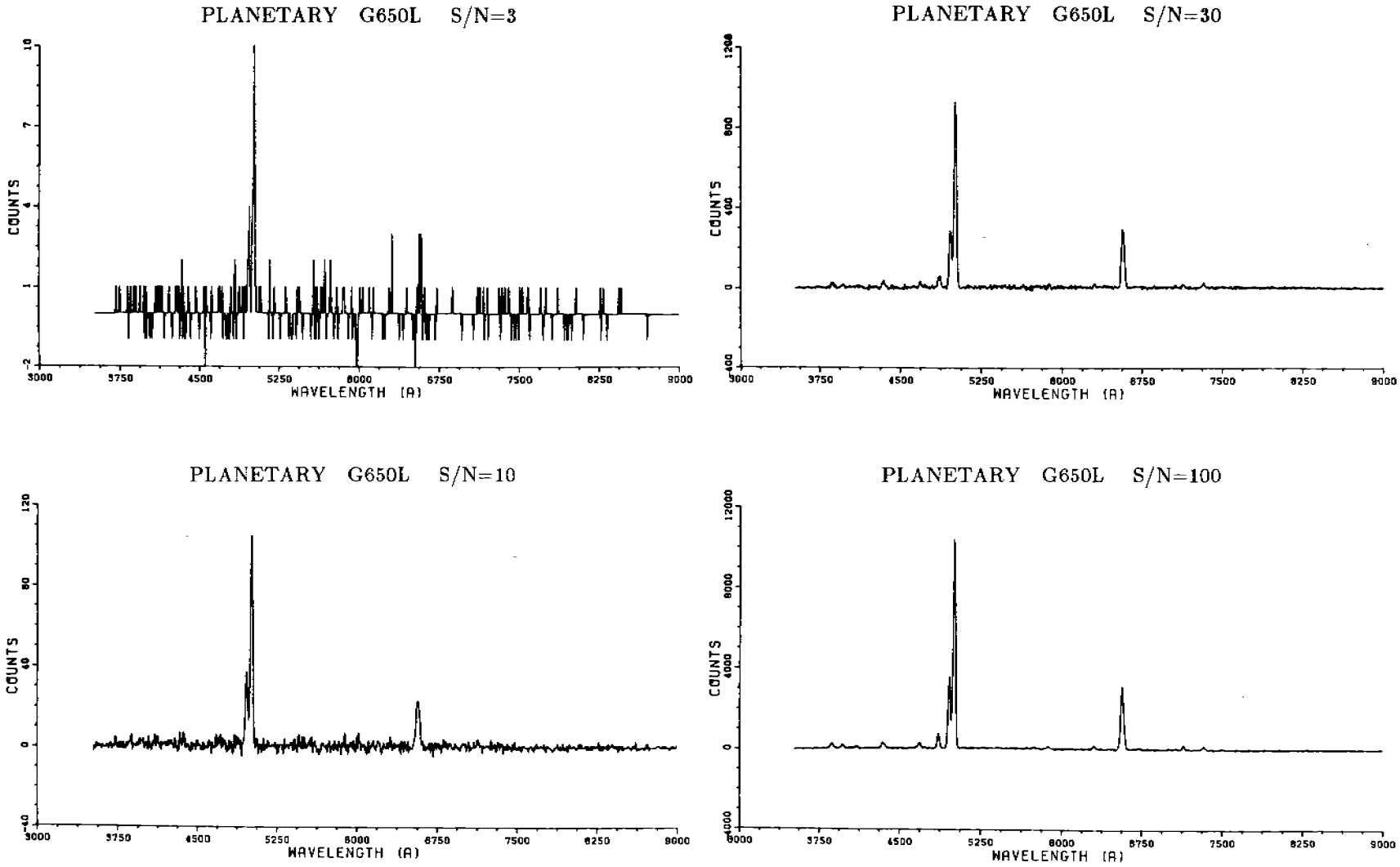

Fig. 4.1-7 Simulated FOS spectra of the high excitation planetary nebula shown in Fig. 4.1-6, taken with grating G650L and the red digicon. The negative counts result from simulating sky subtraction.

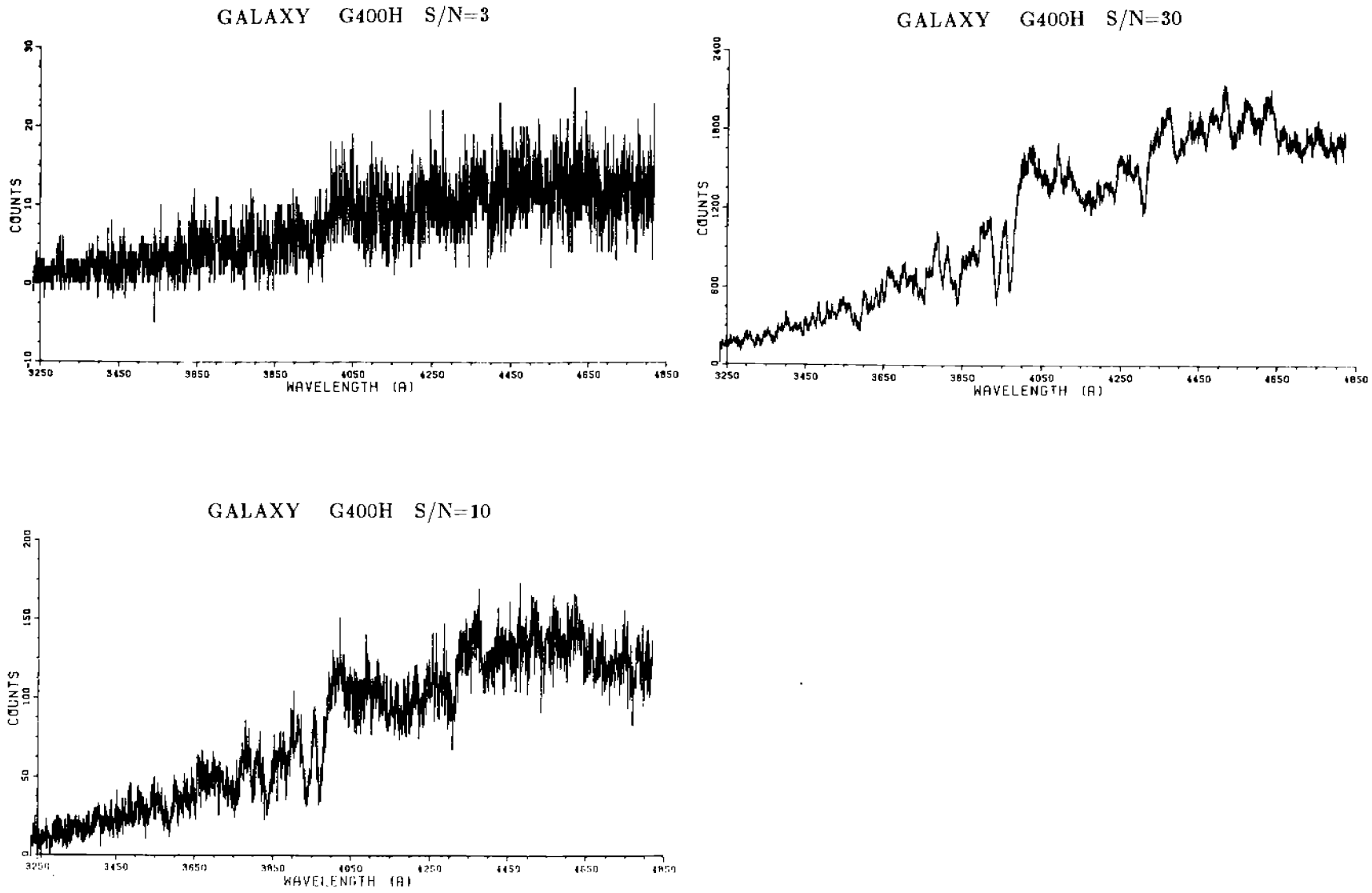

Fig. 4.1-8 Simulated FOS spectra of an early-type galaxy taken with grating G400H and the red digicon. Because the original data had a resolution of 10 Å, which is less than grating G400H's 3 Å resolution, the spectra approximate observations of a galaxy which has a velocity dispersion of several hundred km sec^{-1}.

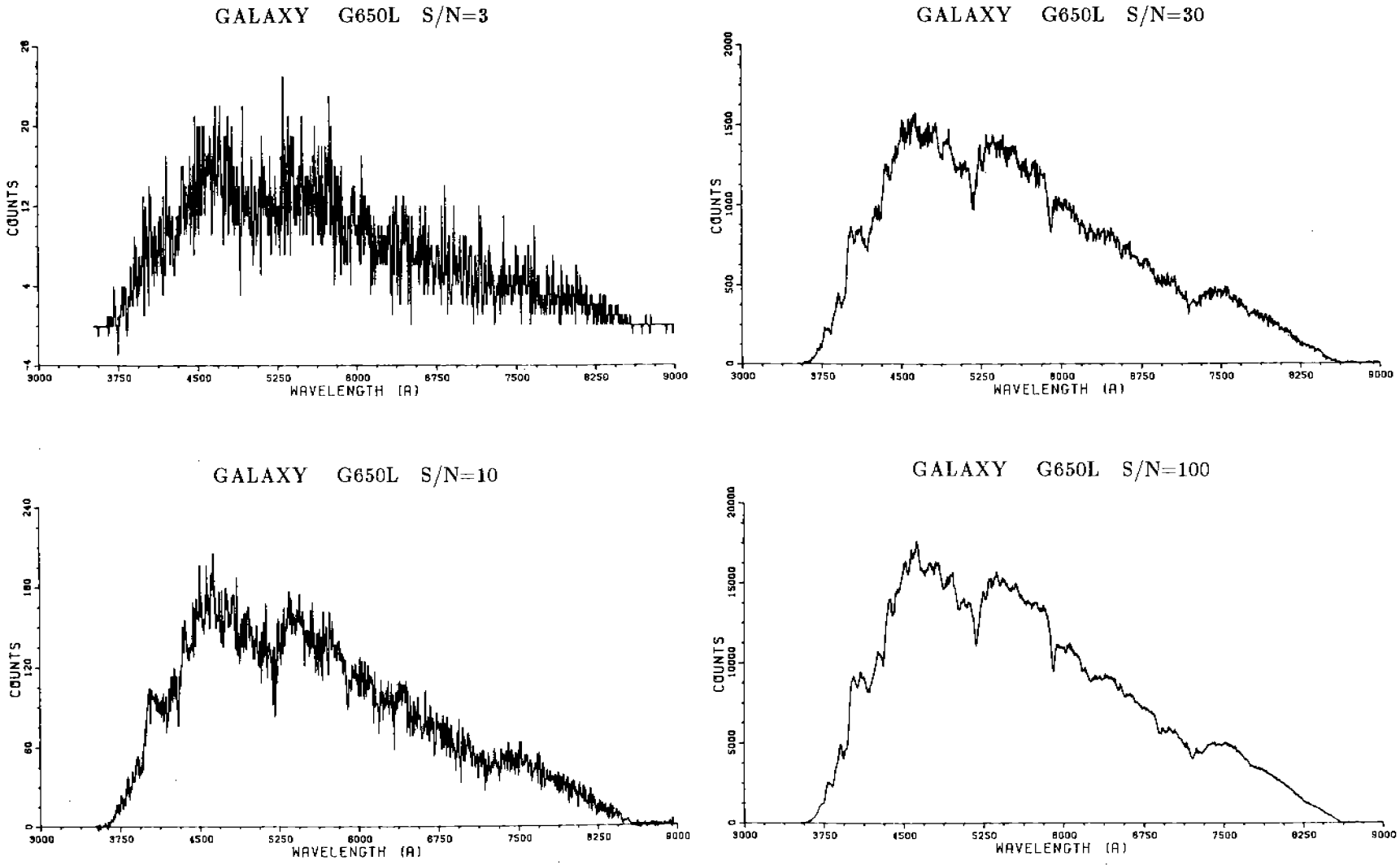

Fig. 4.1-9 Simulated FOS spectra of an early-type galaxy taken with grating G650L and the red digicon. The strong features at 5175 Å and 5890 Å are MgI b and Na D. Reduction of the spectra to a linear intensity scale would make the CaII H and K break at 4000 Å more conspicuous (cf Fig. 4.1-8).

4.2 SNR AND EXPOSURE TIME CALCULATIONS

a) Counts sec^{-1} $diode^{-1}$

The two quantities which go into an exposure time calculation are the SNR(λ) and the anticipated count rate $N(\lambda)$ (counts sec^{-1} $diode^{-1}$). Table 4.2-1 lists seven different equations which can be used to calculate $N(\lambda)$. The choice of which equation to use is dictated by how you choose to specify the spectral energy distribution. If, for example, you are observing stars, a black body approximation may be sufficiently accurate, in which case you could use equation (4) in Table 4.2-1 by specifying an appropriate effective temperature T_{eff}(° K) and magnitude m_{5556}. If you are interested in the continuum distribution of a quasar or nonthermal jet which has a power law energy distribution, you can use equation (7). References for measured spectral energy distributions are given in Table 4.2-3.

The zero point for the equations in Table 4.2-1 was set by assuming a 2.4 m aperture and then using Hayes and Latham's (1975) calibration for Vega at $m_{5556} = 0.0$, which gives 948 photons cm^{-2} sec^{-1} $Å^{-1}$. The quantity $\Delta\lambda$ is the dispersion (Å $diode^{-1}$), and is given in Table 2.2.3-1 for the central wavelength of each grating-digicon combination. The dispersion is constant to 2 or 3 percent across each grating. The efficiency $E(\lambda)$ (fraction of incident photons detected at a given wavelength) is the product of the HST's primary mirror and secondary mirror reflectivities at λ (NASA Announcement of Opportunity No. OSS-1-77 1AO) times the net FOS efficiency as measured during the preflight calibration, and includes the 14% obscuration by the central hole, baffles, and the secondary-mirror support structure. You should be advised that Bob Brown has made calculations which predict that the HST reflectivity and scattering at 1216 Å will put 25% of the light into an image instead of the 40% given in the AO. The efficiency $E(\lambda)$ is plotted as a function of wavelength for each FOS configuration in Figures 4.2-1.

As previously noted, the flight Red Digicon (F3) has been removed from the FOS and will be replaced by one of two flight spares, F8 or F9. The ST+FOS efficiencies $E(\lambda)$ for the two spare Red Digicons are given in Fig. 4.2-1. Unlike the efficiencies for the Blue Digicon, which are based on direct FOS calibration measurements, these efficiencies are necessarily estimates which are based on the measured relative quantum efficiencies of the flight Red Digicon and the flight spares. Once a final selection has been made, you will be advised in the STScI Newsletter which Digicon will be flown in the FOS.

Regrettably, there are still two additional phenomena which reduce the fraction of incident light detected by FOS. The first is due to overfilling of the collimator by the diffraction patterns of the smallest apertures. The fraction of light lost at the collimator was calculated by Richard Allen as a function of wavelength for uniform illumination of the aperture, and is given in Table 4.2-2 for the 0.1-PAIR and the 0.25-PAIR. These factors should be included in $E(\lambda)$ when observing extended objects with the smallest apertures. The second source of light loss is due to the fact that the HST's stellar point spread function overfills the smaller apertures. We have calculated the light lost from a perfectly centered stellar image by integrating the point spread functions given in the NASA Announcement of Opportunity over the area of the apertures. The resulting fractions of transmitted light are shown in Fig. 4.2-2 as a function of wavelength, and should be multiplied times $E(\lambda)$ when observing point sources with the smaller apertures. Although the diffraction pattern for a point source delimited by the aperture edges will be unequal to the diffraction pattern of a uniformly illuminated aperture, as a first approximation we have taken them to be the same. The curves for the 0.1-PAIR and the 0.25-PAIR shown in Fig. 4.2-2 include the light loss tabulated in Table 4.2-2.

Fig. 4.2-1 ST+FOS efficiency E_λ versus λ for four grating-Digicon combinations.

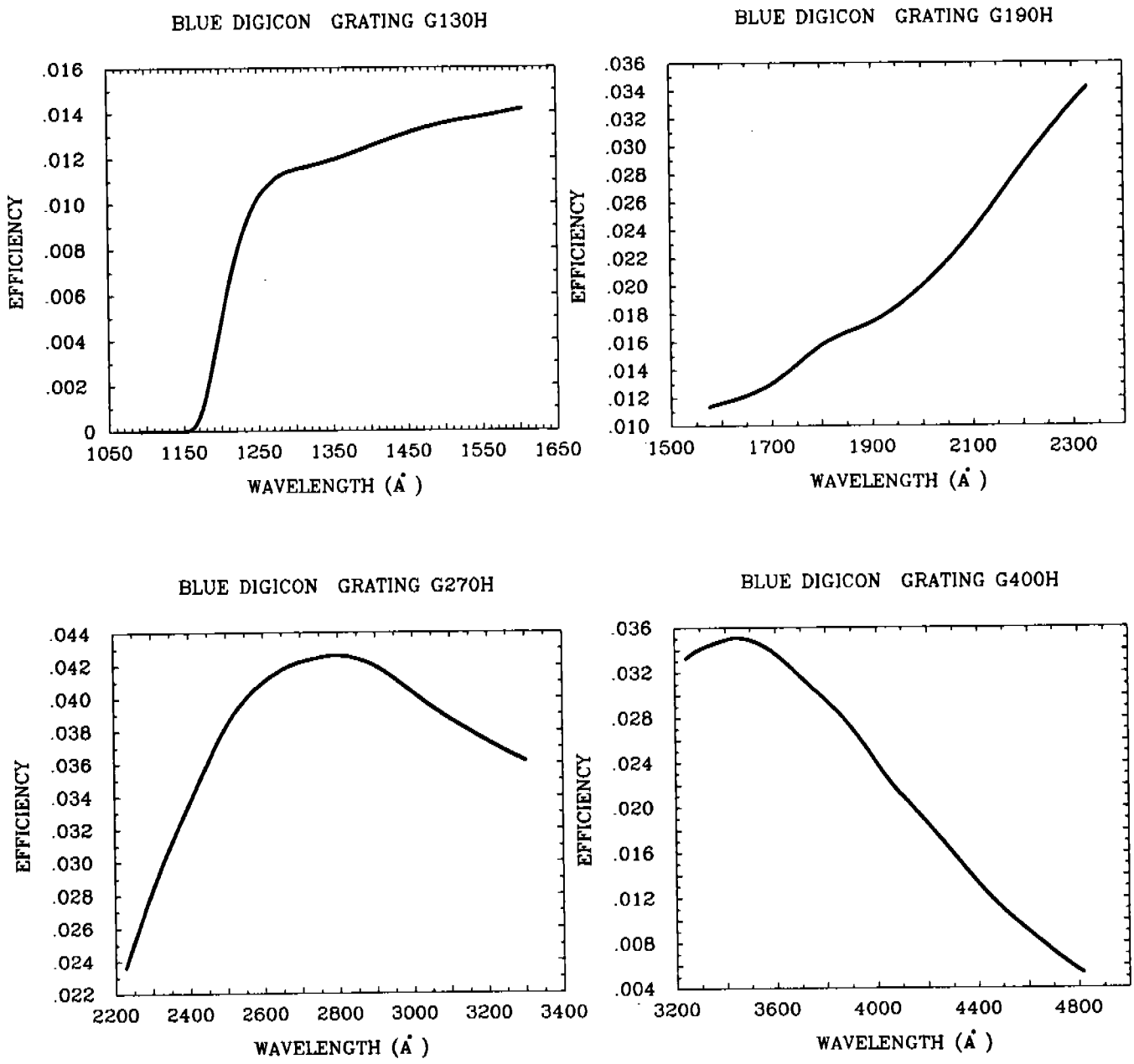

HST–FOS NET EFFICIENCY

Fig. 4.2-1 ST+FOS efficiency E_λ versus λ for three grating-Digicon combinations.

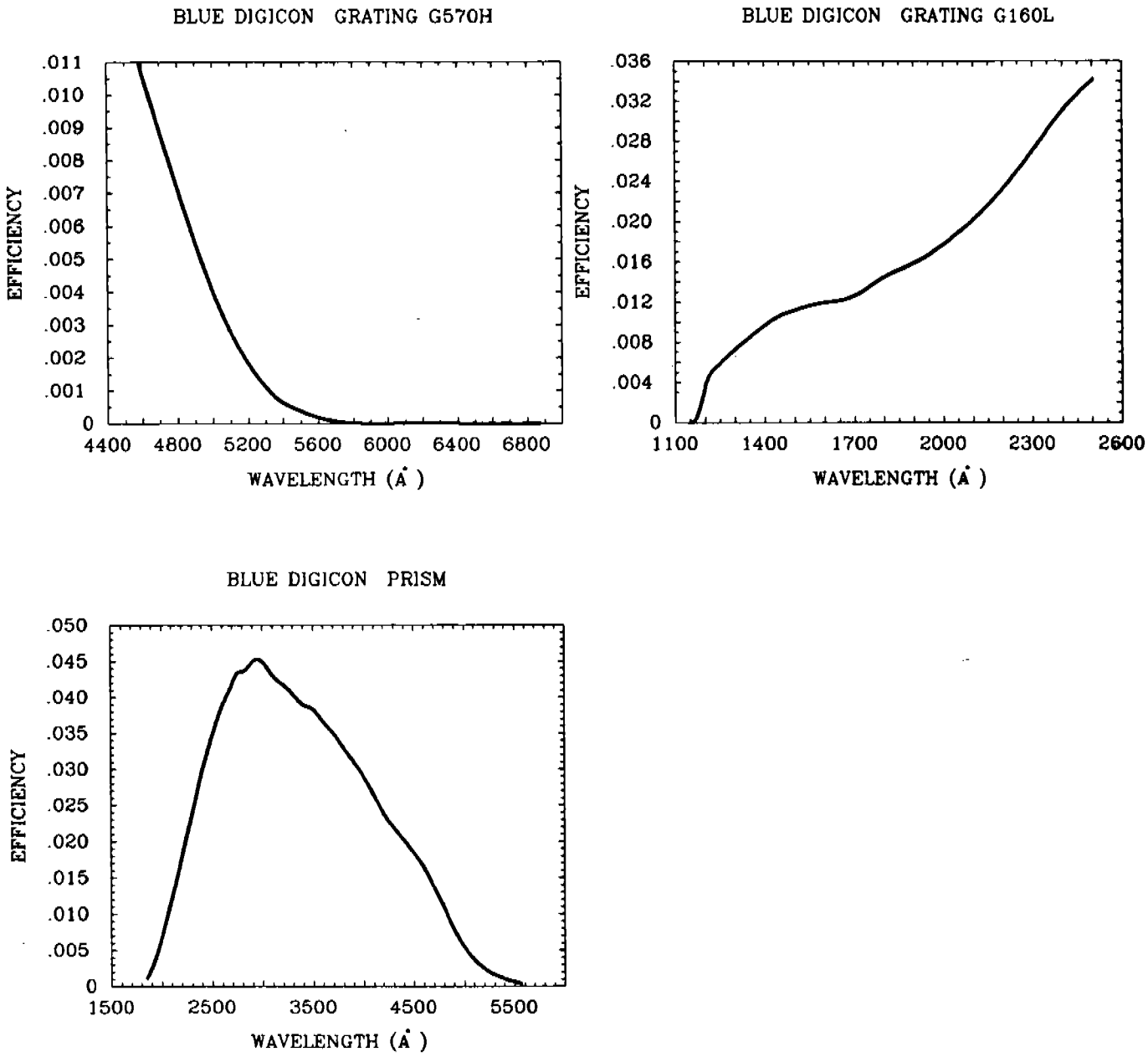

HST–FOS NET EFFICIENCY

Fig. 4.2-1 ST+FOS efficiency E_λ versus λ for four grating-Digicon combinations.

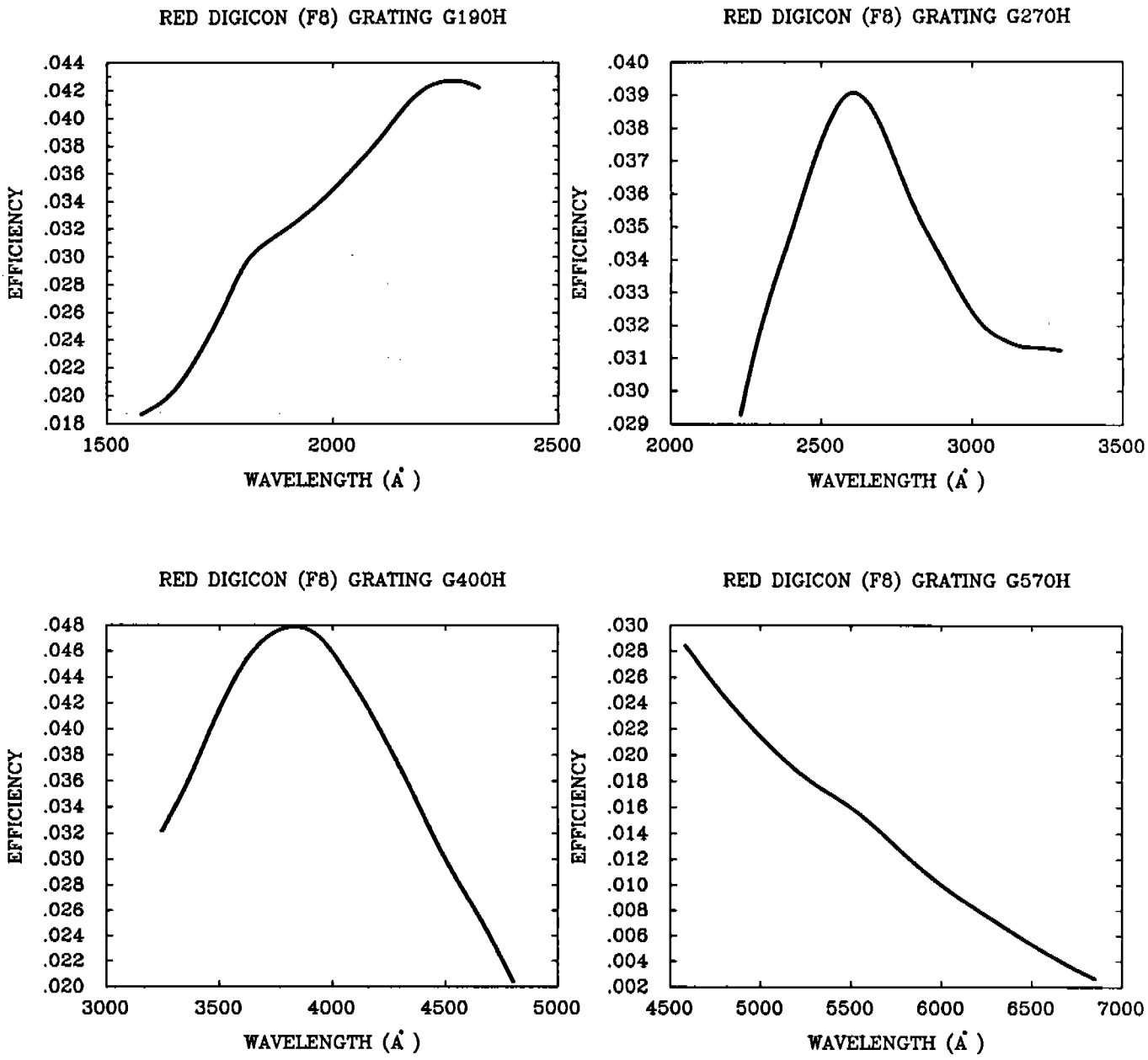

HST–FOS NET EFFICIENCY

Fig. 4.2-1 ST+FOS efficiency E_λ versus λ for three grating-Digicon combinations.

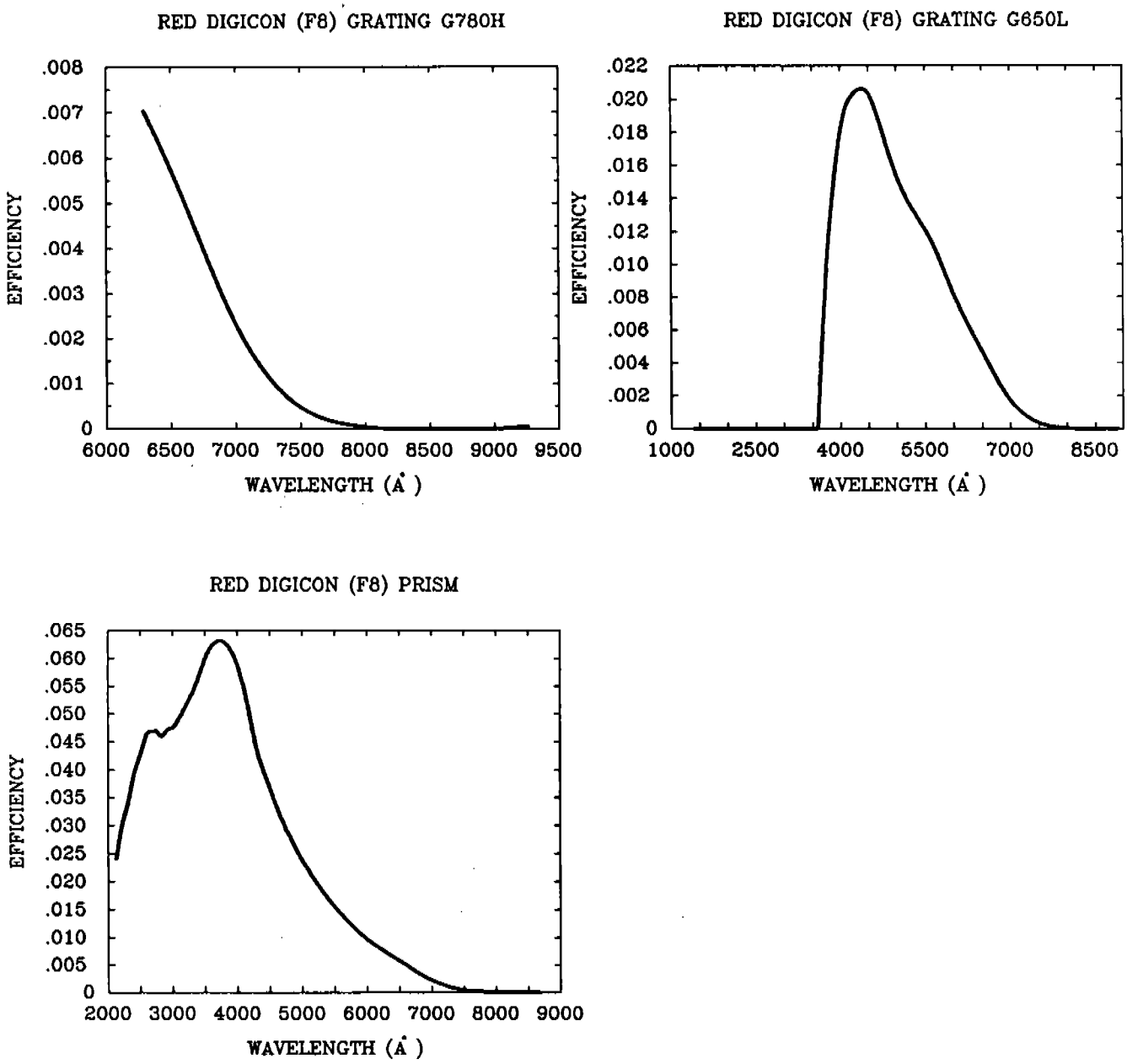

HST–FOS NET EFFICIENCY

Fig. 4.2-1 ST+FOS efficiency E_λ versus λ for four grating-Digicon combinations.

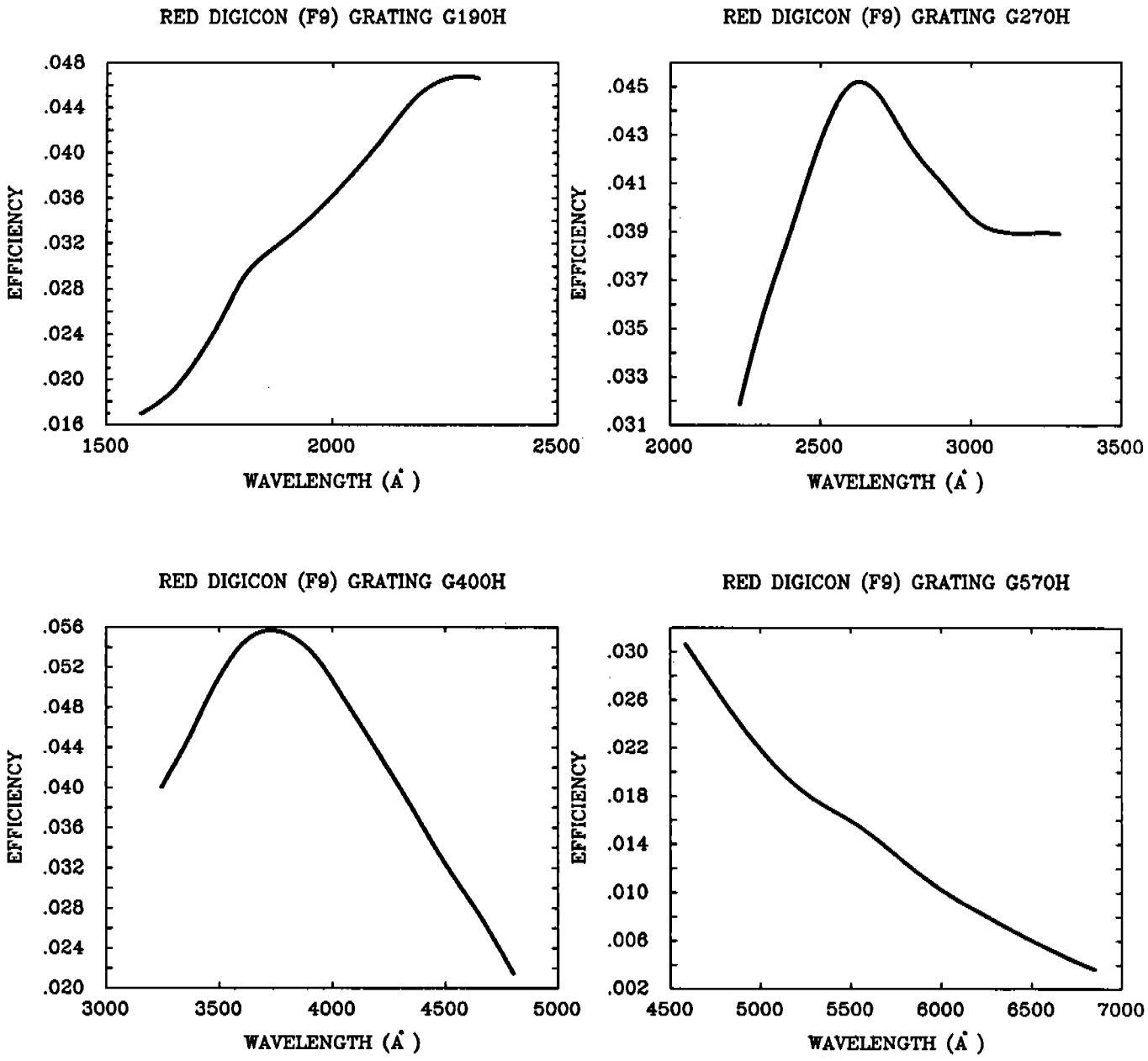

HST–FOS NET EFFICIENCY

Fig. 4.2-1 ST+FOS efficiency E_λ versus λ for three grating-Digicon combinations.

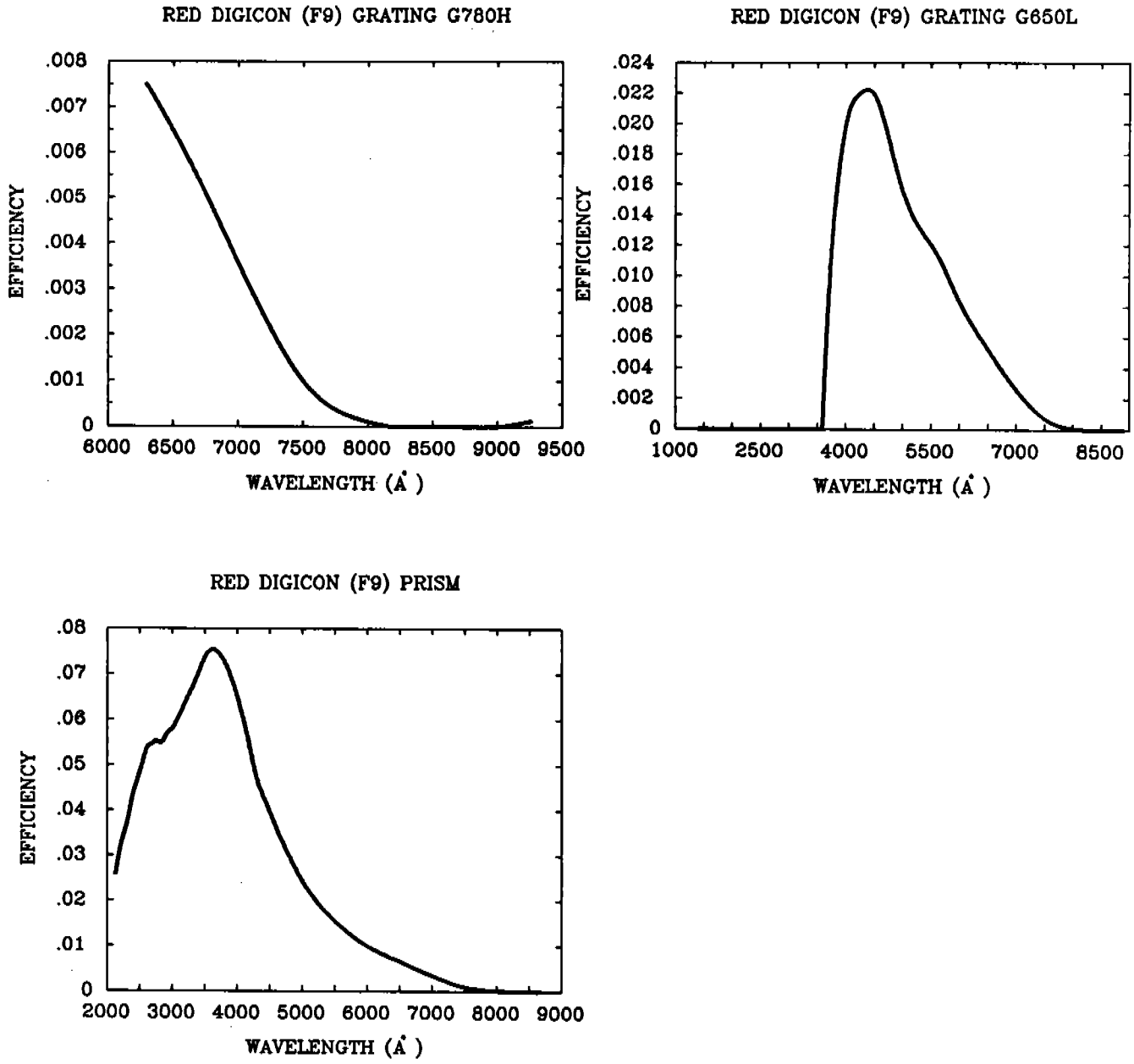

HST–FOS NET EFFICIENCY

TABLE 4.2-1

FOS Observed Counts Sec^{-1} $Diode^{-1}$ (N_λ) for Point Sources at Wavelength $\lambda(\text{Å})$

Flux Distribution	Inputs	Equation for N_λ (counts s^{-1} $diode^{-1}$)	
Continuum	$F_\lambda(\text{ergs cm}^{-2}\text{s}^{-1}\text{Å}^{-1})$	$2.28 \times 10^{12} F_\lambda \lambda \Delta\lambda E_\lambda$	(1)
Monochromatic	$I_\lambda(\text{ergs cm}^{-2}\text{s}^{-1})$	$2.28 \times 10^{12} I_\lambda \lambda E_\lambda$	(2)
Normalized Continuum	$\frac{F_\lambda}{F_{5556}}, m_{5556}$	$7720 \frac{F_\lambda}{F_{5556}} \lambda \Delta\lambda E_\lambda 10^{-0.4 m_{5556}}$	(3)
Planck Function	$T_{eff}(\overset{\circ}{K}), m_{5556}$	$4.09 \times 10^{22} \frac{\left(e^{25897/T}-1\right)}{\left(e^{(1.4388\times10^8)/\lambda T}-1\right)} \Delta\lambda \frac{E_\lambda 10^{-0.4 m_{5556}}}{\lambda^4}$	(4)
Continuum	$F_\nu(\text{ergs cm}^{-2}\text{ s}^{-1}\text{hz}^{-1})$	$6.83 \times 10^{30} \frac{F_\nu \Delta\lambda E_\lambda}{\lambda}$	(5)
Normalized Continuum	$\frac{F_\nu}{F_{\nu,5556}}, m_{5556}$	$2.38 \times 10^{11} \frac{F_\nu}{F_{\nu,5556}} \frac{\Delta\lambda E_\lambda}{\lambda} 10^{-0.4 m_{5556}}$	(6)
Power Law $\nu^{-\alpha}$	α, m_{5556}	$2.38 \times 10^{11} \left(\frac{\lambda}{5556}\right)^\alpha \frac{\Delta\lambda E_\lambda}{\lambda} 10^{-0.4 m_{5556}}$	(7)

E_λ = Net HST Reflectivity x FOS Efficiency at Wavelength $\lambda(\text{Å})$

$\Delta\lambda$ = Number of Angstroms per Diode at Wavelength λ (Å)

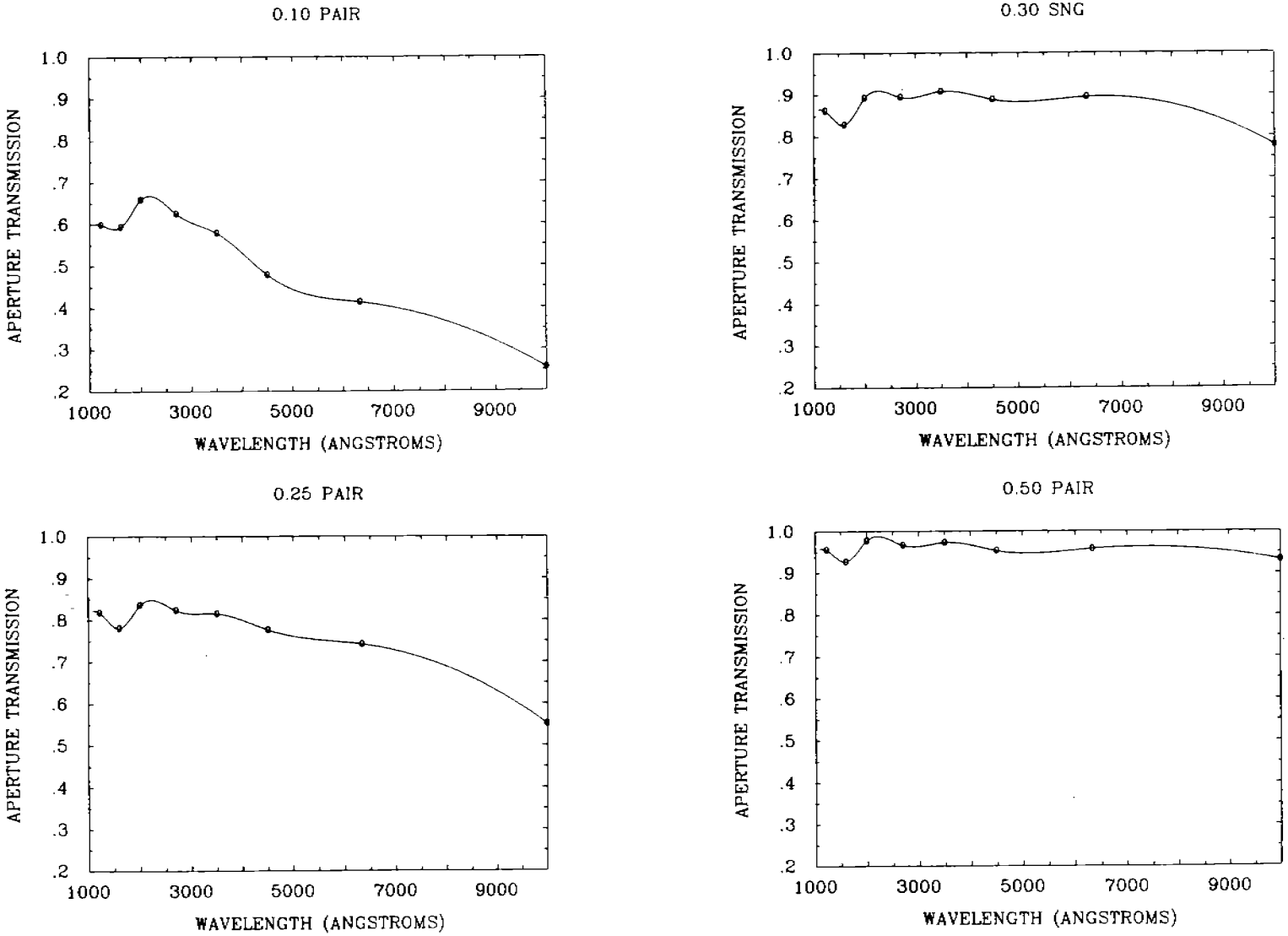

Fig. 4.2-2 Fraction of light transmitted by the apertures for a perfectly centered point source. The curves for the 0.10 PAIR and the 0.25 PAIR include the fraction of light lost from the aperture diffraction pattern which overfills the FOS collimator.

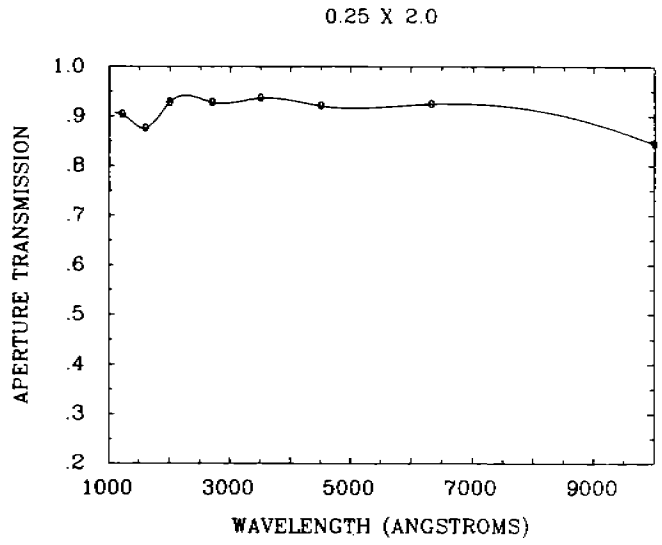

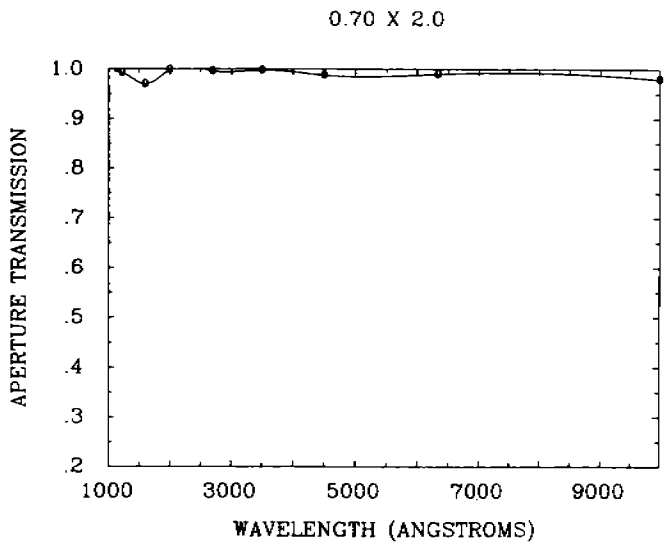

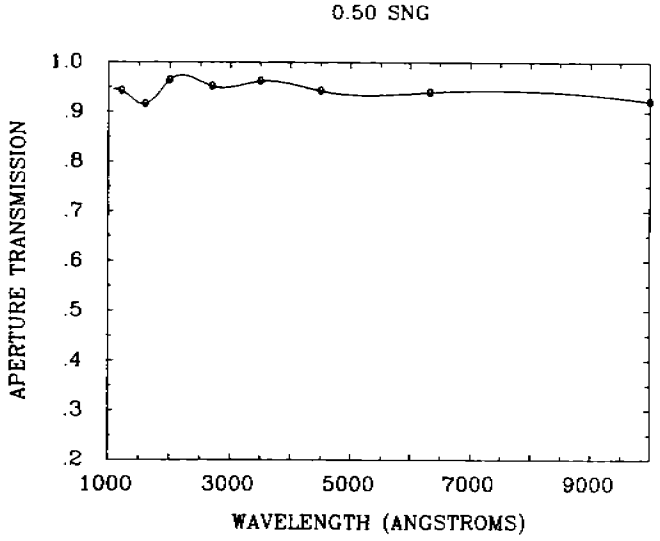

Fig. 4.2-2 Fraction of light transmitted by the apertures for a perfectly centered point source.

TABLE 4.2-2

Per Cent Light Loss by Diffraction

Wavelength (Å)	0.1-PAIR	0.25-PAIR
1500	9.1%	3.9%
3000	18.5%	8.0%
6000	31.9%	15.5%

TABLE 4.2-3

References for Spectral Energy Distributions

Source Type	Flux Distribution	Spectral Range (Å)	Reference
O - M Stars	F_λ	3510–7427	Jacoby *et al.* 1984
O - K Stars	F_λ	1150–3200	Heck *et al.* 1984
O - M Stars	F_λ	1150–3200	Wu *et al.* 1983
O - B Stars	F_λ	1150–3200	Bohlin, 1984
Low Redshift Giant Ellipticals	$-2.5 \log F_\nu + C$	3400– 8000	Schild and Oke, 1971
Low Redshift Giant Ellipticals	$-2.5 \log F_\lambda + C$	3388– 10962	Whitford, 1971
Cluster Galaxies ($0.012 < z < 0.465$)	$-2.5 \log F_\nu + C$	3259–10694	Gunn and Oke, 1975
M31 and M32 Nuclei	F_λ	1000–3400	Johnson, 1979

TABLE 4.2-4

FOS Exposure Time and Signal to Noise Ratio per Substep

No Sky Subtraction

$$SNR_\lambda = \frac{N_\lambda \left(\frac{t_1}{n}\right)^{\frac{1}{2}}}{\left(N_\lambda + N_{sky,\lambda} + N_D\right)^{\frac{1}{2}}} \simeq \left(\frac{N_\lambda t_1}{n}\right)^{\frac{1}{2}} \tag{8}$$

$$t_1 \simeq \frac{nSNR_\lambda^2}{N_\lambda} \tag{9}$$

Sky Subtraction

$$SNR_\lambda = \frac{N_\lambda \left(\frac{t_2}{2n}\right)^{\frac{1}{2}}}{\{N_\lambda + 2\left(N_{sky,\lambda} + N_D\right)\}^{\frac{1}{2}}} \tag{10}$$

$$t_2 = \frac{2n\{N_\lambda + 2(N_{sky,\lambda} + N_D)\}SNR_\lambda^2}{N_\lambda^2} \tag{11}$$

$t_1 =$ total time in seconds spent on the object plus sky and background
$t_2 =$ total integration time in seconds; $\frac{t_2}{2}$ is the integration time on the objects plus sky and background
$n =$ number of substeps (default = 4)
$N_{sky,\lambda} =$ counts s^{-1} $diode^{-1}$ from the sky at wavelength λ
$N_D =$ dark counts s^{-1} diode $^{-1}$

(b) SNR and Exposure Time Calculations

The equations for computing the exposure time or SNR(λ) are given in Table 4.2-4. Because the Digicons are pulse counting detectors and have a sharp peak in the pulse height distribution from photoelectrons, which permits discrimination between photoelectrons and noise in the detector electronics, the noise is very nearly the square root of the observed number of counts. Consequently, in cases where the object is bright enough to make a background subtraction unnecessary, the SNR(λ) per channel will be given by equation (8), and the exposure time by equation (9). $N(\lambda)$ is given by the equations in Table 4.2-1, t_1 is the total integration time, and n is the number of $1/n$-steps ($n = 4$ is the default) which have been taken. If the monochromatic magnitude m_λ of an isolated object is brighter than 21 and the entrance aperture 0.5″ or smaller, background subtraction should be unnecessary.

For the faintest objects, which give count rates comparable to the sky seen through the aperture, or faint objects observed against a bright background (*e.g.*, globular clusters in M87) sky subtraction may be necessary. In this case you should use equations (10) and (11), where t_2 is the total time, with $t_2/2$ spent on the object (plus background) and $t/2$ on the background.

4.3 SKY BRIGHTNESS, DARK CURRENT, AND PARTICLE BACKGROUND

a) Sky Brightness

When observing while the HST is in the Earth's shadow (and perhaps while in sunlight if pointing well away from the sun or the bright limbs of the earth and moon), the major sources of sky brightness in the optical will be zodiacal light, diffuse galactic light (DGL), and, especially at low galactic latitudes, individual faint stars. The latter will not be considered here. In the far ultraviolet the major sources of background light will be diffuse galactic light and emission lines from the ionosphere, the brightest being geocoronal Lyα.

The zodiacal light has a solar spectral energy distribution longward of 2500 Å (Levasseur-Regourd and Dumont, 1980), and a surface brightness which is strongly dependent on heliocentric ecliptic longitude ($\lambda - \lambda_\odot$) and latitude. The maximum surface brightness (within HST observing constraints) will be $m_V \simeq 21.1$ and is obtained in the ecliptic plane 50° from the sun. In equation (12) (*cf.* Table 4.3-1) we have approximated the number of FOS counts $\sec^{-1}$ diode^{-1} from the zodiacal light by using a Planck distribution with the solar effective temperature, 5770° K. Ap is the area of the aperture in square arc seconds and b is the galactic latitude. The zodiacal light surface brightness in equation (12), m_V, is tabulated by Levasseur-Regourd and Dumont (1980) and given in an abbreviated form in Table 4.3-2. If your object is faint enough to require sky subtraction, the observations probably should be scheduled while the HST is in the Earth's shadow. In that case the limited longitude coverage in Table 4.3-2 should be adequate for estimating the zodiacal light contribution to the background.

With the exception of low galactic latitudes and the far ultraviolet, the diffuse galactic light is fainter than the zodiacal light; consequently, there may be appreciable errors in published measurements. Lillie and Witt (1976) tabulate the diffuse galactic light surface brightness, *averaged over galactic longitude*, as a function of wavelength (for $\lambda \leq 4250$) and galactic latitude. We were able to accurately fit the DGL wavelength dependence at $b = 1°$ with a third order polynomial in λ (*cf.* equation 14). With somewhat less accuracy we used the DGL data to derive a wavelength dependent exponential scale height (equation 16). These functional dependencies reproduce Lillie and Witt's data to an accuracy of 30% or better. In order to estimate the DGL background at wavelengths $\lambda \geq 4250$, we scaled Witt's (1968) Blue and Orange DGL brightnesses to Lillie and Witt's brightness at 4250 Å and then derived the effective temperature ($T_{eff} = 6475°$ K which fits the optical data with a Planck function. The result is given in equation (15).

Paresce and Volpe (1984) have developed a background radiation model for the Space Telescope which includes geocoronal airglow. Based on their discussion, there are only three emission lines which will have intensities greater than 0.1 Kilo Rayleighs (KR; $1R = 10^6/4\pi$ $photons^{-1}cm^{-2}s^{-1}sr^{-1}$). These are NI(1200Å), HI(1216Å), and OI(1304 Å). The estimated intensities of these lines in the HST zenith-direction are listed in Table 4.3-3. Note that while the HST is in the Earth's shadow Lyα is the only geocoronal emission

TABLE 4.3-1

Sky Background and Digicon Dark Counts

Source	Equation	Units	
Zodiacal Light	$N_\lambda = 3.6 \times 10^{24} \frac{\Delta\lambda E_\lambda Ap 10^{-0.4 m_V}}{\left\{e^{\frac{24936}{\lambda(\mathring{A})}} - 1\right\} \lambda^4(\mathring{A})}$	counts s^{-1} $diode^{-1}$	(12)
Diffuse Galactic Light	$N_\lambda = 4.2 \times 10^4 f(\lambda) \Delta\lambda E_\lambda Ap$	counts s^{-1} $diode^{-1}$	(13)
	$f(\lambda) = \{1.766 \times 10^{-6} - 1.765 \times 10^{-9}\lambda$	photons cm^{-2} s^{-1} $\mathring{A}^{-1}$ arc-sec^{-2}	(14)
	$+5.613 \times 10^{-13}\lambda^2 - 4.984 \times 10^{-17}\lambda^3\} e^{t_\lambda b},\ \lambda \leq 4250$		
	$f(\lambda) = \frac{3.48 \times 10^{10} e^{t_\lambda b}}{\left(e^{22221/\lambda} - 1\right)\lambda^4}, \lambda > 4250$	photons cm^{-2} s^{-1} $\mathring{A}^{-1}$ arc-sec^{-2}	(15)
	$t_\lambda = -1.14 \times 10^{-2} - 1.0376 \times 10^{-5}\lambda$		(16)
Airglow	$N_\lambda = 84.6 I(KR) E_\lambda f(Ap)$	peak-counts s^{-1} diode-1	(17)
	$f(Ap) = 0.7Ap,\ \sqrt{Ap} \leq 0.35''$		(18)
	$f(Ap) = 0.35\sqrt{Ap},\ \sqrt{Ap} > 0.35''$		(19)

Digicon Dark Counts (N_D) at $-10°$ C

Bialkali Digicon (Blue) counts s^{-1} $diode^{-1}$	Trialkali Digicon (Red) counts s^{-1} $diode^{-1}$
0.00052	0.0027

Ap = aperture area in square arc seconds, refer to Table 2.2.1-1; b = galactic latitude

TABLE 4.3-2
Zodiacal Light Sky Brightness, M_V

$\lambda - \lambda_\odot$	Ecliptic Latitude 0	30	60	90
180	22.1	22.7	23.2	23.3
145	22.4	22.9	23.3	23.3
110	22.3	22.9	23.3	23.3

TABLE 4.3-3
Airglow Emission Line Intensities at the ST Zenith

λ(Å)	Element	I(KR) ST Midnight	I(KR) ST Noon
1200	NI	–	0.22
1216	HI	2.5	22
1304	OI	–	2.1

TABLE 4.3-4

Average Counts s^{-1} $Diode^{-1}$× 1000 As a Function of Rejection Threshold and Percentage of Signal Lost

Percentage of Signal Lost (%)	Rejection Threshold 2	3	4	5	10
1	1.465	4.297	8.105	12.45	40.04
10	5.195	10.74	17.04	23.73	60.79
25	9.375	16.89	24.76	32.91	75.44

TABLE 4.3-5

Mean HST Reflectivity × FOS Efficiency

Grating	Digicon	$\overline{\lambda\Delta\lambda E_\lambda}$ (Å)	Grating	Digicon	$\overline{\lambda\Delta\lambda E_\lambda}$ (Å)
G130H	Blue	14	G130H	Red	—
G190H	Blue	61	G190H	Red	60
G270H	Blue	221	G270H	Red	182
G400H	Blue	262	G400H	Red	418
G570H	Blue	37	G570H	Red	352
G780H	Blue	—	G780H	Red	122
G160L	Blue	217	G650L	Red	747

line which will be observed with a strength $I > 0.1KR$. The emission line intensities in Table 4.3-3 will approximately double as the HST changes its pointing from the zenith to the horizon. Equation (17) gives the FOS count rate as a function of geocoronal emission line intensity. The aperture functions $f(Ap)$ in equations (18) and (19)allow for either overfilling or underfilling a diode with the image of the aperture.

b) Dark Current

The dark current due to thermionic emission and particle-induced diffuse glow may depend weakly on the Digicon photocathode temperature and strongly on the ST's orbital position relative to the South Atlantic Anomaly (SAA). Until data is obtained in orbit, you may assume that the dark count outside the SAA will be given by the values in Table 4.3-1.

c) Discrete Particle Events

Discrete particle events which result in more than one detected count can be discriminated against by commanding the FOS microprocessor to sum the counts in the accumulators at the end of the innermost integration time (livetime, which can be as short as 10 msec; *cf.* 3.6) and reject the integration if the sum exceeds a preset level. A parameter is set in the microprocessor which causes the logic to either keep a count of the number of rejected integrations, or keep retrying the integration until successful. The latter option will not be used until we have a thorough understanding of the particle background in orbit.

The average count rates at which there will be 1%, 10%, and 25% losses of data due to rejection of signal counts instead of cosmic ray events are given in Table 4.3-4 as a function of the rejection threshold, assuming 512 msec per INT. The average count rates can be converted to a mean monochromatic magnitude, m_λ, by using the equation

$$m_\lambda = -2.5 \log \frac{N_\lambda}{7734(\overline{\lambda\Delta\lambda E_\lambda})} \qquad (20)$$

where the mean sensitivity $\overline{\lambda\Delta\lambda E_\lambda}$ is given for each grating-digicon combination in Table 4.3-5. Advice on strategies for choosing the optimum rejection threshold must await orbital observations of the particle-induced amplitude and frequency distribution.

4.4 INTERSTELLAR REDDENING

You should be reminded that a little bit of $E(B-V)$ goes a long way in the far ultraviolet. If the foreground reddening in the direction of your object isn't known, you may choose to use either the global representation given by de Vaucouleurs, de Vaucouleurs, and Corwin (1976), or an estimate based on the observed HI column density in the direction of your object, using the precepts of Bohlin *et al.* (1978). For your convenience, these equations are summarized in Table 4.4-1. The HI column density, N_H (cm^{-2}) can be taken from Heiles (1976) for declinations greater than $-23°$ and from Cleary, Heiles, and Haslam (1979) for declinations less than $-30°$.

To convert $E(B-V)$ to the extinction A_λ(mag), you can use Seaton's (1979) UV extinction curve, which is summarized in analytical and numerical form in Table 4.4-2. If you use an apparent magnitude m_{5556} in equations (3), (4), (6), or (7), you must multiply the equations by the additional factor $10^{-0.4(A_\lambda - A_{5556})}$ to correct for interstellar extinction. If you put an unreddened flux into equations (1), (2), or (5), you should correct for extinction by multiplying by $10^{-0.4A_\lambda}$. Finally, the interstellar dust in another galaxy (*e.g.*, the Magellanic Clouds) may be different than the galactic dust, in which case Seaton's extinction curve will not be appropriate.

TABLE 4.4-1

Estimation of Interstellar Extinction

Source	Equations	
de Vaucouleurs *et al.* 1976	$A_B = 0.19(1 + S_N \cos b)\lvert C\rvert \quad (b > 0)$ $A_B = 0.21(1 + S_S \cos b)\lvert C\rvert \quad (b < 0)$	(21)
	where	
	$S_N(\ell) = 0.1948\cos\ell + 0.0725\sin\ell$ $+0.1168\cos 2\ell - 0.0921\sin 2\ell$ $+0.1147\cos 3\ell + 0.0784\sin 3\ell$ $+0.0479\cos 4\ell + 0.0847\sin 4\ell,$ $S_S(\ell) = 0.2090\cos\ell - 0.0133\sin\ell$ $+0.1719\cos 2\ell - 0.0214\sin 2\ell$ $-0.1071\cos 3\ell - 0.0014\sin 3\ell$ $+0.0681\cos 4\ell + 0.0519\sin 4\ell,$	
	with, for both hemispheres,	
	$C = \csc[b - b_0(\ell)] = \csc(b + 0.25° - 1.7°\sin\ell - 1.0°\cos 3\ell$	(22)
de Vaucouleurs *et al.* 1976	$E(B-V) = A_B(R+1)^{-1}$	(23)
de Vaucouleurs *et al.* 1976	$4.20 \le R + 1 \le 4.41$ for $0.3 \le (B-V) \le 1.0$	(24)
Bohlin *et al.* 1978	$E(B-V) = 2.1 \times 10^{-22} N_H \ (\mathrm{cm}^{-2})$	(25)

Table 4.4-2

Seaton's Interstellar Extinction

	Range of $1/\lambda(\mu)$	$A_\lambda/E(B-V)$
(26)	$2.70 \leq 1/\lambda \leq 3.65$	$1.56 + 1.048/\lambda + 1.01/\{(1/\lambda - 4.60)^2 + 0.280\}$
(27)	$3.65 \leq 1/\lambda \leq 7.14$	$2.29 + 0.848/\lambda + 1.01/\{(1/\lambda - 4.60)^2 + 0.280\}$
(28)	$7.14 \leq 1/\lambda \leq 10.0$	$16.17 - 3.20/\lambda + 0.2975/\lambda^2$

Values of $A_\lambda/E(B-V)$ for $1.0 \leq 1/\lambda \leq 2.7$

$1/\lambda$	$A_\lambda/E(B-V)$	$1/\lambda$	$A_\lambda/E(B-V)$
1.0	1.36	1.9	3.36
1.1	1.44	2.0	3.56
1.2	1.84	2.1	3.77
1.3	2.04	2.2	3.96
1.4	2.24	2.3	4.15
1.5	2.44	2.4	4.26
1.6	2.66	2.5	4.40
1.7	2.88	2.6	4.52
1.8	3.14	2.7	4.64

4.5 SUMMARY OF SNR AND EXPOSURE TIME CALCULATIONS

In case you lost the thread through the preceding discussion, the following summarizes the procedure for calculating FOS exposure times.

1. Decide on the SNR that will allow you to accomplish your scientific goals.
2. Estimate the counts sec^{-1} $\text{diode}^{-1} N_\lambda$ by using one of equations (1) through (7), taking $\Delta\lambda$ from Table 2.2.3-1 and E_λ from Figure 4.2-1 for the appropriate FOS configuration. If you are satisfied with a Planck distribution, use equations (4). If your object has a power law distribution, use equation (7).
3. Estimate $E(B-V)$ from equations (23) or (25) (or use an observed $E(B-V)$) to calculate A_λ with the help of Table 4.4-2. Correct N_λ for extinction by multiplying by either $10^{-0.4(A_\lambda - A_{5556})}$ or $10^{-0.4A_\lambda}$, as explained in the preceding section.
4. If you are not going to subtract the sky from your object plus sky spectrum, use equation (9) to estimate the exposure time.

5. If you plan to sky subtract, estimate the sky counts sec^{-1} $diode^{-1}$ by using equations (12) and (13) (and equation (17) if observing at wavelengths below 1350Å), and then add the dark counts sec^{-1} $diode^{-1}$ (Table 4.3-1) to the estimated background counts sec^{-1} $diode^{-1}$. Finally, use equation (11) to calculate the total exposure time.

4.6 NOISE PERFORMANCE

In order to achieve faint limiting magnitudes, extreme reduction of instrumental background noise sources is essential. The favorable pulse-height-distribution of the Digicons makes false counts due to random analog signals exceeding the discriminator threshold very rare (approximately one such false count per Hubble time). The noise sources which can be significant to the FOS are: 1) straylight, 2) fluorescence and phosphorescence due to energetic particle bombardment, 3) thermionic emission, and 4) electromagnetic interference.

The HST itself includes many safeguards against straylight—sun shield, baffles, and high quality optics. The FOS apertures limit incoming light, filters block unwanted short-wavelength photons, while internal baffling must suffice to control other straylight. Unfortunately, no measurements of stray light performance are yet possible, and predictions of straylight performance are rather uncertain. Of course, we intend and expect that for most observations straylight will not be a limiting factor. One likely exception can already be identified. Because the FOS is a single-pass spectrometer with broad wavelength sensitivity, ultraviolet spectra of very red objects may suffer some red straylight contamination. This problem will be clarified during post launch science verification by comparing FOS and HRS (solar blind) UV observations of late type stars.

The sapphire prism and the windowed detectors each contribute unwanted counts due to fluorescence and phosphorescence under energetic-particle bombardment such as will be seen in orbit. Due to this concern, we have measured the light-producing properties of the materials used to manufacture the FOS. Major lot-to-lot variations occur, so the measured samples should come from adjacent parts of the same boule if the actual flight article cannot be tested. In addition to the trapped-particle radiation, decay from materials which become radioactive under such bombardment must also be considered (primarily if it is part of the detector assembly). The sapphire prism light emission is acceptable (both particles and ultraviolet light produce fluorescence) because it is distant enough from the detectors that the direct illumination of the Digicons is small, and it is sufficiently defocused that light transmitted by the optical train is small also. The prism should never produce detectable levels of diffuse straylight background. The detectors are another matter. Fluorescence from the windows would be a major (and unacceptable) source of instrumental background if not suppressed. We use the 512-element diode array as self- anticoincidence detectors, relying on the circumstance that such bursts can be eliminated by enabling a software-selectable threshold which rejects any "INT" of data in which the sum of counts over a selected set (generally, all operational) of channels exceeds the software limit. With this burst noise rejection scheme operating, we expect fluorescence to contribute less than 0.001 count sec^{-1} $diode^{-1}$ outside the South Atlantic Anomaly (SAA). Inside the SAA, such noise may be much greater, and it may not be possible to observe at all (the software may eliminate all data if noise bursts occur too frequently).

The dominant instrumental noise is expected to be the thermionic photocathode emission from each Digicon. During HST operation, the photocathode temperatures are calculated to lie between $-10°$ C and $-28°$ C. At the warm end of this range, the red Digicon noise has been measured to lie between 0.001 and 0.0027 counts $\sec^{-1}$ diode^{-1}. At $-10°$ C, the blue detector background is about 0.0005 counts $\sec^{-1}$ diode^{-1}.

Electromagnetic disturbances, if severe enough, can cause the FOS electronics to produce spurious counts. All the HST instruments including the FOS incorporate normal good engineering practice (single-point grounds to eliminate ground loops, shielding from conducted and radiated electrical fields, *etc.*) and, of course, each instrument's production of electromagnetic interference is controlled. Additional protection for the FOS is provided by the burst-noise rejection scheme discussion above. Still, such sources of noise can only be eliminated with certainty at the HST integration level by thorough testing.

In conclusion, all instrumental background noise sources outside the SAA are expected to be less than our goal of 0.002 counts $\sec^{-1}$ diode^{-1}.

4.7 FOS PULSE COINCIDENCE CORRECTION AND DYNAMIC RANGE

The minimum detectable source levels are set by instrumental background, while the maximum accurately measurable source levels are determined by the response times of the FOS electronics. Each of the digicons has 512 independent photon counting detectors. Each of the 512 channels has its own charge sensitive preamplifier, charge to voltage converter and voltage amplifier, voltage-pulse-height discriminator, and accumulator. The digital signal from the discriminator is rate- limited by digitally gating off the electronic channel for 10.5 micro sec after accepting a pulse. This technique forces each channel to have the same input to output counting characteristics. In order to remove the nonlinearity in the relationship between the true input count rate and the observed output count rate, we assume an equation of the standard form:

$$R_{true} = \frac{R_{observed}}{1 - tR_{observed}} \text{counts s}^{-1}\text{diode}^{-1} \tag{21}$$

$$t = 9.5 \times 10^{-6} sec \qquad (R_{observed} \leq 51000) \tag{22}$$

$$t = 9.5 \times 10^{-6} + 2.607 \times 10^{-10}(R_{observed} - 51000) \qquad (R_{observed} > 51000) \tag{23}$$

In equation (21) t is the dead time and and is given by equations (22) and (23). The solid line in Figure 4.7-1 is a plot of the observed count rate versus the inferred true count rate, and shows our fit through the data using equations (21), (22), and (23). It is evident that a single time constant gives an excellent fit to the calibration data at count rates lower than 51000 $counts\ s^{-1} diode^{-1}$. At higher observed count rates the data behaves as though the photocathode is progressively limiting the photoelectric current. We have chosen to represent this turnover in the observed count rate by an increasing dead time as given in equation (23). When a true maximum rate of 10^5 is divided by the instrumental background, a large dynamic range results (at least 2.5×10^7), showing that sources over a range of 18 magnitudes in apparent luminosity can be observed with the FOS.

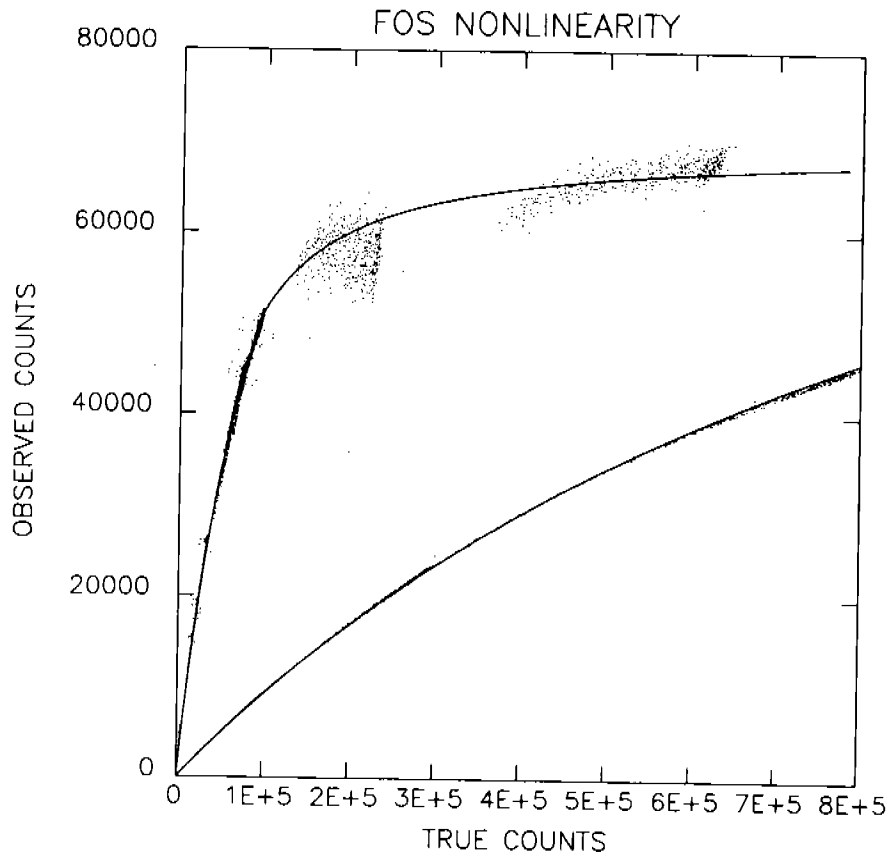

FIGURE 4.7-1. Measured count rate versus true count rate (provided by D. Lindler and R. Bohlin). The lower curve is a plot of the upper curve expanded by 10 in the x-direction.

5.0 FOS CALIBRATION OBSERVATIONS

Calibration of FOS spectra involves the following steps:

1. Correction of the observed count rates for counts lost during discriminator dead times ("paired-pulse" correction). The dead time corrections will be based on measurements made before launch.
2. Correction of the spectra for dead diodes and noisy diodes which have been turned off. This procedure, which is arithmetic and does not require a calibration observation, is possible only if "overscan" has been used (*cf.* 3.4).
3. Removal of small scale irregularities in the photocathode response by division of the spectrum with observations of smooth continuum sources.
4. Assignment of wavelengths to the pixels (*e.g.*, each 1/4-step is a pixel) by fitting polynomials to spectra of the internal calibration lamps. Although third order polynomials are used, the FOS spectra are very linear (except the prism), and the second and third order terms are small.
5. Conversion of the corrected count rate to incident flux by division with a spectral sensitivity function which has been derived from observations of stars with known flux distributions.

In order to accomplish these calibrations, the ST ScI will schedule FOS calibration observations at intervals which will be determined by the stability of FOS mechanisms, electronics, and photometric response. Calibration functions which are derived from these observations will be incorporated in the Science Operations Ground System (SOGS) and will be used for routine and automatic reduction of your data. The time required to make the necessary calibration observations will not be charged to your program. However, it does mean that your data will be reduced with calibration observations which were taken hours, days, or weeks earlier, and if appropriate, reduced by using mean calibration functions which have been derived from many observations.

The standard reductions may not be suitable for some programs. For example, if your program requires highly accurate radial velocities, you may want to use a comparison spectrum taken immediately before or after your observations at the same aperture wheel and filter-grating settings, rather than a comparison spectrum taken a week earlier. Alternatively, or additionally, you may need special observations of a radial velocity standard in order to tie your velocities into a particular radial velocity system. As another example, you might need observations of special flux standards in order to tie your spectrophotometry into a particular photometric system. If you must ask for special calibration observations, two facts should be kept in mind. First, the time required to take the special calibration observations will be charged to your program. Second, your data will still be reduced with the standard calibration functions by SOGS. In order to use your calibration observations, you must use Science Data and Analysis Software (SDAS) to create new calibration functions, which you then use to rereduce your data.

6.0 FOS DATA PRODUCTS

Your FOS observations will be given to you on magnetic tape, as hardcopy plots, and, in some instances, as pictures. The breakdown in each of the categories is given in the following sections.

6.1 MAGNETIC TAPE

The tapes will include the following data.

1) All edited raw data, including the target acquisition data. If, for example, the spectra were taken with the STAR-SKY step pattern, summed into the FOS memory at four minute intervals for thirty-two minutes, and nondestructively read at the end of each four minute sum, there will be eight pairs of spectra on the tape.
2) If you took special calibration observations (*e.g.*, spectra of the internal calibration lamps), the tape will include all raw calibration data.
3) An intermediate reduction of all the data in 1). The reduction will consist of paired pulse corrections and removal of small scale irregularities in the photocathode response. You also will be given functions for assigning wavelengths to the channels. By separating the intermediate reduction from the final reduction at this point, it should not be too difficult to recalibrate the spectra if the sensitivity functions change or improve.
4) A complete reduction of all the data in 1) to an absolute flux scale, plus the final "star plus sky" minus "sky" difference if the data was taken in a beam switching mode.
5) The calibration functions which were used to reduce the data, including:
    i) the time constants used for the paired pulse corrections.
    ii) the polynomial coefficients for wavelength calculation.
    iii) the spectra or functions used to remove small scale irregularities in the photocathode response.
    iv) the sensitivity functions.
6) An error array which shows the pixel-by-pixel noise and includes data quality flags for dead diodes and noisy diodes.

6.2 HARDCOPY

In addition to the tape, you will receive the following hardcopy.

1) A listing of all file headers which are on the tape.
2) Plots of the final "star plus sky," "sky," and difference sums for the edited raw spectra, the intermediate- reduction spectra, and the flux calibrated spectra.

6.3 PICTURES

If you used FOS imaging target acquisition, you will receive a gray scale copy of each target acquisition picture.

7.0 ACKNOWLEDGEMENTS

I am grateful to Ralph Bohlin and George Hartig for critical readings of this manual and for comments which clarified a number of technical issues. Many of the FOS performance characteristics summarized in this manual are based on long hours of hard work by Ralph and George. I am indebted to Richard Harms and Ed Beaver for much of my FOS source material, and especially for material on detector performance. Likewise, Roger Angel and Richard Allen have provided all the source material for performance of the FOS polarizer. Ross Cohen deserves special thanks for his excellent preparation of the simulated FOS observations in chapter 4. Robin Ciardullo has been the key person in the development of the FOS simulator, an extremely versatile program which has been indispensable in writing this manual. Anne Kinney has done an excellent job in producing many of the final figures and tables for the manual. I wish to thank Nolan Walborn for very carefully reading the handbook and making many suggestions which improved the style and clarity.

Last, but by no means least, the FOS Instrument Definition Team, consisting of Roger Angel, Frank Bartko, Edward Beaver, Ralph Bohlin, Margaret Burbidge, Arthur Davidsen, Holland Ford, Richard Harms (Principal Investigator), and Bruce Margon, has put an enormous effort into building and calibrating the FOS.

REFERENCES

Allen, R.G. and Angel, J.R.P. 1982, *Proc. SPIE (Instrumentation in Astronomy IV)*, **331**, 259

Bohlin, R.C. 1984, *IUE NASA Newsletter No. 26*

Bohlin, R.C., Savage, B.D. and Drake, J.F. 1978, *Ap. J.*, **224**, 132

Cleary, M.N., Heiles, C. and Haslam,C.G. 1979, *Astron. Astrophys. Suppl.*, **36**, 95

de Vaucouleurs, G., de Vaucouleurs, A., and Corwin, Jr., H.G. 1976, *Second Reference Catalogue of Bright Galaxies* (University of Texas Press:Austin and London)

Gunn, J.E. and Oke, J.B. 1975, *Ap. J.*, **195**, 255

Harms, R. J., Angel, R., Bartko, F., Beaver, E., Bloomquist, W., Bohlin, R., Burbidge, E. M., Davidsen, A. F., Flemming, J. C., Ford, H., and Margon, B., 1979, *SPIE Vol.* **183** *Space Optics*, 74

Harms, R. J. 1982, *The Space Telescope Observatory*, ed. D.N.B. Hall, (Special Session of Commission 44, IAU General Assembly, Patras, Greece, August, 1982; NASA CP-2244)

Hayes, D.S. and Latham, D.W. 1975, *Ap. J.*, **197**, 593

Heck, A., Egret, D., Jaschek, M., and Jaschek, C. 1984, *ESA Document SP-1052* (ESA Scientific and Technical Publications Branch, ESTEC, Noordwijk, The Netherlands

Heiles, C. 1976, *Ap. J.*, **204**, 379

Jacoby, G.H., Hunter, D.A., and Christian, C.A. 1984, *Ap. J. Suppl.*, **56**, 257

Johnson, H.M. 1979, *Ap. J.*, **230**, L137

Kaler, J.B. 1976, *Ap. J. Suppl.*, **31**, 517

Levasseur-Regourd, A.C. and Dumont, R. 1980, *Astron. Astrophys.*, **84**, 277

Lillie, C.F. and Witt, A.N. 1976, *Ap. J.*, **208**, 64

Paresce, F. and Volpe, R. 1984, *The Background Radiation Model for the Space Telescope*

Schild, R. and Oke, J.B. 1971, *Ap. J.*, **169**, 209

Seaton, M.J. 1979, *M.N.R.A.S.*, **187**, 73P

Sirk, M. and Bohlin, R. 1985, *FOS Wavelength Calibration (STScI FOS Calibration Report, Jan. 1985*

Whitford, A.E. 1971 *Ap. J.*, **169**, 215

Witt, A.N. 1968 *Ap.J.*, **152**, 59

Wu, C.C., Ake, T.B., Boggess, A., Bohlin, R.C., Imhoff, C.L., Holm, A.V., Levay, Z.G., Panek, R.J., Schiffer, F.H., and Turnrose, B.E. 1983, *IUE NASA Newsletter No. 22*

APPENDIX A

FOS Wavelength Calibration

M. SIRK and R. BOHLIN
SPACE TELESCOPE SCIENCE INSTITUTE

Instrument Science Report **Jan–85**
Revised **Jun–85**

Two internal Pt–Cr–Ne vacuum data sets obtained using the 0.1 arcsec (A4) lower aperture were available for wavelength calibrations. Third order polynomials were fit to all gratings except G160H on the red side which had too few unblended reference lines to properly constrain a cubic fit. Figures 1 through 7 are the FOS spectra used for this analysis. Figure 8 shows typical systematic residuals for a linear fit to grating G270H (bottom plot) and motivates the use of a cubic fit (upper plot). The coefficients of the polynomial fit for all gratings and the prism are listed in Table 1 for the red Digicon and in Table 2 for the blue Digicon. Table 3 lists the wavelength range and average dispersion for each disperser. The RMS scatter of the residuals for the high dispersion gratings ranges from .023 pixels to .054 pixels on the blue side and from .023 pixels to .041 pixels on the red side (see Tables 1 and 2, and Fig. 8). The RMS scatter for grating G160L is about .067 pixels for both sides and for G650H it is .073 pixels on the blue side and .022 on the red side. The prism was fit by a fourth order expansion in $1/x$ with a RMS residual of 0.11 and 0.13 pixels for the red and blue tube, respectively (see Figs. 9 and 10). For gratings G270H and G400H there is a systematic residual in the fits for the blue detector. Fifth order polynomials only reduced the RMS error from .038 pixel to .031 pixel for G270H and from .047 pixel to .035 pixel for G400H. A scatter diagram depicting the residuals from G270H and G400H on the blue side of the July 19 vacuum data vs. the residuals of the July 13 vacuum data shows a very strong correlation (R=0.915, see Fig. 11). Since this systematic error is present in

four different blue spectra taken with two different gratings and at two different FOS operating temperatures, non–uniform spacing of the diode elements may be the source of the systematic errors at the few micron level.

Changes in the dispersion relations due to the use of all apertures other than the A4 lower will be deferred to the aperture offset report.

Figure Captions

Figures 1 through 7. FOS calibration spectra. All spectra are obtained with the 0.1 arcsec (A4) aperture. The lines that are used for the wavelength calibrations are labeled with their air wavelengths in Å except for gratings G130H and G190H which are labeled with vacuum wavelengths (Fig. 1). All wavelengths are converted to vacuum wavelengths before the dispersion relation calculations are performed. Grating spectra of G190H, G270H, and G400H for the red tube are not shown since they are nearly identical to the blue tube spectra.

Figure 8. The upper plot shows the residuals of a cubic fit in pixels vs. wavelength for grating G270H, red Digicon. The residuals are fairly randomly distributed with the majority confined to $\pm.04$ pixels. The lower plot shows the residuals of a linear fit to the same data. Note the systematic curvature which motivates the use of cubic fits.

Figure 9. Wavelength as a function of pixel number for the prism, blue Digicon. The points are the measured pixel values and the curve is the non–linear least squares fit to the points.

Figure 10. Plot of residuals from the fourth order expansion in $1/x$ vs. wavelength for the prism, blue detector.

Figure 11. Scatter diagram of the residuals for the two independent vacuum data sets, blue detector. The cubic residuals (in pixels) from gratings G270H and G400H from the July 19 data are plotted against the cubic residuals from the July 13 data. Note the very strong correlation ($R = .915$).

TABLE 1
Red Tube Dispersion coefficients

16 JULY 84

GRATING	A	B	C	D	SIGMA(px)
G190H	2322.513	-1.45718	6.58573E-6	4.43439E-9	.032
G270H	3292.711	-2.07717	7.25595E-6	1.07575E-8	.028
G400H	4802.383	-3.04342	5.40444E-6	1.91643E-8	.023
G570H	6849.174	-4.42790	1.04729E-5	2.16783E-8	.030
G780H	9259.337	-5.79737	-2.36782E-5	8.16690E-8	.023
G160L	2473.402	-6.95873	0.0	0.0	.067
G650L	8904.327	-25.1923	1.05742E-3	-1.52250E-6	.018

17 JULY 84

G190H	2322.212	-1.45708	2.20500E-6	1.10397E-8	.041
G270H	3292.243	-2.07911	1.05702E-5	7.67617E-9	.029
G400H	4802.257	-3.04698	1.51817E-5	6.74792E-9	.022
G570H	6848.519	-4.43086	1.67005E-5	1.26003E-8	.032
G780H	9261.217	-5.79513	-3.58795E-5	9.19218E-8	.023
G160L	2471.840	-6.96511	0.0	0.0	.067
G650L	8895.502	-25.1598	8.08459E-4	-1.13636E-6	.022

PRISM 16 JULY 84

X_o	A_o	A_1	A_2	A_3	A_4
525.911	1042.83	-1.65523E+5	-2.50311E+6	-9.58158E+7	+8.46986E+8

SIGMA=0.11px

PRISM 17 JULY 84

525.292	1036.08	-1.66333E+5	-2.48682E+6	-9.09195E+7	+9.200415E+8

SIGMA=0.10px

$$\lambda_G = A + B(px) + C(px)^2 + D(px)^3$$

$$\lambda_P = A_0 + \frac{A_1}{(px - X_0)} + \frac{A_2}{(px - X_0)^2} + \frac{A_3}{(px - X_0)^3} + \frac{A_4}{(px - X_0)^4}$$

TABLE 2

Blue Tube Dispersion Coefficients

13 JULY 84

GRATING	A	B	C	D	SIGMA(px)
G130H	1090.385	0.99652	4.86964E-5	-7.13150E-8	.023
G190H	1575.250	1.47056	3.43885E-5	-7.55204E-8	.036
G270H	2226.658	2.10005	3.62150E-5	-9.35269E-8	.038
G400H	3244.323	3.07613	5.53993E-5	-1.38085E-7	.047
G570H	4583.391	4.47959	5.72694E-5	-1.73970E-7	.048
G160L	-838.888	5.32069	3.93095E-3	-3.12077E-6	.069
G650L	-3854.154	24.4235	3.18666E-3	-3.79766E-6	.073

19 JULY 84

G130H	1090.334	1.00116	3.31290E-5	-5.59020E-8	.026
G190H	1575.893	1.47067	3.37199E-5	-7.58713E-8	.032
G270H	2227.256	2.10037	3.29076E-5	-8.94733E-8	.042
G400H	3248.346	3.07326	6.82611E-5	-1.56275E-7	.054
G570H	4588.035	4.47360	1.00810E-4	-2.68694E-7	.045
G160L	-954.675	6.15569	2.02297E-3	-1.68022E-6	.061
G650L	-3837.019	24.3629	3.43342E-3	-4.09577E-6	.066

PRISM 13 JULY 84

X_o	A_o	A_1	A_2	A_3	A_4
3.05910	1135.29	1.34469E+5	-1.63028E+6	2.74478E+7	-8.24012E+7

SIGMA=0.13px

PRISM 19 JULY 84

1.07279	1126.15	1.36901E+5	-1.65014E+6	3.07381E+7	-7.69851E+7

SIGMA=0.13px

TABLE 3

WAVELENGTH COVERAGE OF FOS DISPERSERS AND AVERAGE DISPERSIONS WITH MAXIMUM DEVIATIONS FROM THE MEAN.

RED TUBE

GRATING	LOW(Å)	HIGH(Å)	DISP(Å/px)	MAX DEV(%)
G190H	1573[b]	2323	-1.4527	.385
G270H	2225	3293	-2.0707	.442
G400H	3237	4802	-3.0357	.411
G570H	4571	6849	-4.4170	.370
G780H	6274	9259[g]	-5.7882	.511
L160L	1600[b] (px126)	2473[c]	-6.9587	0.0
G650L	3850 (px202)	8904[d]	-25.0509	.599
PRISM	1850[e] (px332)	8950[g] (px497)		

BLUE TUBE

G130H	1150[a] (px60)	1608	1.0027	1.16
G190H	1575	2332	1.4680	1.46
G270H	2227	3306	2.0942	1.40
G400H	3244	4827	3.0685	1.38
G570H	4583	6885[f]	4.4636	1.33
G160L	1150[a] (px318)	2523[c]	6.5023	2.43
G650L	3530 (px296)	9910[d,f]	25.0435	2.56
PRISM	1850[e] (px175)	5500[f] (px25)		

All wavelengths are for the extreme pixel values of 0 and 516 except as noted.

[a] MgF_2 cutoff is at 1150Å.

[b] The red tube's quartz window begins to attenuate strongly below 1750Å. See the absolute photometric calibration curves for the amount of attenuation.

[c] Second order overlaps first order longward of 2300Å.

[d] Second order overlaps first order longward of 7900Å.

[e] Sapphire cutoff is 1650Å, but because of the large dispersion of the prism at the shortest wavelengths, the effective cutoff is longward of 1650Å (see the absolute photometric calibration).

[f] Blue tube attenuates strongly above 5500Å.

[g] Red tube attenuates strongly above 8950Å.

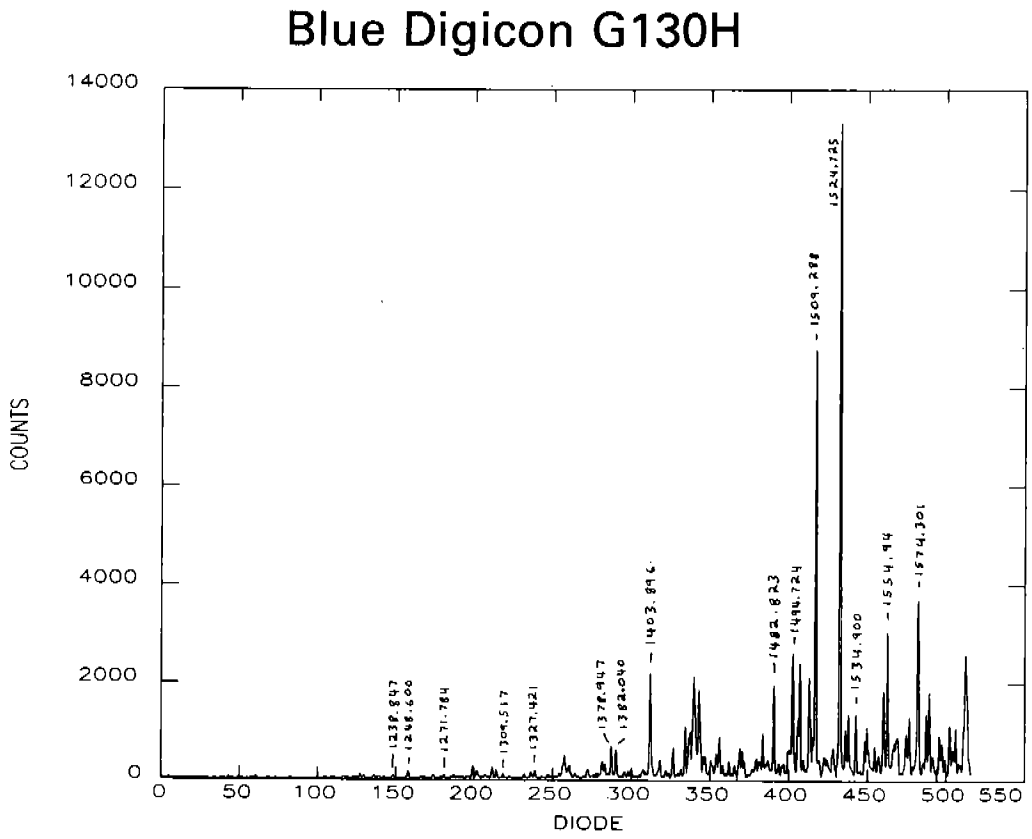
Blue Digicon G130H
COUNTS
DIODE
0
2000
4000
6000
8000
10000
12000
14000
0
50
100
150
200
250
300
350
400
450
500
550
1239.847
1246.606
1271.784
1305.517
1327.421
1378.947
1382.040
1403.896
1482.823
1494.724
1509.288
1524.735
1534.900
1554.194
1674.301

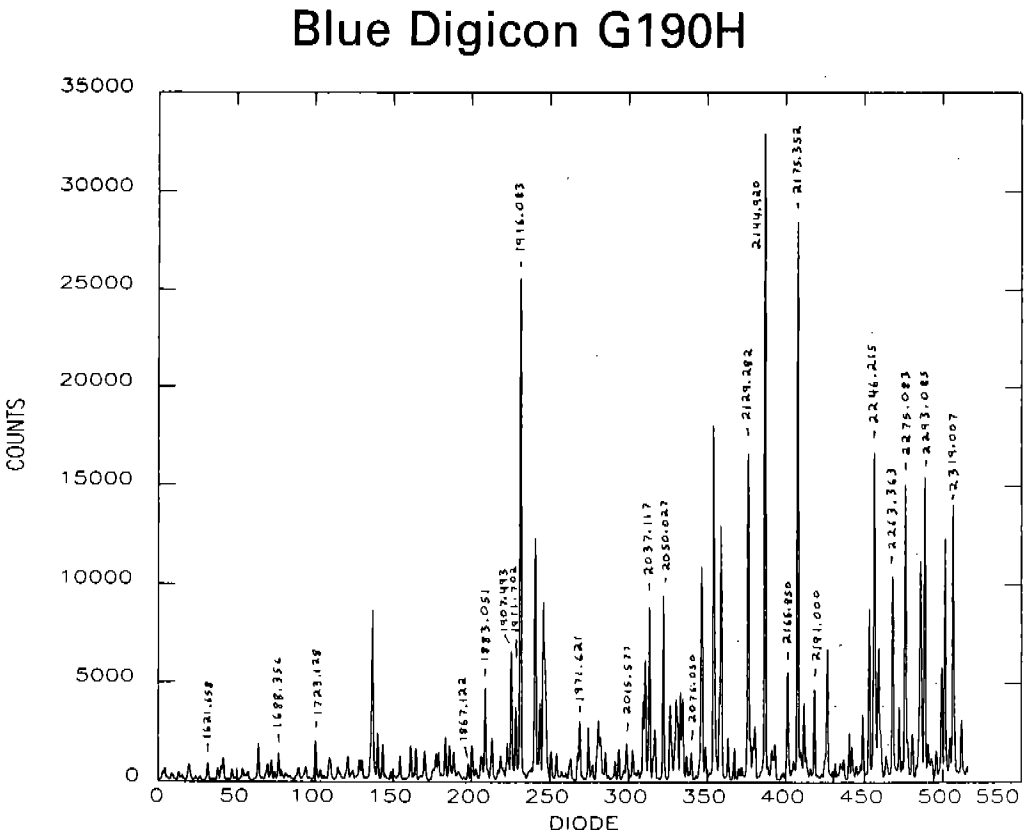
Blue Digicon G190H
COUNTS
DIODE
0
5000
10000
15000
20000
25000
30000
35000
0
50
100
150
200
250
300
350
400
450
500
550
1621.658
1688.356
1723.158
1867.122
1883.051
1907.493
1916.083
1971.621
2016.577
2037.117
2050.027
2076.050
2129.292
2144.920
2166.850
2175.352
2191.000
2243.085
2276.083
2319.007

Figure 1.

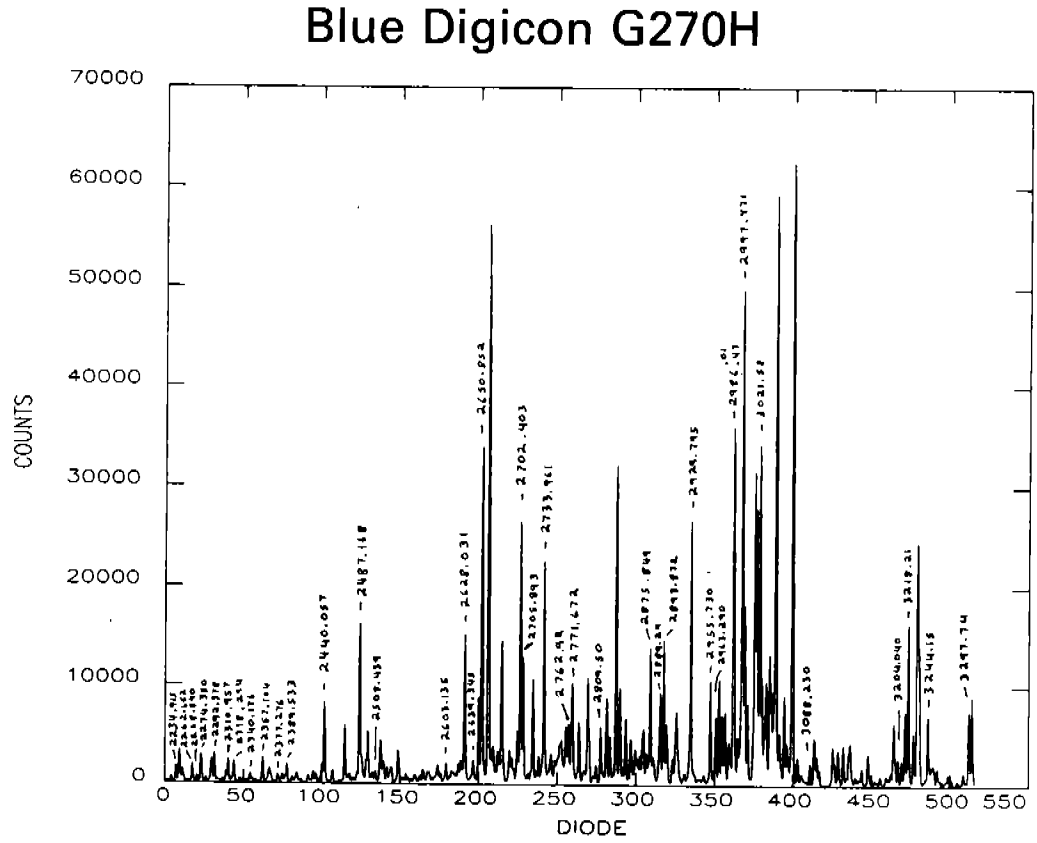
Blue Digicon G270H
COUNTS
DIODE
0
10000
20000
30000
40000
50000
60000
70000
0
50
100
150
200
250
300
350
400
450
500
550

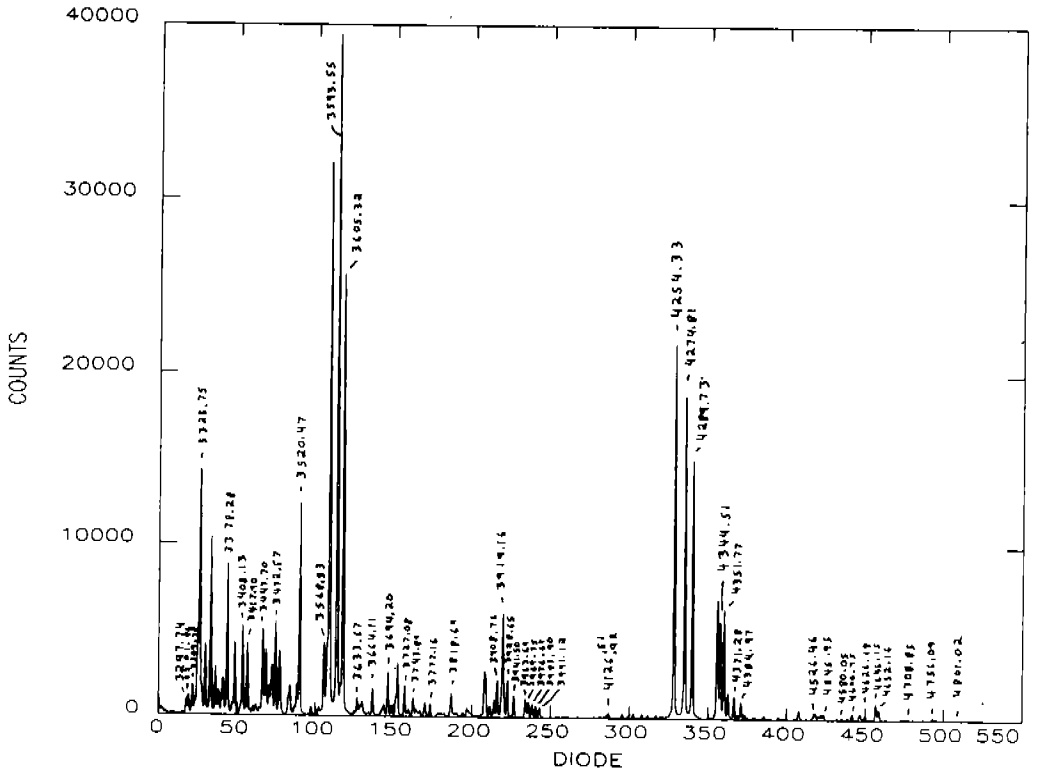
Blue Digicon G400H
COUNTS
DIODE
0
10000
20000
30000
40000
0
50
100
150
200
250
300
350
400
450
500
550

Figure 2.

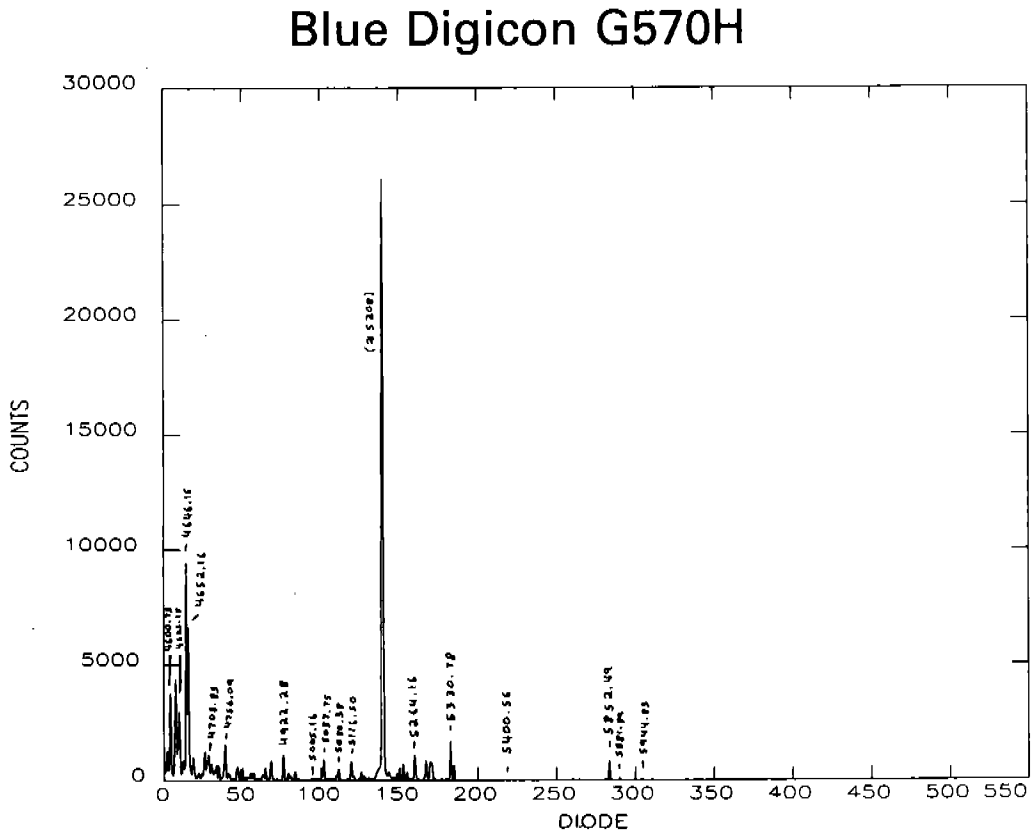
Blue Digicon G570H
30000
25000
20000
15000
10000
5000
0
COUNTS
0
50
100
150
200
250
300
350
400
450
500
550
DIODE

Figure 3.

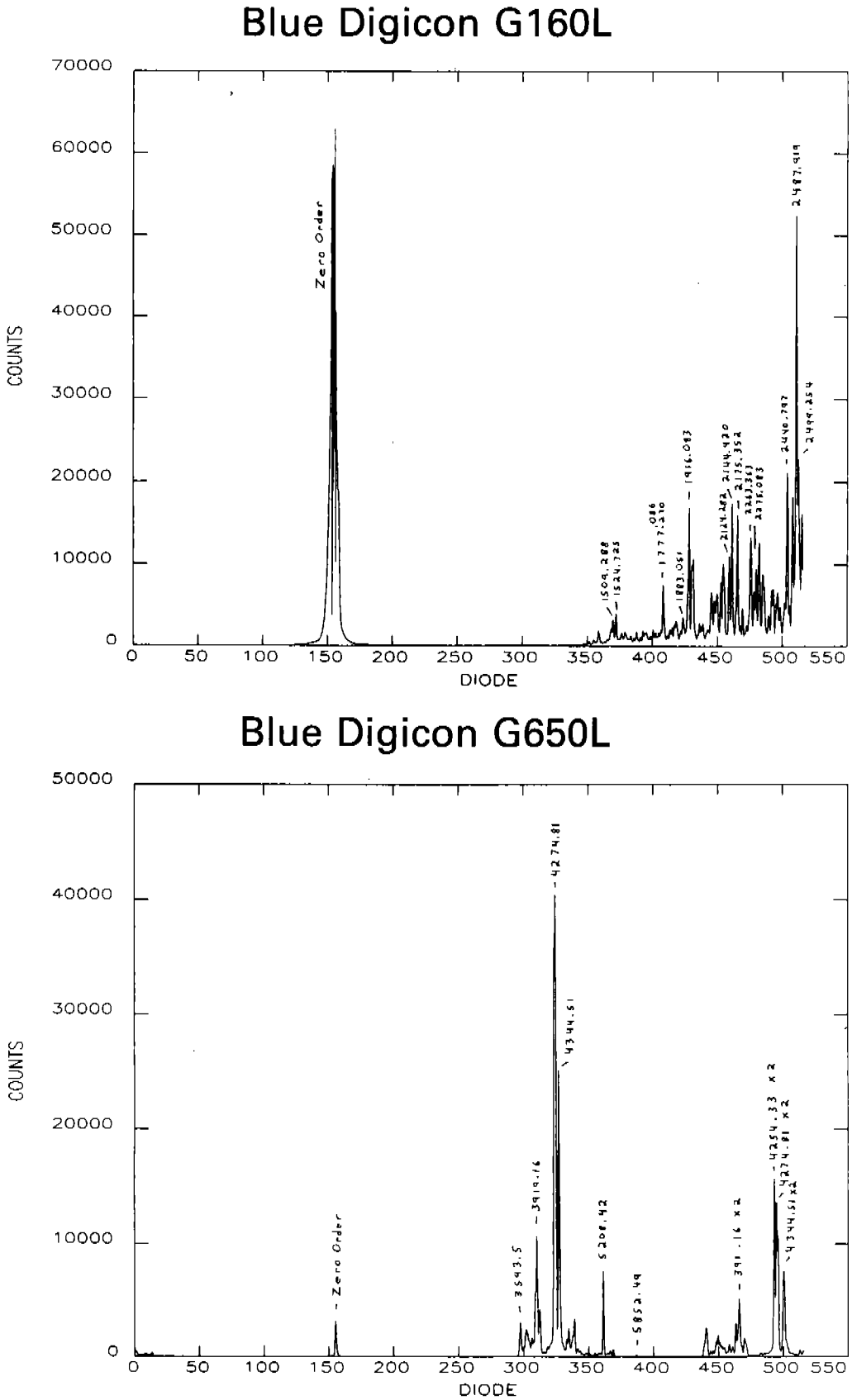
Blue Digicon G160L
COUNTS
DIODE
Zero Order
Blue Digicon G650L
COUNTS
DIODE
Zero Order

Figure 4.

Blue Digicon Prism

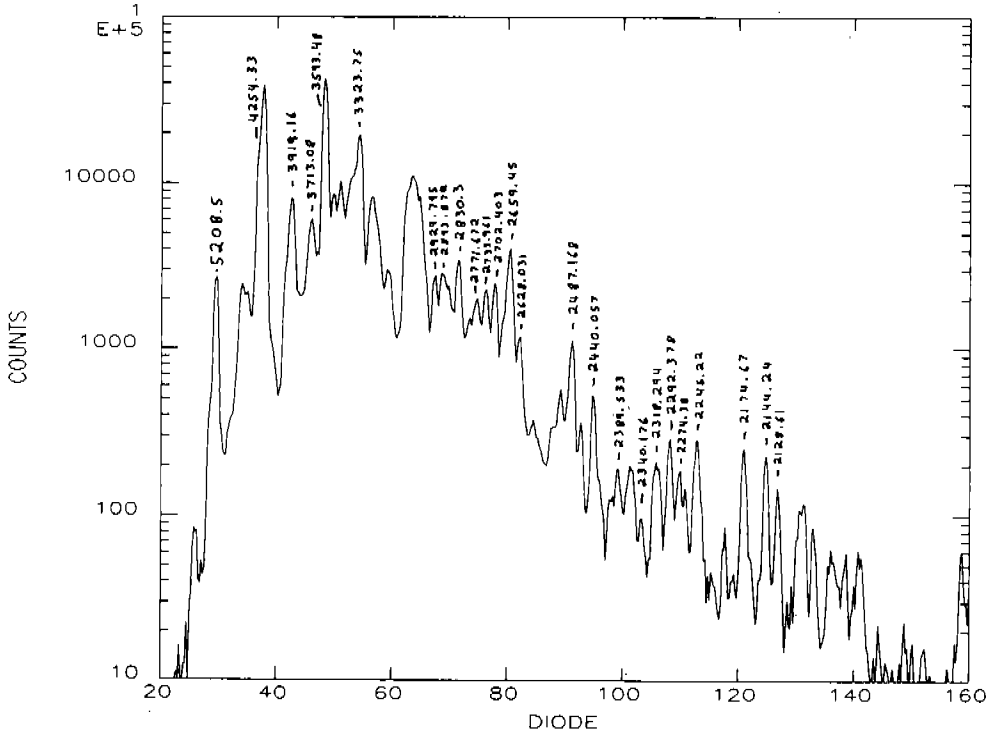

Red Digicon Prism

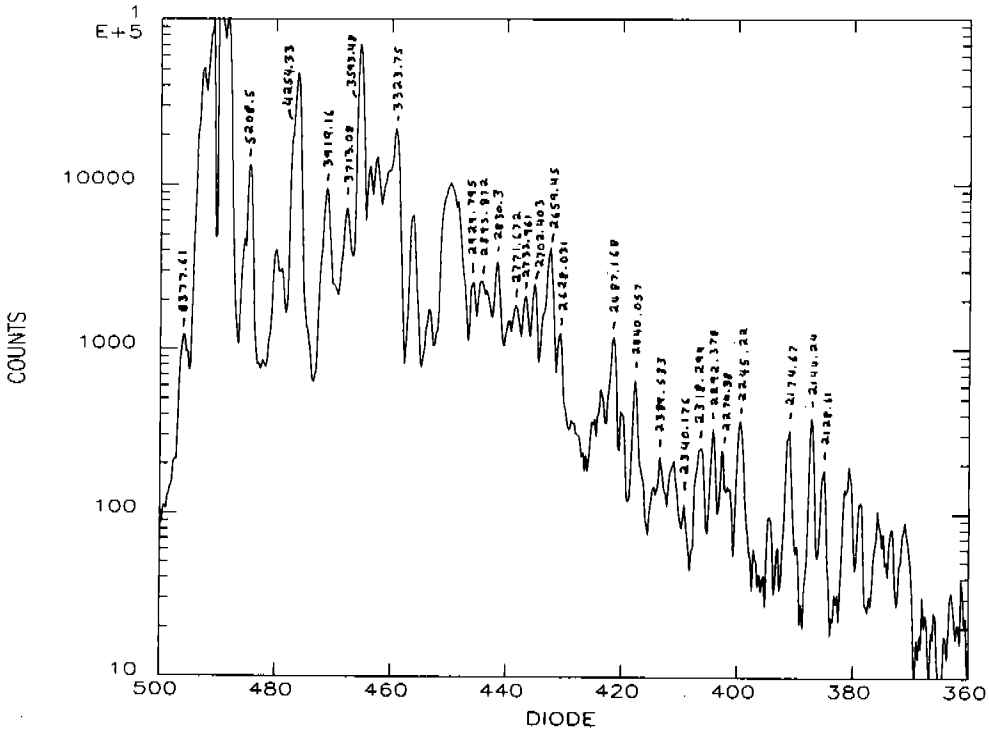

Figure 5.

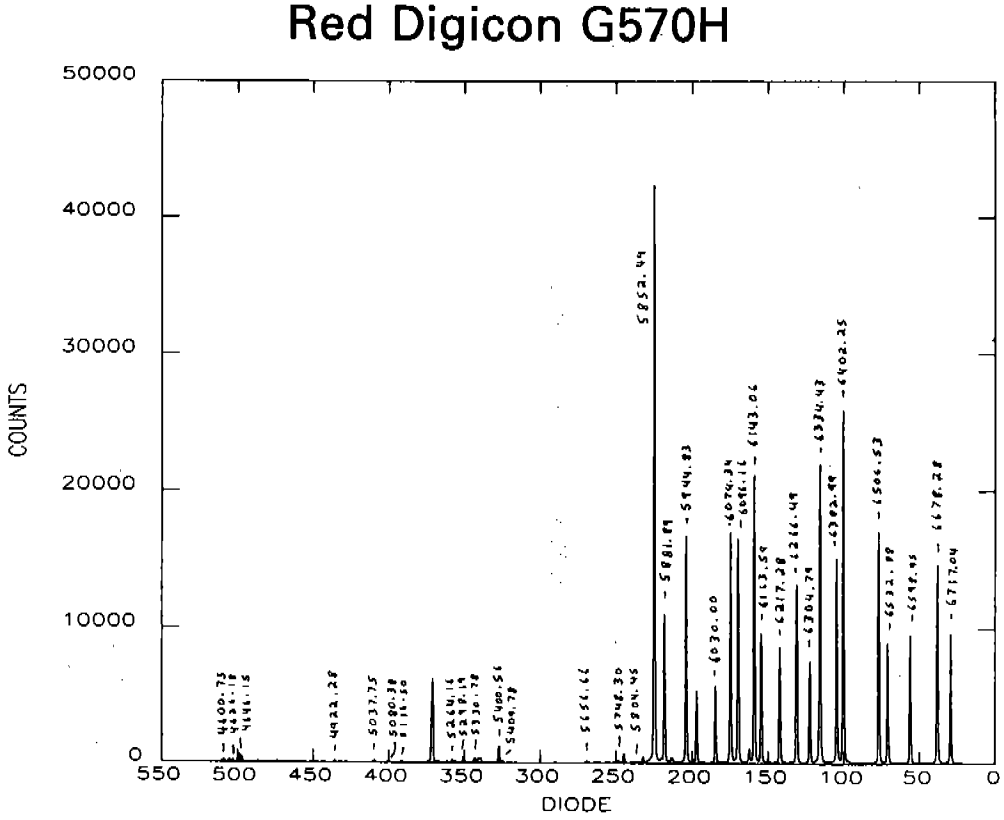
Red Digicon G570H
COUNTS
DIODE
50000
40000
30000
20000
10000
0
550
500
450
400
350
300
250
200
150
100
50
0

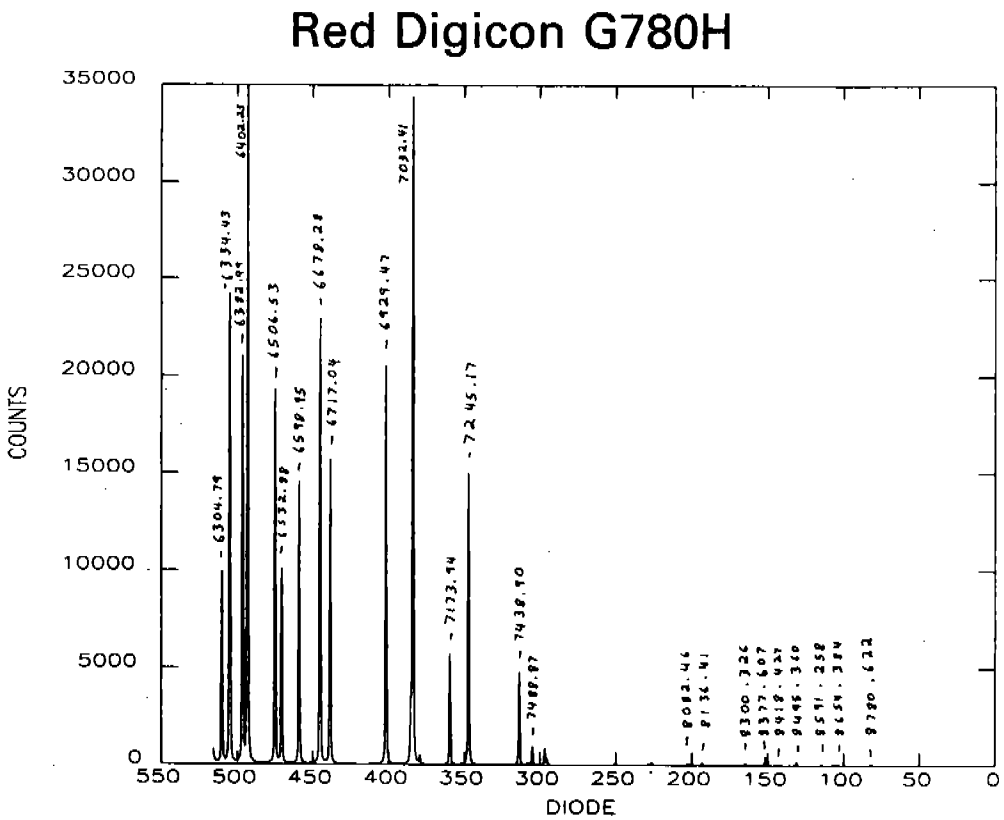
Red Digicon G780H
COUNTS
DIODE
35000
30000
25000
20000
15000
10000
5000
0
550
500
450
400
350
300
250
200
150
100
50
0

Figure 6.

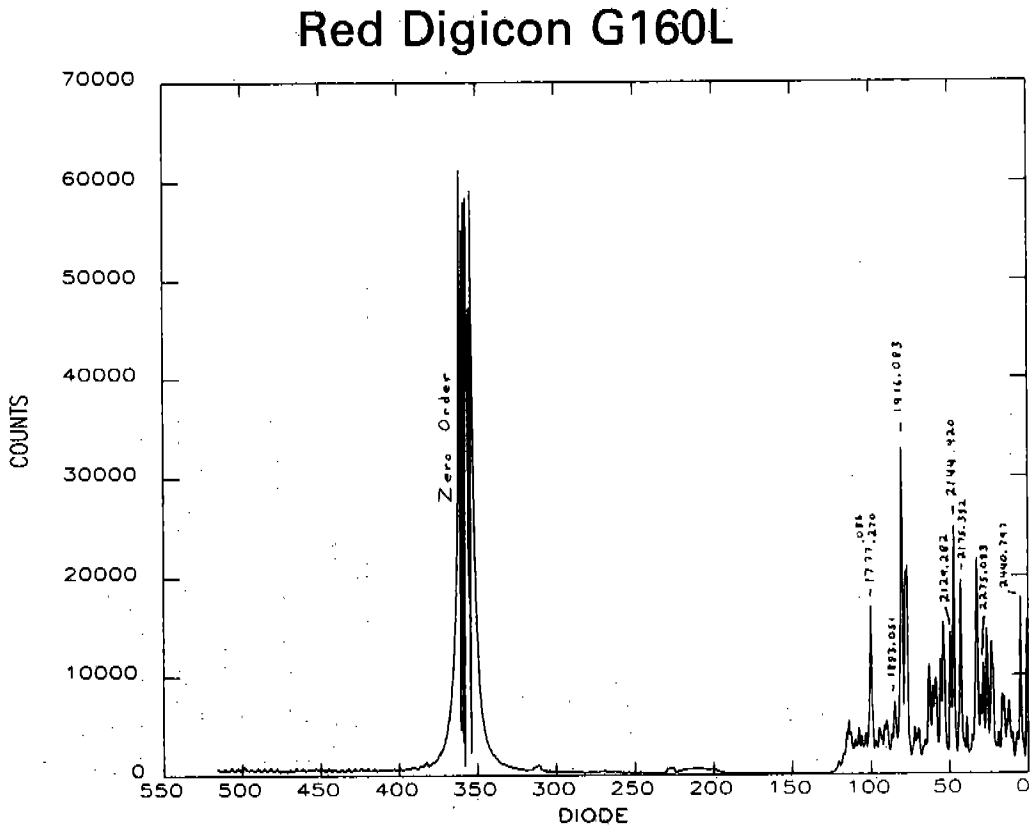
Red Digicon G160L
COUNTS
DIODE
Zero Order
70000
60000
50000
40000
30000
20000
10000
0
550
500
450
400
350
300
250
200
150
100
50
0

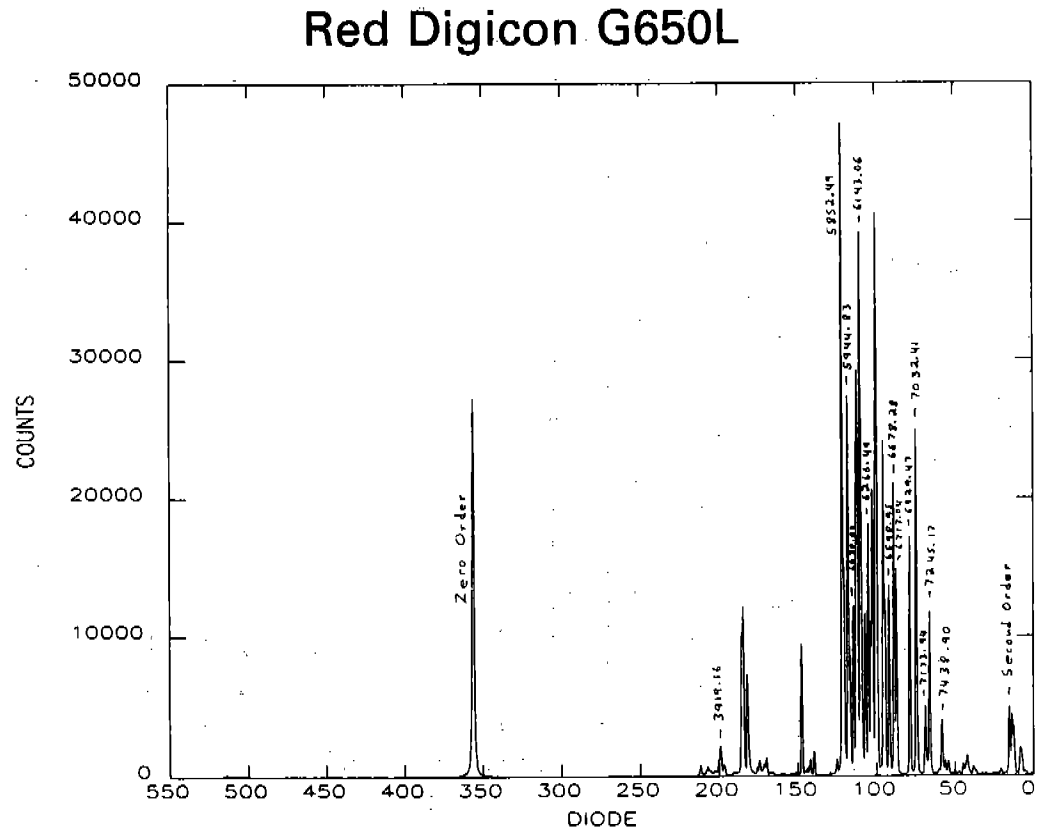
Red Digicon G650L
COUNTS
DIODE
Zero Order
Second Order
50000
40000
30000
20000
10000
0
550
500
450
400
350
300
250
200
150
100
50
0

Figure 7.

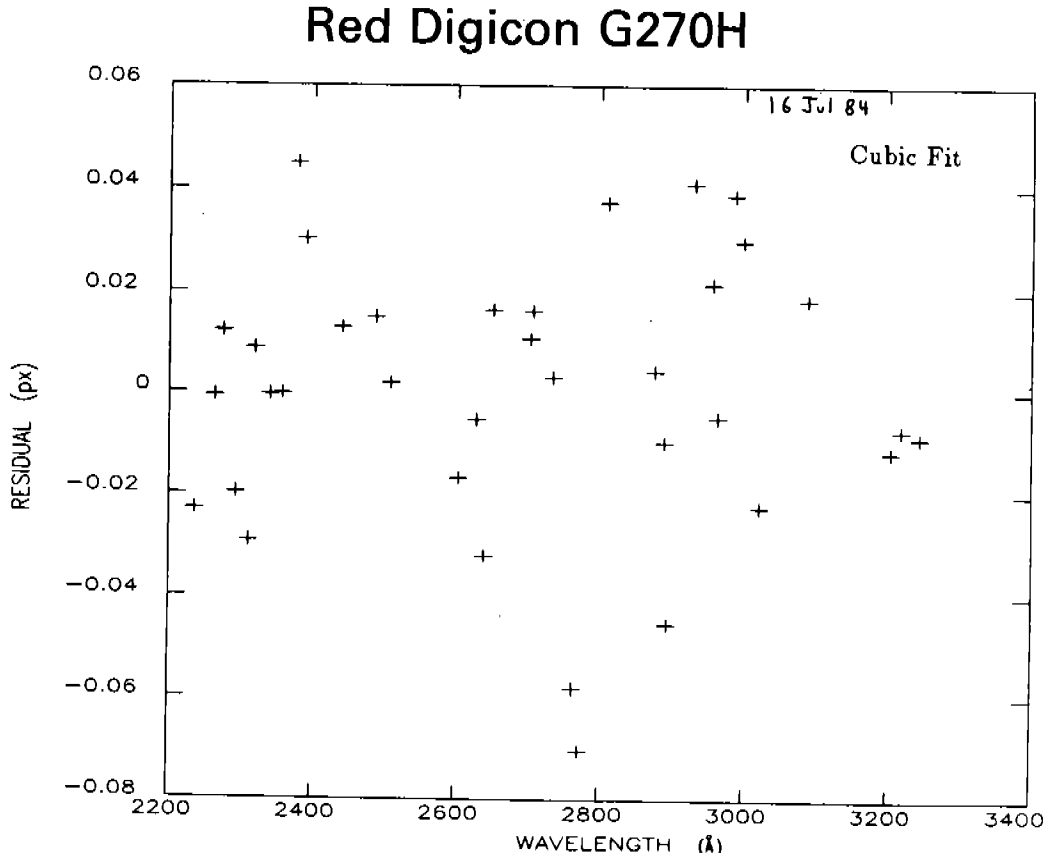
Red Digicon G270H
16 Jul 84
Cubic Fit
RESIDUAL (px)
0.06
0.04
0.02
0
−0.02
−0.04
−0.06
−0.08
2200
2400
2600
2800
3000
3200
3400
WAVELENGTH (Å)

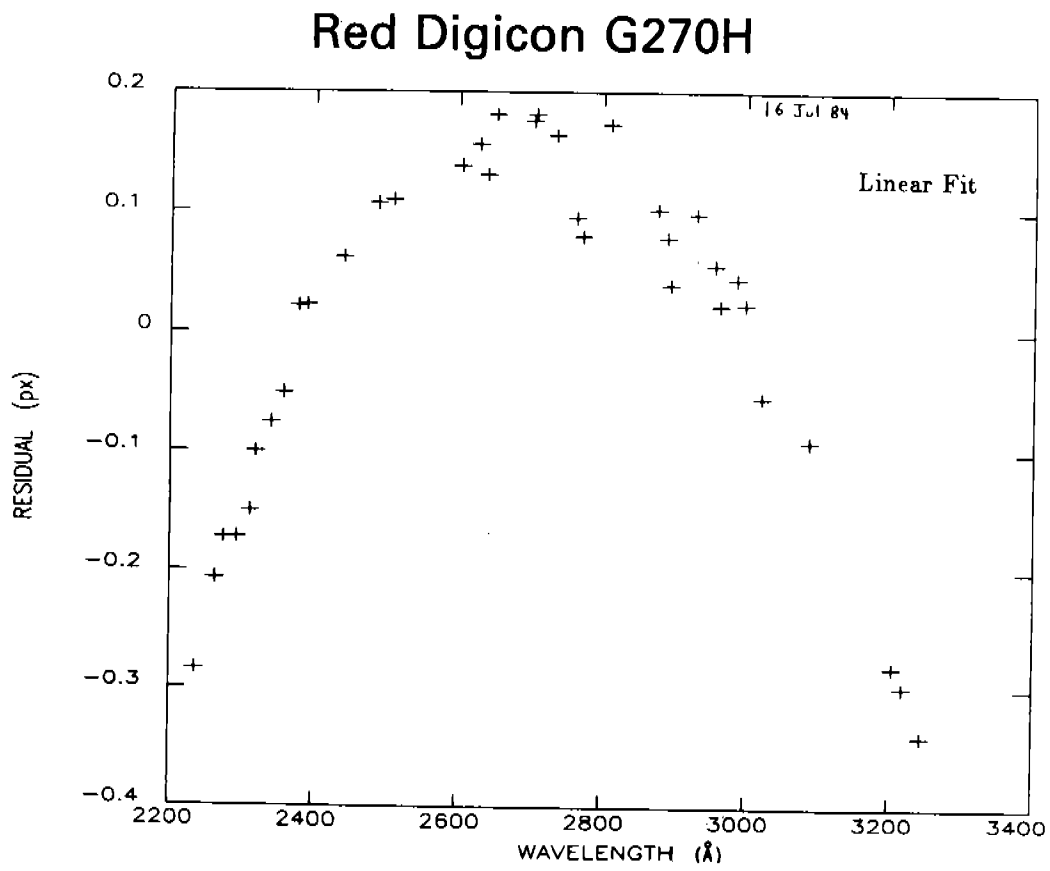
Red Digicon G270H
16 Jul 84
Linear Fit
RESIDUAL (px)
0.2
0.1
0
−0.1
−0.2
−0.3
−0.4
2200
2400
2600
2800
3000
3200
3400
WAVELENGTH (Å)

Figure 8.

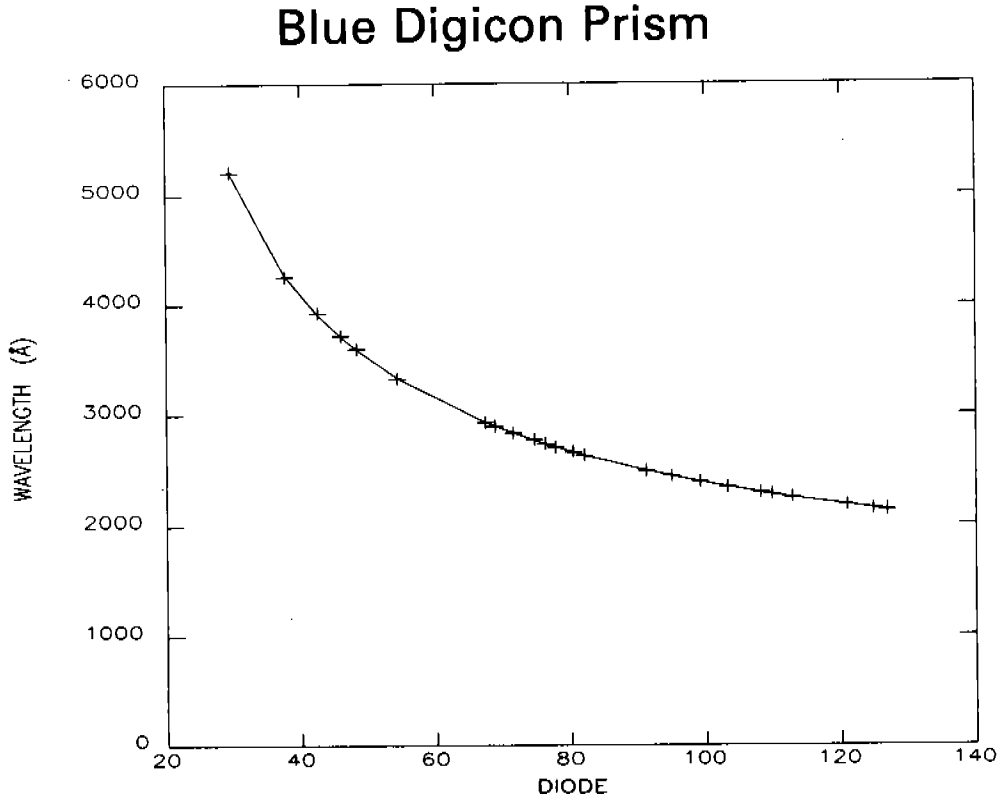

Figure 9.

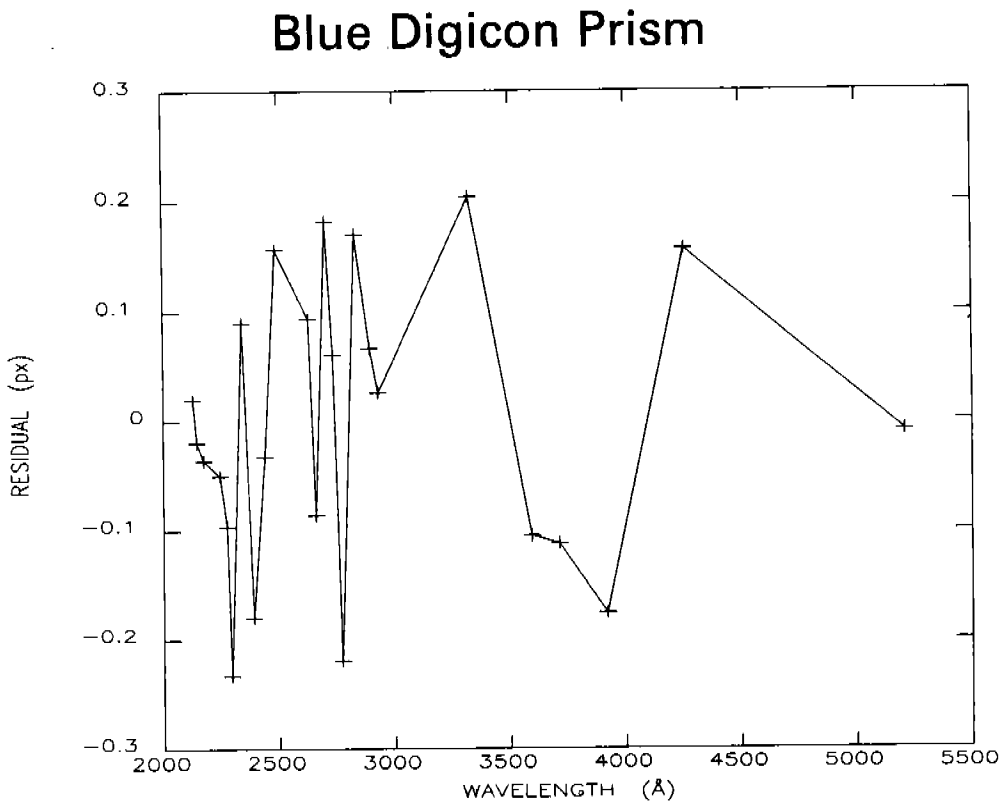

Figure 10.

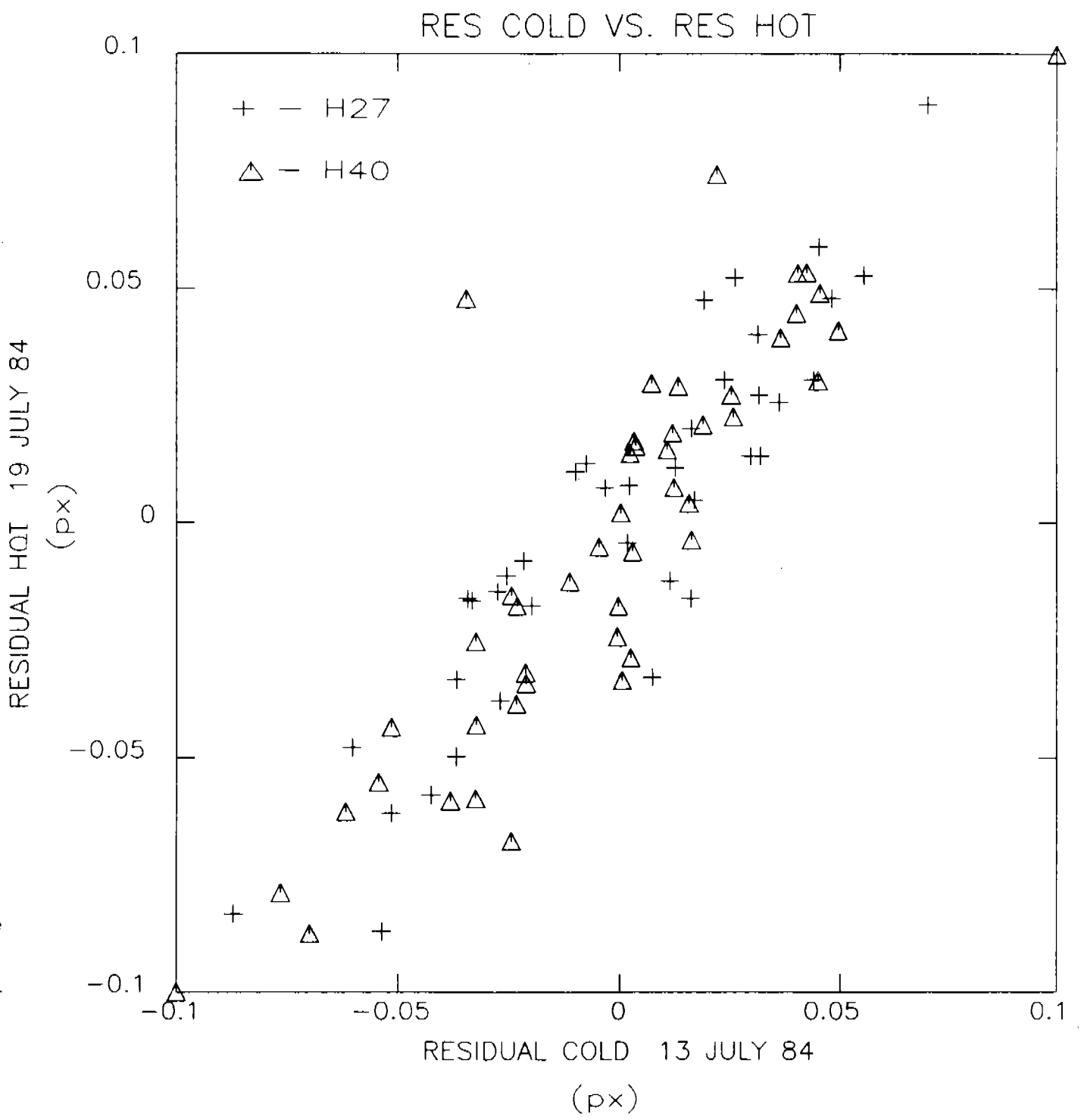
RES COLD VS. RES HOT
+ — H27
△ — H40
0.1
0.05
0
−0.05
−0.1
−0.1
−0.05
0
0.05
0.1
RESIDUAL HOT 19 JULY 84
(px)
RESIDUAL COLD 13 JULY 84
(px)

Figure 11.

APPENDIX B
FOS Optical Components Calibrations

The following pages present the spectral reflectivities and transmissions of the FOS optical components. The reflectivities of the grazing incidence mirrors, collimators, and gratings were measured in Arthur Davidsen's laboratory at the Johns Hopkins University. George Hartig has subsequently reviewed and checked the records of the original measurements. Unfortunately, the product of the efficiencies of the individual components times the measured quantum efficiency of the digicon detectors predicts a net FOS sensitivity which is approximately 40% higher than the net sensitivity measured during the preflight calibration.

PRISM

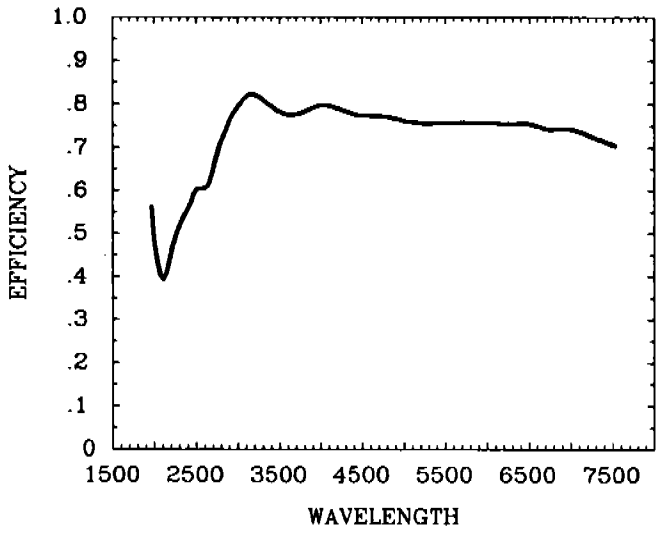

GRAZING INCIDENCE MIRROR

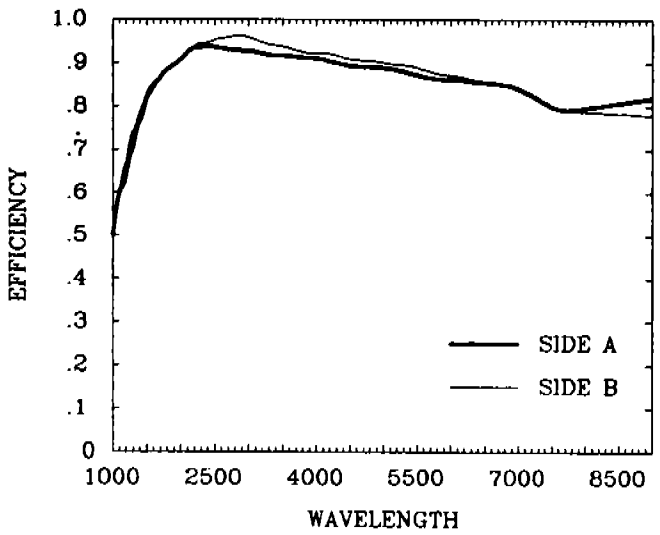

COLLIMATOR

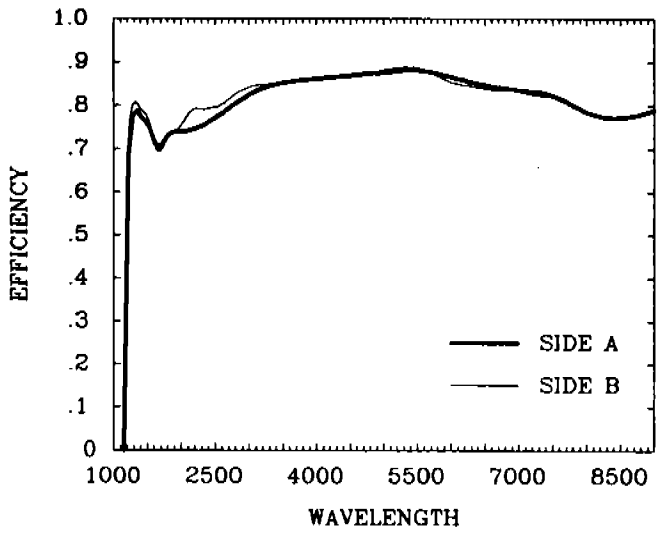

ASSUMED SPACE TELESCOPE EFFICIENCY

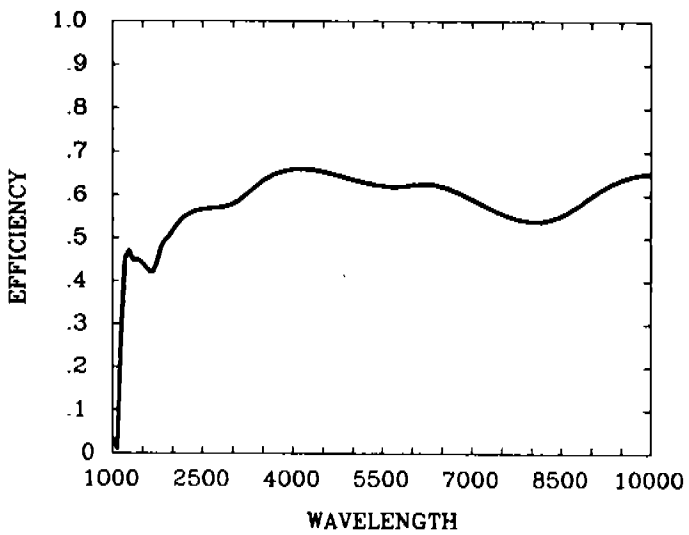

FOS COMPONENT CALIBRATIONS

SCHOTT WG305 BLOCKING FILTER

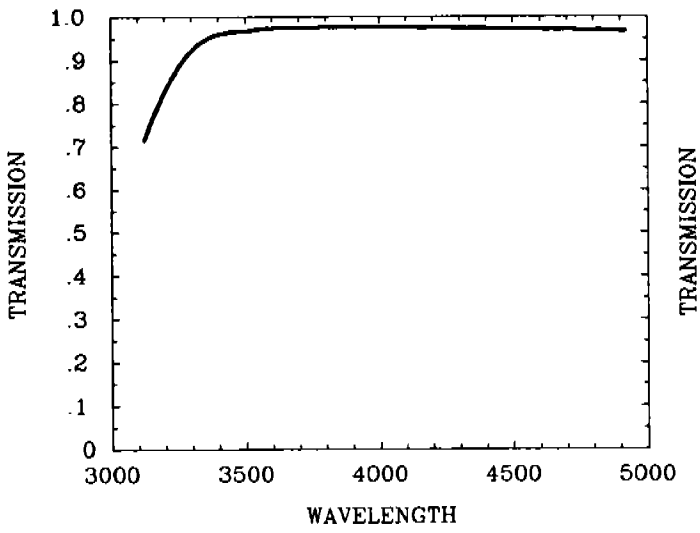

GG375 BLOCKING FILTER

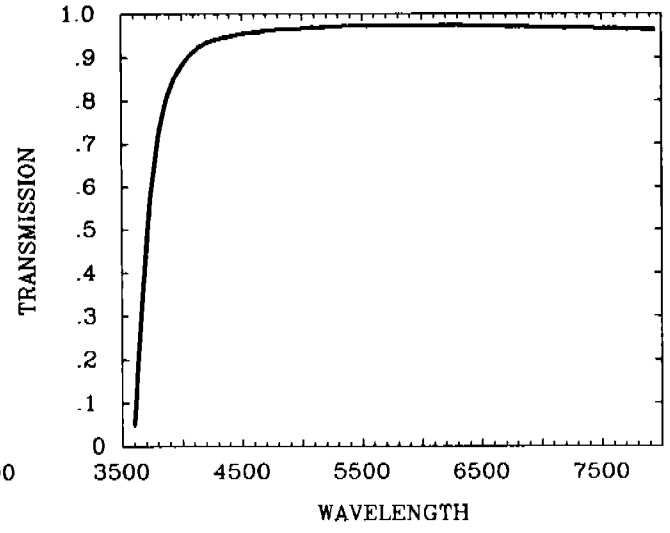

OG530 BLOCKING FILTER

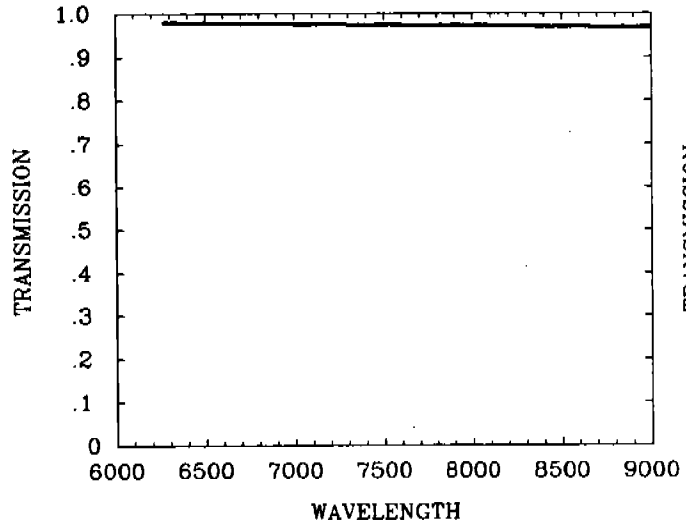

ULTRAVIOLET BLOCKING FILTER

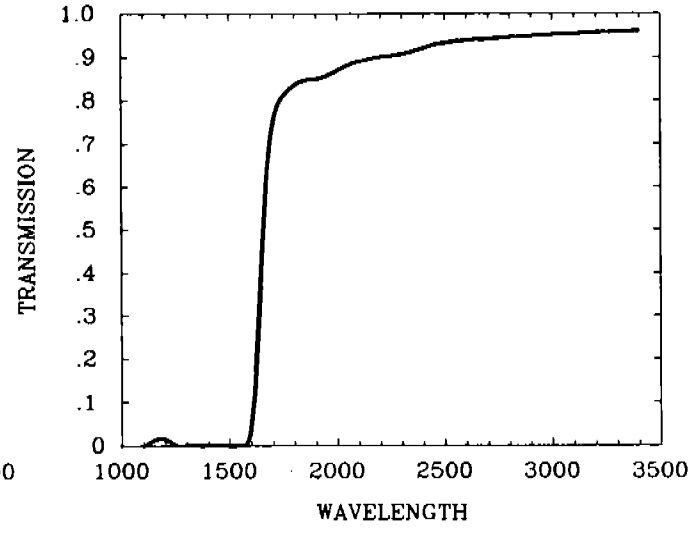

FOS FILTER CALIBRATIONS

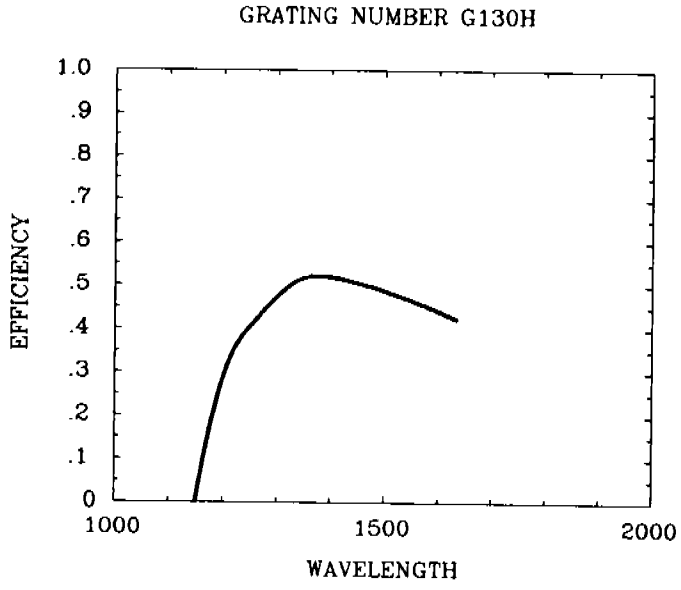

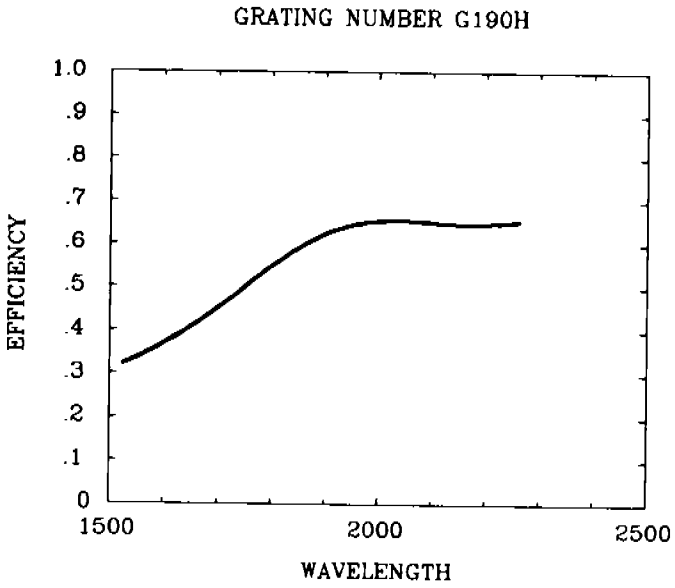

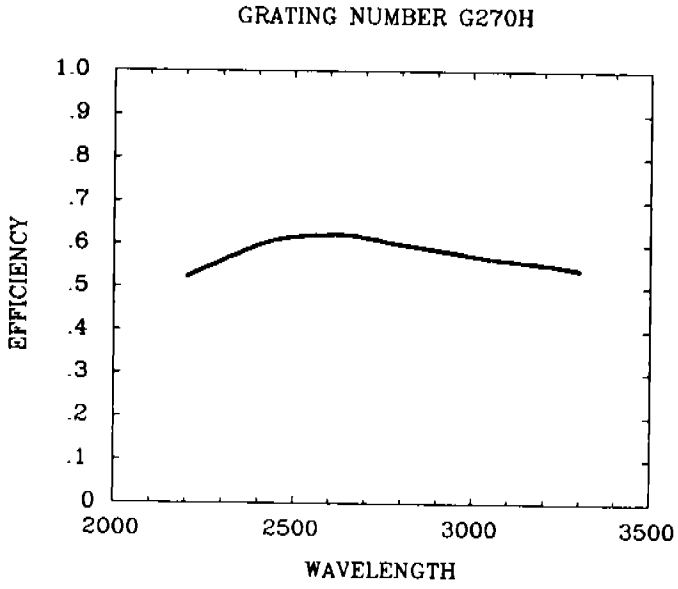

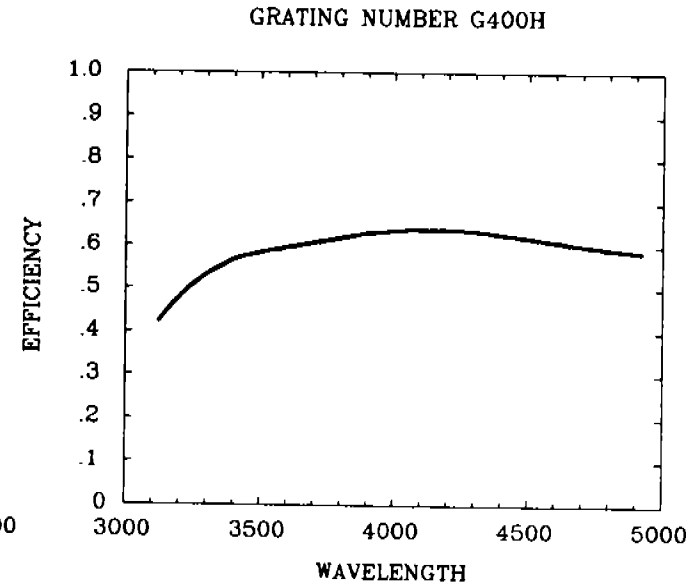

FOS GRATING CALIBRATIONS

GRATING NUMBER G570H

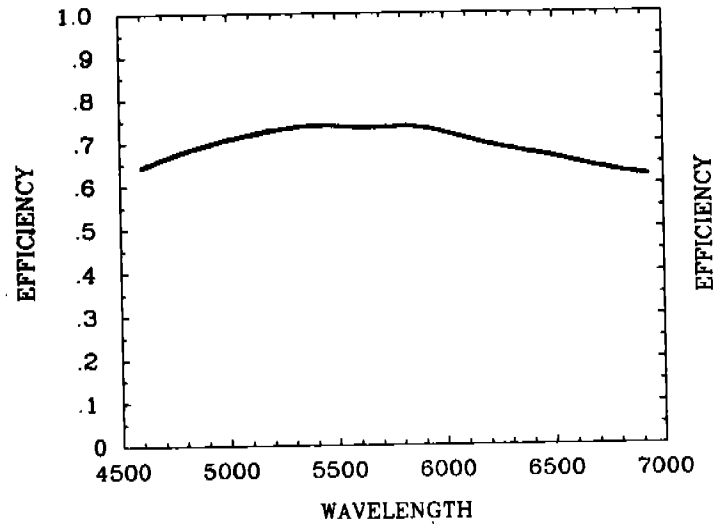

GRATING NUMBER G780H

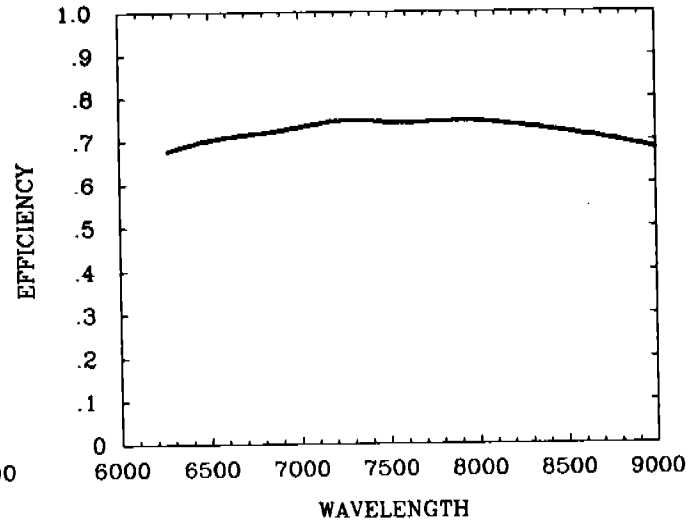

GRATING NUMBER G160L

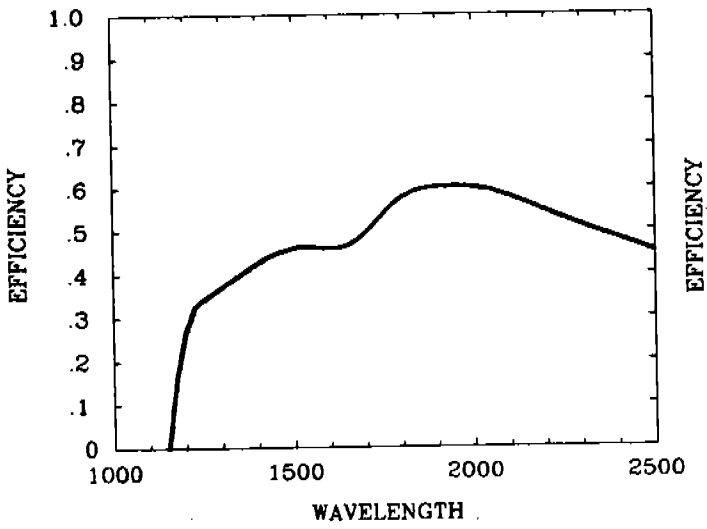

GRATING NUMBER G650L

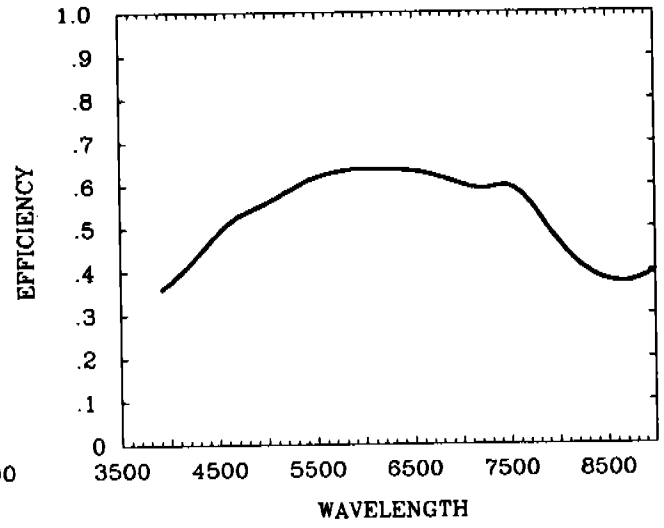

FOS GRATING CALIBRATIONS

APPENDIX C

FOS Spectropolarimeter Performance

Performance of the Spectropolarimeter for the Space Telescope Faint Object Spectrograph

R. G. Allen and J. R. P. Angel

Steward Observatory, University of Arizona
Tucson, Arizona 85721

Abstract

The Faint Object Spectrograph of the Space Telescope will be able to obtain spectropolarimetric data on faint astronomical objects. This is done by introducing a Wollaston prism and rotating waveplate behind the spectrograph entrance apertures. Fabrication of the polarimeter assembly has now been completed at the Martin Marietta Aerospace Co. in Denver, Colorado. Recent tests of the polarimeter and its optics have demonstrated that the device is capable of excellent performance. The magnesium flouride optical components of the polarimeter permit measurements of linear and circular polarization throughout the ultraviolet, down to Lyman α at 1216 Å. The mechanical stability and repeatability of the mechanism are demonstrated to yield position angles of the incoming plane of polarization to better than ± 0.5°, and we anticipate that measurements of the degree of polarization could be made to an accuracy of at least 0.1%. The accuracy for faint objects will depend on the integration times available for the observations, because of noise from photoelectron statistics. A 20-minute integration at 15th magnitude gives typically errors of 1% in each 100 Å wide spectral band.

Introduction

Polarization measurements are a powerful tool for astronomers, especially useful for studying some of the more extreme phenomena. Radiation originating in regions of magnetic field is often linearly or circularly polarized. The Zeeman effect, synchrotron and cyclotron emission are well known. Scattering processes in asymmetric geometry also cause linear polarization. Resonance scattering, electron scattering and dust scattering often modify light on its way from the point of emission, leaving clues in the polarization. We can use these clues to study phenomena as diverse as the composition and shape of dust grains a few hundred Angstroms across to the brilliant emission coming from the edge of very massive black holes in the nuclei of galaxies.

High sensitivity polarization measurements are now made from the ground in the range 0.32 - 1 μm and in the near IR to 2.2 μm. Space Telescope gives us the opportunity to add another factor 3 in wavelength, extending the lower limit to 1200 Å. This extra baseline will be especially helpful in interpreting continuum sources. Also, it makes accessible strong resonance lines and other spectral features of particular value in polarimetry.

Large aperture and high throughput are at a premium for polarization work, particularly spectropolarimetry. Integrations of many hours with the largest ground-based telescopes are made to get the high accuracy often needed in these measurements. Multichannel detectors are essential if spectropolarimetry of faint objects is to be attempted. Photoelectron counting systems are ideal for the high accuracy measurements; the digicon has been used extensively for spectropolarimetry on the ground[1], as well as the Oke multichannel scanner.[2] Recently the Lick IDS has also been modified for spectropolarimetry, and has obtained data of very high quality.[3] The Faint Object Spectrograph, FOS, is optimized for high efficiency, and with its digicon photon counting detectors is an ideal instrument for extending measurements to the far UV with the ST.

The technique used for spectropolarimetry in the FOS is very similar to that developed for ground-based instruments. A polarizing prism of doubly refractive material is introduced into the spectrophotometer, so as to form twin dispersed images of the slit in opposite senses of polarization at the detector. This analyzer is left fixed, and a waveplate is introduced ahead of it which is turned to analyze for linear and circular polarization. In this way the polarization effects in the dispersing optics following the analyzing prism are of no consequence, and have no effect on the accuracy of the measurement.

The FOS has two entrance ports, separated by 16 mm, where the entrance apertures are located. The polarimeter assembly is located 150 mm behind the apertures, and is constructed so that polarizing optics can be introduced into either beam. Since the FOS is discussed at length elsewhere in these proceedings[4], we give here just a short summary of the complete instrument. The beams passing through the polarimeter strike a roof-shaped grazing incidence mirror, which separates them and directs them away from the enclosure

corner that lies along the main telescope axis. Each of the redirected beams then strikes an off-axis collimator which sends the light to a grating/filter wheel. The concave gratings of the filter/grating wheel disperse the light and simultaneously reimage it onto a digicon detector. There are thus separate collimators and digicons for each entrance port. One digicon has a multi-alkali photocathode and is red sensitive (1800 - 8000 Å); while the other has bi-alkali photocathode and is blue sensitive (1150 - 5000 Å). The red and blue responses of the digicons are usually used to distinguish between the two optical paths through the FOS. The polarimeter can be used with either digicon. It can also be moved so that both paths are clear.

Basic principles

The polarization of a source can be characterized by the four Stoke's parameters I_1, Q_1, U_1, V_1 in the coordinate system shown in Figure 1. The degree of linear polarization in such a system is

$$P = \frac{(Q_1^2 + U_1^2)^{1/2}}{I_1}, \qquad (1)$$

the position angle of the plane of polarization is

$$\theta = 1/2 \tan^{-1}\left(\frac{U_1}{Q_1}\right),$$

the degree of circular polarization is

$$P_V = \frac{V_1}{I_1}, \qquad (2)$$

and the intensity is

$$I_1 = I_0 + (Q_1^2 + U_1^2 + V_1^2)^{1/2} \qquad (3)$$

where I_0 is the unpolarized component of I_1.

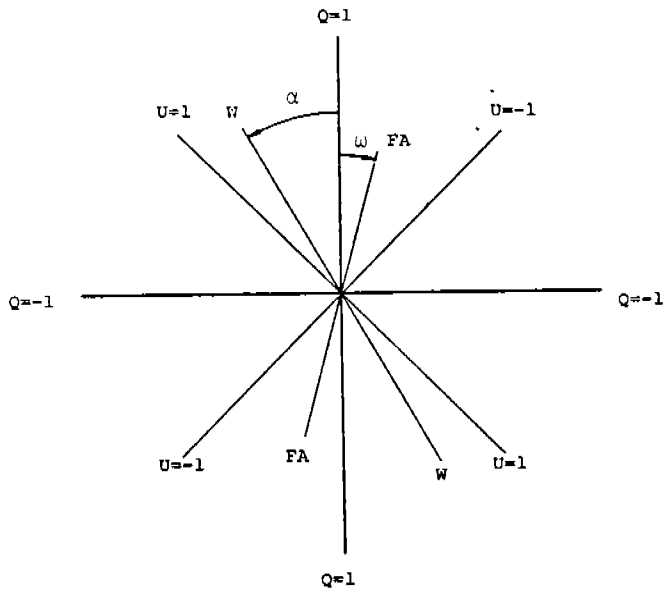

Figure 1. Coordinate system used in the polarization analysis. The view is toward the source. The line W-W is the pass direction of the Wollaston; while FA-FA is the fast axis of the waveplate.

If a waveplate with a fast axis at an angle ω and a retardation δ is inserted between the source and an observer, the transmitted radiation will have a new polarization state

$$I_2 = I_1, \qquad (4)$$

$$Q_2 = (1/2(1+\cos\delta) + 1/2(1-\cos\delta)\cos 4\omega)Q_1 - (1/2(1-\cos\delta)\sin 4\omega)U_1 + (\sin\delta \sin 2\omega)V_1, \qquad (5)$$

$$U_2 = -(1/2(1-\cos\delta) \sin 4\omega)Q_1 + (1/2(1+\cos\delta) - 1/2(1-\cos\delta)\cos 4\omega)U_1 + (\sin\delta \cos 2\omega)V_1, \qquad (6)$$

and

$$V_2 = -(\sin\delta \sin 2\omega)Q_1 - (\sin\delta \cos 2\omega) U_1 + (\cos\delta)V_1. \qquad (7)$$

If the observer then places an analyzer at an angle α in back of the waveplate, he will detect a signal

$$J = 1/2(I_2 + Q_2\cos 2\alpha + U_2\sin 2\alpha). \qquad (8)$$

In cases where the analyzer and coordinate system are aligned so that $\alpha = 0$, the observer receives a signal

$$J = \frac{I_1}{2} + \frac{Q_1}{4}(1 + \cos\delta) + \frac{Q_1}{4}(1 - \cos\delta)\cos 4\omega - \frac{U_1}{4}(1 - \cos\delta)\sin 4\omega + \frac{V_1}{2}\sin\delta \sin 2\omega. \quad (9)$$

By defining a phase factor $\varepsilon = 2\theta + 90°$ such that

$$\sin\varepsilon = \frac{Q_1}{(Q_1^2 + U_1^2)^{1/2}} = +\cos 2\theta \quad (10)$$

and

$$\cos\varepsilon = \frac{-U_1}{(Q_1^2 + U_1^2)^{1/2}} = -\sin 2\theta, \quad (11)$$

this expression can be reduced to

$$J = \frac{I_1}{2} + \frac{Q_1}{4}(1 + \cos\delta) + \frac{(Q_1^2 + U_1^2)^{1/2}}{4}(1 - \cos\delta)\sin(4\omega + \varepsilon) + \frac{V_1}{2}\sin\delta \sin 2\omega. \quad (12)$$

The functional dependence of J on ω in this equation shows that a rotating waveplate in front of an analyzer will modulate a linearly polarized beam at 4 times its rotation rate; while a circularly polarized beam will be modulated at 2 times its rotation rate. This equation also shows that, if one can determine the waveplate retardation δ, measures of J as a function of ω can be used to determine the Stoke's parameters I_1, Q_1, U_1, V_1 of the source.

The retardation of the rotating waveplate can be determined experimentally with 100% linearly polarized light. Under such conditions, $I_1 = (Q_1^2 + U_1^2)^{1/2}$ and

$$\delta = 2\cos^{-1}\left(\frac{1 - M}{1 + M\sin\varepsilon}\right)^{1/2} \quad (13)$$

where $M = \frac{J_{max} - J_{min}}{J_{max} + J_{min}}$ is the observed modulation of the signal. If the plane of polarization of the incoming radiation is aligned with the pass direction of the Wollaston prism, then $\sin\varepsilon = 1$ and

$$\delta = 2\cos^{-1}\left(\frac{J_{min}}{J_{max}}\right)^{1/2} \quad (14)$$

This is the best configuration for measuring δ. When the incoming plane of polarization is more nearly perpendicular to the Wollaston prism pass direction, δ is very uncertain because $1 - M$ and $1 + M\sin\varepsilon$ are both very small.

The polarimeter mechanism

The FOS polarimeter contains two rotatable waveplate retarders and two Wollaston prisms. One waveplate is permanently located in front of each Wollaston. The polarimeter is designed so that only a single motor is required to rotate the waveplates and to move either of the Wollaston/waveplate pairs from one entrance port to the other or out of the way. The mechanism that accomplishes this is shown in Figure 2. The drum, which is only 1.9 inches in diameter, contains the two Wollaston/waveplate pairs. The Wollastons are permanently fixed to the drum, but the waveplates are mounted in rotatable cylinders inside the drum. The waveplate cylinders have a 16-tooth gear on the outside which meshes with a 17-tooth fixed center gear inside the drum. One revolution of the drum rotates the Wollastons by 360°. The waveplates, however, rotate 382.5°. Each rotation of the drum thus increments the position angle of the waveplate fast axis by a net 22.5°. Sixteen rotations of the drum bring the mechanism back to its original configuration.

The drum is driven by a 90° permanent magnet stepper motor. A total of 420 motor steps are required to rotate the drum 360°. Errors in the positions of the optical components result from tolerances on the motor (±4.5°) and from errors in the gear train. Anti-backlash gears have been used wherever possible, and clearances between bearings and their

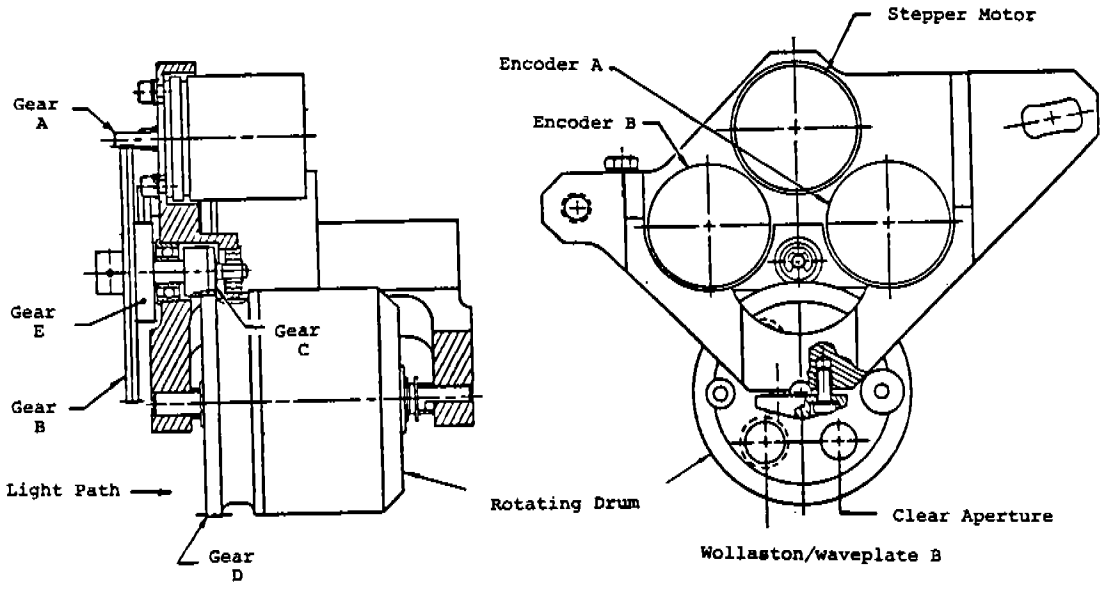

Figure 2. Side and rear views of the polarimeter.

housings and shafts have been held to less than .0001". Each bearing is also preloaded axially to eliminate radial play within the bearing itself. Belleville washers and compression springs provide the necessary preloads. Repeatability tolerances on θ_z (rotation about the optical axis) are ± 2.8 arc min for the Wollaston prisms and ± 10.0 arc min for the waveplates. Tolerances on θ_x and θ_y are ± 1.7 arc min for the Wollaston prisms and ± 3.0 arc min for the waveplates. These mechanical tolerances are better than those originally specified for the mechanism and will help to minimize uncertainties in the measurements that might be introduced by errors in the positions of the components.

Figure 3 shows the relative positions of the two Wollaston/waveplate pairs, labelled A and B, and the clear apertures, labelled C. The clear apertures are located in the red and blue beams. Motor step counts and angles between the various elements are indicated. It should be noted that this view of the polarimeter is from inside the spectrograph looking back at the entrance ports. This convention will be retained in all subsequent diagrams.

Two eight-bit pin encoders provide positional information on the mechanism. One revolution of the drum rotates encoder A five times and encoder B 5.0625 times. In 16 cycles, encoder A rotates 80 times and encoder B 81 times, bringing both back to their original counts. Encoder A changes by 3.0476 bits and encoder B by 3.0857 bits with each step of the motor. Both encoders increase with a CCW rotation of the drum as viewed in Figure 3. If the motor should ever fail, the entire mechanism can be removed from the optical path by activating a hot wire pinpuller.

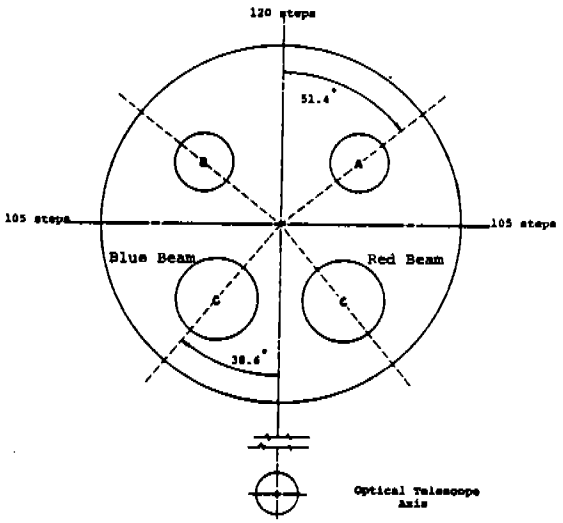

Figure 3. Relative configuration of the optical elements as viewed from inside the FOS in the direction of the entrance ports.

The optical components

The Wollaston prisms and waveplates for the polarimeter were manufactured by the Karl Lambrecht Corp. of Chicago, Illinois. Magnesium flouride was the birefringent crystal selected for the polarizing elements because of its transmission to below 1200 Å. The birefringence of magnesium flouride changes slowly in the visible and near UV. Around 1200 Å, however, it falls to zero and then has a reversed sign down to the transmission cutoff of the crystal. The Wollaston prisms both have an internal wedge angle of 20°. This angle was chosen so that the weak birefringence at Lyman α would still give adequate separation of the spectra at the detector. Two waveplates with different retardations are used in the polarimeter. The thickness differential of waveplate A is 137μm; that for waveplate B is 68.5μm. The actual retardations and transmissions of the flight waveplates were measured as a function of wavelength at the Marshall Space Flight Center in Huntsville, Alabama. The retardations of the two flight waveplates are listed in Table 1. The wavelength of zero retardation is slightly different for the two, which we believe must be due to slightly different chemical compositions. Retardations in the far UV are presented graphically in Figure 4.

Table 1. Retardations of the Flight Waveplates

λ(Å)	Waveplate A			Waveplate B		
	δ	Efficiency linear	Efficiency circular	δ	Efficiency linear	Efficiency circular
1175	-108°	.65	.95	-93°	.53	1.00
1200	100°	.59	.98	0°	0	0
1216	215°	.91	.57	90°	.50	1.00
1250	360°	0	0	161°	.97	.33
1300	460°	.59	.98	228°	.83	.74
1350	482°	.76	.85	247°	.70	.92
1400	485°	.79	.82	250°	.67	.94
1450	480°	.75	.87	241°	.74	.87
1500	468°	.65	.95	238°	.76	.85
1600	439°	.85	.98	226°	.85	.72
2537	251°	.66	.94	123°	.77	.86
3650	163°	.98	.29	84°	.45	.99
6328	95°	.54	.99	43°	.13	.68

The modulation efficiency of a waveplate is equal to $1/2(1 - \cos\delta)$ for linearly polarized light and $\sin\delta$ for circularly polarized light (see equation 12). Each waveplate is therefore most efficient at modulating linearly polarized light when $\delta = 180°$ and least efficient when $\delta = 0°$ or 360°. For circular polarization the efficiency peaks at $\delta = 90°$ and 270°. The modulation efficiency of each waveplate as a function of wavelength has been included in Table 1. In particular, note that waveplate A has a high modulation efficiency for linear polarization at Lyman α; while waveplate B does not. Together, the two waveplates provide adequate coverage of the spectrum.

A transmission curve for the complete polarizer is shown in Figure 5. Only a single curve is shown since both Wollaston/waveplate pairs are very similar. The fairly high transmission in the far UV was achieved by carefully selecting components and by making them as thin as possible. The Wollaston prisms are 3.5 mm thick; while the waveplates are only 1.0 mm thick. All elements have an 8 mm clear aperture.

Although the manufacturer came very close to achieving the specified values of retardation for the waveplates, they were unable to optically contact them as originally desired. There is therefore some light lost at the internal boundaries of the two halves of the waveplates. The Wollaston prisms are also not optically contacted. Optically contacting the optical components would probably have been possible if the components had been scaled up in thickness. This is a tradeoff, however, that would have significantly increased the absorption losses in the far UV.

Dow Corning 6-1104 sealant was applied to the edges of the Wollastons and waveplates to hold them together during testing. The flight components were later glued into their holders in the polarimeter with the same material.

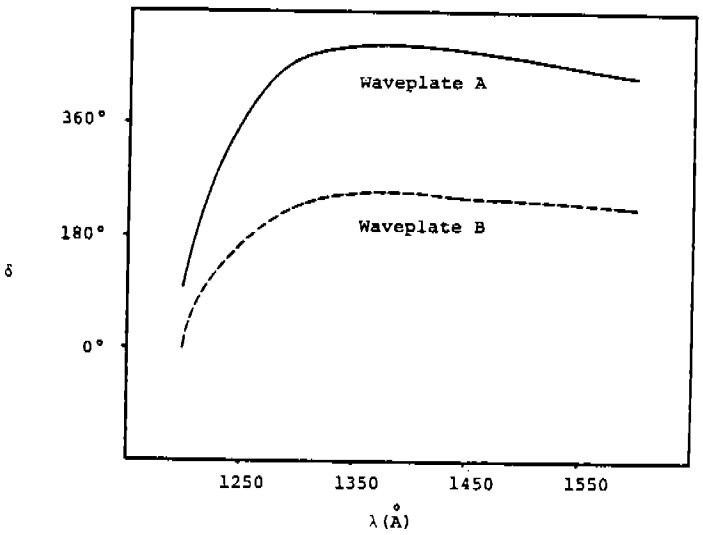

Figure 4. Retardations of the flight waveplates.

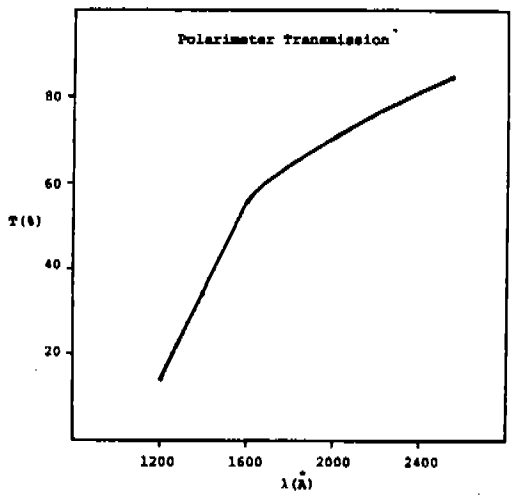

Figure 5. The transmission of the polarimeter as a function of wavelength.

Laboratory measurements

Operational tests of the polarimeter assembly were carried out at the Martin Marietta Aerospace Co. in Denver, Colorado. In the first phase of testing, the polarimeter was placed in auxiliary optical system that accurately simulated its operation in the FOS, and the position of each image in the focal plane was measured to an accuracy of ± 2.5 μm as the polarimeter was cycled from one waveplate position to the next. No systematic variations were observed with either Wollaston/waveplate pair, and random variations in the positions of the images were less than ± 5.0μm. Since the digicon diodes are 50 μm wide, there should be no significant image motion problems with the polarimeter.

The measurements of image motion were used to compute the position angles of the image splitting for the four normal configurations of the polarimeter. Figure 6 summarizes these measurements. It also shows how the images are rotated by the grazing incidence mirror and then inverted by the collimator and grating before reaching the detector. Figure 6 has a rotational orientation that is identical to that of Figure 3.

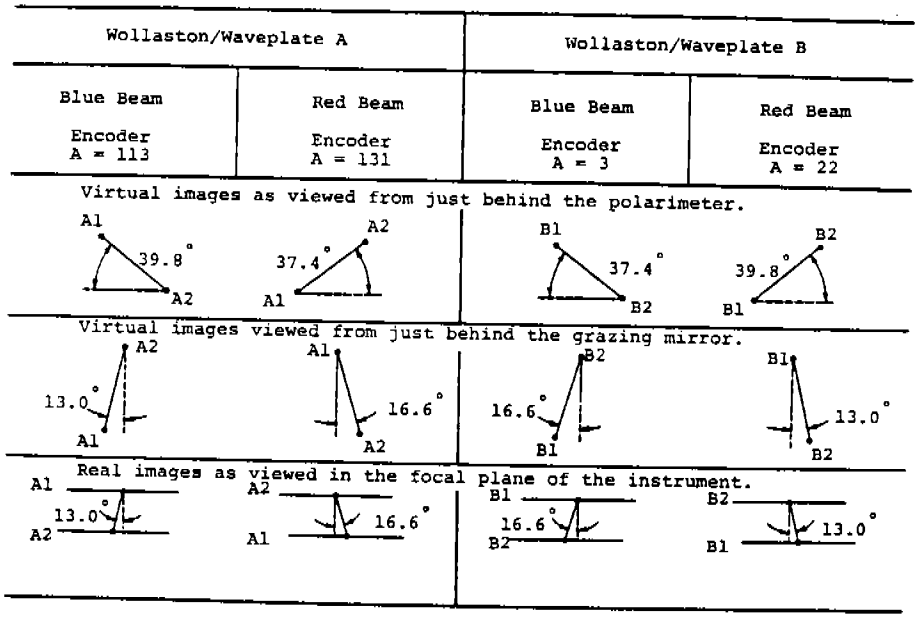

Figure 6. Split images of the entrance ports as viewed from various locations in the FOS.

The twin images at the detector are separated by an amount

$$s = 150\ |n_e - n_o|\ \tan 20° \qquad (15)$$

where $n_e - n_o$ is the birefringence of the magnesium flouride and s is in millimeters. Maximum splitting is 780 μm at 1530 A. Images at Lyman α are separated by only 242 μm. Figure 6 shows that splitting is not precisely perpendicular to the dispersion. This is a consequence of requiring either waveplate to be operable in either beam.

The second phase of the operational tests involved actually measuring the polarization angle θ of a known source. In this stage of the testing, a pinhole light source at 3650 A was placed 150 mm in front of the polarimeter. A lens after the polarimeter limited the transmitted beam to f/24 and reimaged the light onto a photomultiplier. The 2:1 imaging in the FOS was also reproduced. A chopper was used to reduce the effects of stray light. During the actual tests, an HNP'B polarizer was aligned at θ = 0°, 45°, 90°, and 135° in front of the polarimeter. At each angle of incoming polarization, two sets of sixteen measures of the intensity J as a function of waveplate angle γ were taken with each Wollaston/waveplate pair. One set was taken with each split image. The waveplate angle γ changed by 22.5° between measures and was defined to be zero at the initial position of the waveplate in each data set.

The individual data sets from the tests were fitted with an equation of the form

$$J = C_1 + C_2 \sin (4\gamma + \psi). \qquad (16)$$

The phase angle ψ in this equation equals $4\omega_1 + \varepsilon$, where ω_1 is the initial position of the waveplate with respect to the Wollaston pass direction and ε is the phase factor in equations (10), (11), and (12). The angle γ is thus equal to $\omega - \omega_1$ where ω_1 was determined from the eight sets of data that were taken with each Wollaston/waveplate pair. Each individual data set then yielded a final value for the angle of polarization θ and the waveplate retardation δ. Results of the test observations are summarized in Figure 7. The standard deviation of θ about its known direction is 0.15° for waveplate A and 0.22° for waveplate B. Waveplate A has a high modulation efficiency at the test wavelength; while waveplate B has a modulation efficiency of only 45%. Since these errors are consistent with known sources of error and instability in the test measurements, we can anticipate even better accuracy in the FOS.

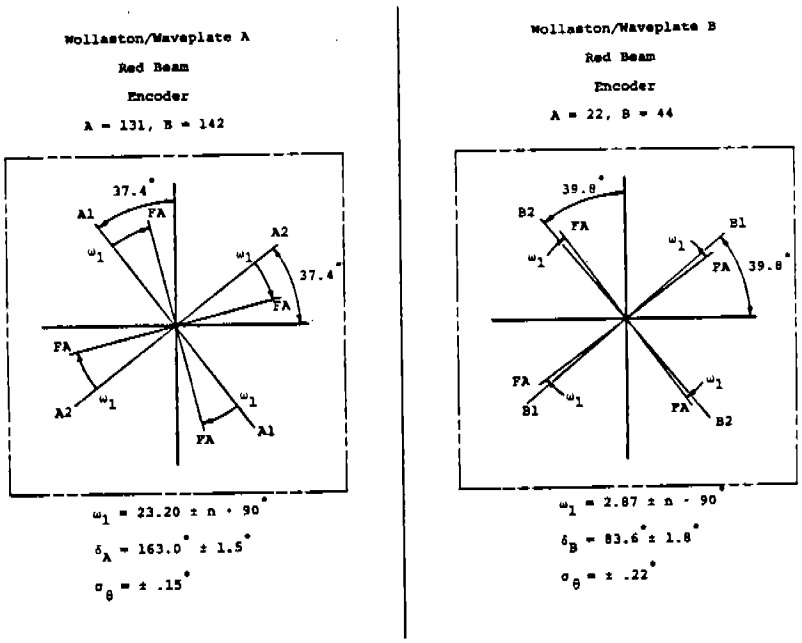

Figure 7. Diagrams of the Wollaston pass directions and the initial positions of the waveplates that were derived from the operational tests of the polarimeter.

Accuracy for faint objects

For many objects studied with the FOS polarimeter, the accuracy of measurement will be set entirely by photoelectron statistics. This is the case now for most ground-based polarimetry. With the transmission and modulation efficiency of the flight polarimeter determined, and the efficiency of the FOS known, the measurement accuracy can be predicted with a high degree of confidence.

In Table 2 we have carried through estimates for an AO star with V = 15th magnitude. Its flux is typical of many objects that will be of interest, such as Seyfert nuclei, bright QSO's, BL Lac Objects, the bright knots of M87's jet, magnetic white dwarfs and AM Her objects. Column 1 gives wavelengths from 1216 to 3000 Å, and column 2 the source flux in ergs/cm^2/Å/sec. In column 3 is the calculated number of photoelectron events per 100 Å bandwidth that will be recorded in an integration going through all 16 waveplate positions in 20 minutes. 134.4 seconds is lost to mechanical cycling through 16 rotations of the drum. We have taken account of losses in the ST main optics, in the FOS and polarimeter, and the fact that the digicon can detect only one of the two spectra at any moment. The FOS efficiency is not strongly dependent on resolution; the counts will be somewhat higher when the sapphire dispersing prism is used to cover the region above 1800 Å in one integration.

Table 2. Count Rate and Polarization Accuracy for AO star, V = 15

(1) λ(Å)	(2) log F_λ	(3) Count in 20 minutes in 100 Å Band	(4)		(5)	
			η(P)	σ(P)	η(V)	σ(V)
1216	-14.6	595	.91	6.4%	1.00	5.8%
1500	-14.2	9,500	.76	1.9%	.95	1.5%
2000	-14.1	39,550	.80	0.89%	.96	0.74%
2500	-14.2	78,000	.77	0.66%	.94	0.54%
3000	-14.4	69,500	.85	0.63%	.92	0.58%

Columns 4 and 5 give the efficiency for the optimum waveplate at each wavelength and the error in measuring linear polarization; $\sigma(P)$ is given by $\sqrt{2}/\eta\sqrt{N}$, and is the standard deviation of each Q/I and U/I. When appreciable polarization is detected, it is also equal to the error in P, the degree of polarization. (Errors in P are not gaussian when P is null or weak). The last two columns give the higher of the two waveplate efficiencies for V, and the standard deviation in V, also given by $\sqrt{2}/\eta\sqrt{N}$.

We see that the errors in a 20-minute measurement in the 100 Å bandwidth vary from 0.6% to 6% over the range from 3000 to 1216 Å. For some objects with high polarization this will already be a useful measurement; when higher accuracy is needed, longer exposures and/or wider bands will be required. For example, the band 1500 - 2000 Å could be measured to $\sim$ 0.2% accuracy in a 3-hour integration.

Acknowledgements

The authors would like to thank Dr. Donald Griner at the Marshall Spaceflight Center and Mr. Jack Eastman of the Martin Marietta Aerospace Co. for their assistance in testing the polarimeter and its optics. Financial assistance in performing these tasks has been provided by the University of California, San Diego under NASA Contract NAS5-24463.

References

1. Angel, J. R. P., and Landstreet, J. D. 1974, Ap. J. 191, 457.
2. Angel, J. R. P., Carswell, B. F., Strittmatter, P. A., Beaver, E. A., and Harms, R. 1974, Ap. J. (Letters) 194, L47.
3. Schmidt, G. D. and Miller, J. S. 1980, Ap. J. 240, 759.
4. Proceedings of the S.P.I.E., Vol. 331, 1982.